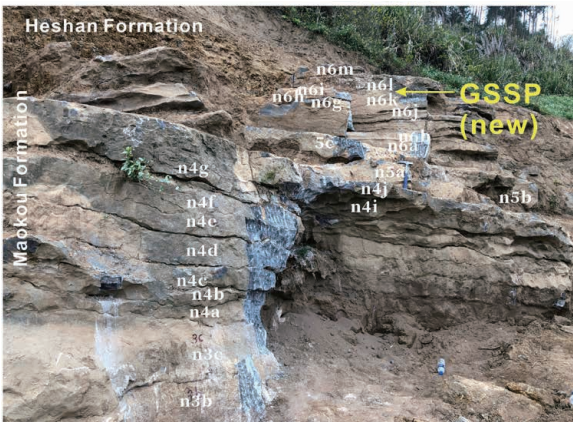
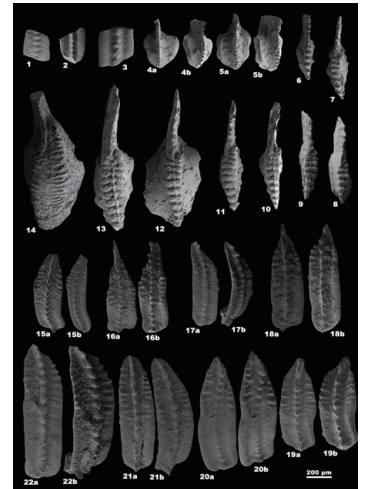
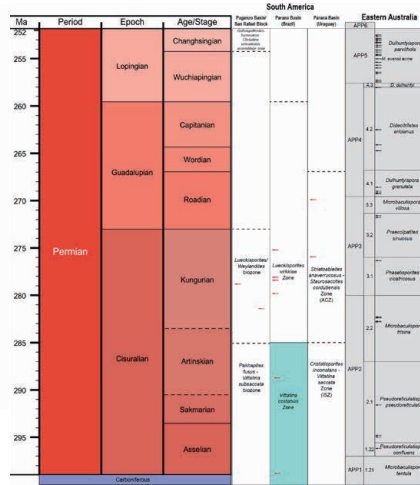
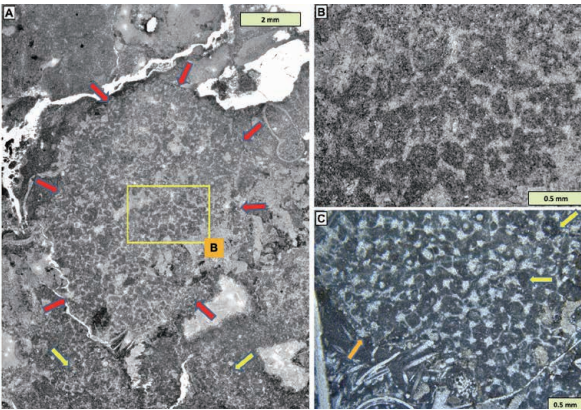




Permophiles

International Commission on Stratigraphy



Newsletter of the
 Subcommittee on
 Permian Stratigraphy
 Number 74
 ISSN 1684-5927
 January 2023

Table of Contents

Notes from SPS Secretary Yichun Zhang	3
Notes from SPS Chair Lucia Angiolini	3
Annual Report 2022	4
Henderson's Harangue #11 Charles Henderson	7
Redefinition of the Global Stratotype Section and Point (GSSP) and new Standard Auxiliary Boundary Stratotype (SABS) for the base of Wuchiapingian Stage (Lopingian Series, Permian) in South China Shu-zhong Shen, Dong-xun Yuan, Yi-chun Zhang, Charles M. Henderson, Quan-feng Zheng, Hua Zhang, Min Zhang, Yu Dai, Hai-peng Xu, Wen-qian Wang, Qian Li, Yue Wang, Xiang-dong Wang, Jahandar Ramezani, Douglas H. Erwin, Lucia Angiolini, Fei-fei Zhang, Zhang-shuai Hou, Xi-yang Zhang, Shu-han Zhang, Yong-xin Pan, Michael Stephenson, Shi-long Mei	9
The Once and Future Quest: the Kungurian GSSP candidate at Rockland Section and SABS at Carlin Canyon, Nevada Lucia Angiolini, Benoit Beauchamp, Luke Bratton, Bryana Fraser, Charles Henderson, Walt Snyder, Andrea Zanchi	37
Correlation chart for the Lower Permian of the western USA Charles Henderson, Michael T. Read	41
Additional conodonts from the Cisuralian-Guadalupian boundary interval in South China Dong-xun Yuan, Shu-zhong Shen, Hua Zhang, Hai-peng Xu, Zhang-shuai Hou, Quan-feng Zheng, Wen-qian Wang	44
Do Permian-Triassic boundary microbialites contain keratose sponges? Stephen Kershaw	47
Tackling species variation in palynology Michael H. Stephenson	51
Rebuilding terrestrial Gondwana: challenges and opportunities of a palynological approach Annette E. Götz, Alexander Wheeler	54
Wuchiapingian brachiopods from Iran: potential and perspectives as archives of the past Marco Viaretti, Gaia Crippa, Lucia Angiolini	58
News from the Permian of Northern Albania at the base of the Albanian Alps Micha Horacek, Leopold Krystyn, Rainer Brandner, Cerciz Durmishi, Kujtim Onuzi	62
Announcement of Strati 2023, a conference in Switzerland and a call for funded participation in STRATI 2023	68
SUBMISSION GUIDELINES FOR ISSUE 75	69

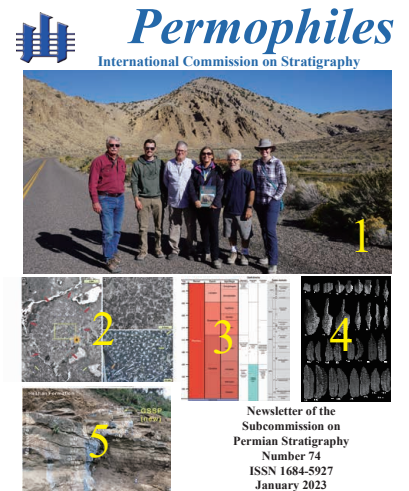
Fig. 1. Group photo in front of the Carlin Canyon section, USA. Angiolini et al., this issue.

Fig. 2. Mineral sponges (lithistids). Stephen Kershaw, this issue.

Fig. 3. Palynological zonation schemes of South America and eastern Australia. Götz and Wheeler, this issue.

Fig. 4. Conodont specimens from the Chihhsia-Kuhfeng boundary interval in South China. Yuan et al., this issue.

Fig. 5. New base-Wuchiapingian GSSP section in Laibin, Guangxi, China. Shen et al., this issue.



Notes from the SPS secretary Yichun Zhang

Introductions and thanks

Time runs so fast and it's time for me again to edit a new issue of *Permophiles*. Coincidentally, it is also the time of the Spring Festival of China (Chinese New Year). I am editing this issue to the sound of firecrackers.

This issue contains significant studies and comments. Many thanks to all the contributors of this issue: Charles Henderson, Shu-zhong Shen and co-authors, Lucia Angiolini and co-authors, Michael T. Read, Dong-xun Yuan and co-authors, Stephen Kershaw, Michael H. Stephenson, Annette E. Götz and Alexander Wheeler, Marco Viaretti and co-authors, and Micha Horacek and co-authors.

I would like to keep drawing your attention to the SPS website <https://permian.stratigraphy.org/>, where you can find all issues of *Permophiles*, updated Permian Timescale, presentation videos and news about the Permian Subcommittee. In addition, a new item "Taxonomy" has been created to show some photos of critical palynomorph species from the Usolka, base Sakmarian GSSP.

Permophiles 74

This issue starts with the eleventh harangue by Prof. Charles Henderson. He tells the story of the discovery of the true age of the conodonts *Sweetognathus whitei* and has highlighted again that *S. whitei* and *S. asymmetricus* are two different species separated by 5 Ma.

Shu-zhong Shen and co-authors have proposed a new section for the GSSP and a Standard Auxiliary Boundary Stratotype for the base of the Wuchiapingian stage because the original Penglaitan section is permanently flooded due to a hydroelectric dam. In the new section, the first appearance datum (FAD) of the conodont *C. postbitteri* sensu lato within the lineage *Jinogondolella granti* → *Clarkina postbitteri* → *C. dukouensis* is proposed as a marker to recognize and correlate the base of the Wuchiapingian.

Lucia Angiolini and co-authors reported their recent fieldwork in the Carlin Canyon section (potential Standard Auxiliary Boundary Stratotype for base-Sakmarian, base-Artinskian and possible base-Kungurian) and the Rockland section (base-Kungurian GSSP candidate) in Nevada, USA.

Charles M. Henderson and Michael T. Read provided an updated Cisuralian correlation chart showing chronostratigraphic correlations between the international scale and the North American scale, based on recent studies on fusulines and conodonts.

Dong-xun Yuan and co-authors reported new conodonts from the Chihhsia-Kuhfeng boundary at the Zhengpanshan and Maweshan sections. Unlike the Zhengpanshan section, *Jinogondolella nankingensis* was found in the upper part of the Chihhsia Formation.

Stephen Kershaw discussed the vermiform structures in Permian-Triassic boundary microbialites. The discussion is focused on whether keratose sponges are responsible for the formation of such structures in microbialites.

Michael Stephenson introduced the application online taxonomy in studying palynology. This method is useful for palynological taxonomists in examining the taxonomy of a specific species and finding possible bridge taxa for inter-continental correlations.

Annette E. Götz and Alexander Wheeler reviewed the latest progress in the study of Permian palynozones in Australia, South America and South Africa. They highlighted that the palynology-based regional correlation should be improved as it is linked to paleoclimates.

Marco Viaretti and co-authors introduced their recent work on oxygen isotopes from Wuchiapingian brachiopod shells from Iran. They found that *Araxilevis intermedius* is the most reliable species for paleoenvironmental reconstructions.

Micha Horacek revisited the Permian sequence in the Albanian Alps. He found that the Permian is not a continuous sedimentary sequence as previously recognized, but mostly composed of mass-flows/olistoliths.

Finally, two symposia/meetings are announced, respectively STRATI 2023 in France and a conference in Lausanne, Switzerland. I call your attention on STRATI 2023 session SC10: Correlation of glacial events and extinctions: the Permian and beyond, and welcome you to submit abstracts on Permian topics.

Future issues of Permophiles

The next issue of *Permophiles* will be the 75th issue. We welcome contributions related to Permian studies around the world. So, I kindly invite our colleagues to contribute harangues, papers, reports, comments and communications.

The deadline for submission to Issue 75 is 31 July 2023. Manuscripts and figures can be submitted via email address (yczhang@nigpas.ac.cn) as attachment.

To format the manuscript, please follow the TEMPLATE on SPS website.

Notes from the SPS Chair Lucia Angiolini

I am very proud to open this issue of *Permophiles*, because it is fervent with topics of discussion, such as the insightful harangue of Charles Henderson, the thoughtful analysis of Mike Stephenson, and the very interesting and in-depth contributions of some of our new voting members and our corresponding members. I am sure that this issue will be a source of discussions and contributions which will vividly flow into the next issue, showing that Permian research is progressing fast and deeply.

Notwithstanding this positive premise, geopolitical tensions remain high, highlighting problems of collaboration, and hampering transparency and coherence in Science. As all SPS members are aware, SPS is following the IUGS statement of March 18, 2022 recommending sanctions in reaction to the invasion of Ukraine by the Russian Federation, but no action has been personally directed towards our Russian colleagues. The sanctions mean that the decision on the Russian-led manuscript on the base-Artinskian GSSP submitted to *Episodes* and positively reviewed is at the moment suspended, even if the base-Artinskian GSSP has been ratified by IUGS on February 1, 2022.

This was widely communicated to SPS members in the last issue of *Permophiles*.

However, some of the co-authors on the base-Artinskian GSSP manuscript submitted to *Episodes* (in stand-by for about one year) were disappointed to discover that part of the contents of the proposal have been just published by Afanasieva et al. (2022, *Paleontological Journal*), without any notice or communication in advance. This paper contains the descriptions of the radiolarians and palynomorphs of the Dal'ny Tulkas section and trench, which can be deleted from the *Episodes* manuscript (the radiolarians), or are not up to date (palynomorphs) with respect to the original proposal. However, it also contains an important discussion on the conodont bioevents and their correlation, which resulted from the common work of Charles Henderson and Valery Chernykh. Some of these conodont bioevents were not understood before the conjunct work for the proposal. See for instance the discussion on the complex history in the understanding of the concept of *Sweetognathus asymmetricus* in Charles Henderson's harangue, this issue. The Afanasieva et al. paper also contains some inconsistencies which will be underscored in the final version of the *Episodes* manuscript.

I would like to discourage citation of this manuscript as a reference for the base-Artinskian GSSP, because this is not the formal proposal. Also, I hope that this practice of lack of transparency and lack of communication will not happen again in SPS and its working groups. My personal thought is that the SPS officers and the co-authors of the original proposal should have been informed in advance and Charles Henderson involved, or at least acknowledged, in this paper.

Going beyond this, a visit to the Rockland section (Nevada, USA), described in this issue, confirmed its validity as the best GSSP candidate for the base-Kungurian. Charles Henderson, Walter Snyder and colleagues will soon submit a GSSP proposal for discussion inside SPS and then voting. Additional conodont samples are being processed by Charles Henderson and some specimens will be analysed for Sr isotopes by his MSc student Luke Bratton. Strontium isotope analysis on whole rock material is also being done by Kate Tierney (Department of Earth and Environmental Sciences, University of Iowa) with the support of SPS funds. The Rockland section is well exposed and continuous, it records a long time interval (all the Artinskian and Kungurian), an expanded boundary interval in carbonate facies, a rich benthic fossil content (allowing correlation with the Tethyan sections), and it has permanent free access. Not far from the Rockland Canyon, the Carlin Canyon succession is very promising to establish complementary boundary intervals, i.e. a Standard Auxiliary Boundary Stratotype (SABS), for the base Sakmarian and base Artinskian, as outlined in Charles Henderson's harangue and in Angiolini et al., this issue. I suggest the Permian Community to read the paper by Head et al. (2022, *Episodes*) on SABS, because it is really clear and interesting.

Another very important piece of work to complete the Permian GSSPs is the proposal by Shen et al. on the replacement section for the previously-defined base of the Lopingian GSSP at the Penglaitan section in Guangxi, South China that has been permanently flooded since 2020; its auxiliary section at Tieqiao has been flooded too. A new section along the Hongshui River

has been excavated and studied at a place higher on the same bank as the original GSSP at Penglaitan, and it is presented in this issue. A new Standard Auxiliary Boundary Stratotype is also proposed at the Fengshan section near the Liuzhou City of Guangxi Province. The proposal will be soon sent to the voting members with a request for comments, immediately followed by call for a vote of SPS voting members.

To continue our good practice to organize webinars on Permian topics and promote discussion, on November 2, 2022, the webinar "The Science of Permian Conodonts" by Charles Henderson was organized live online through MS Teams:

<https://permian.stratigraphy.org/Interests/Charles>

We are planning a new webinar for April, and we will keep the Permian community informed.

We have important news: the "Gondwana to Euramerica correlations Working Group" is working hard and Mike Stephenson has launched a very good proposal to "tackle species variation" publishing a photo-gallery in the SPS website (<https://permian.stratigraphy.org/Gallery/Usolka>). Please also read his contribution in this issue.

Finally, I am pleased to announce that a compilation of selected papers published on Permian topics in 2022 prepared by Marco Viaretti (University of Milano) will be soon available on the SPS website.

I want to thank Yichun Zhang for his very good work in preparing *Permophiles* and managing the workflow of SPS, and I am sure that, based on the content of this issue, we will receive very interesting contributions, comments and opinions for the next one.

ANNUAL REPORT 2022

1. TITLE OF CONSTITUENT BODY and NAME OF REPORTER

International Subcommittee on Permian Stratigraphy (SPS)

Submitted by: Lucia Angiolini, SPS Chair

Dipartimento di Scienze della Terra "A. Desio", Via Mangiagalli 34, 20133 Milano, Italy, E-mail: lucia.angiolini@unimi.it

2. OVERALL OBJECTIVES, AND FIT WITHIN IUGS SCIENCE POLICY

Subcommittee Objectives: The Subcommittee's primary objective is to define the series and stages of the Permian by means of internationally agreed GSSPs and establish a high-resolution temporal framework based on multidisciplinary (biostratigraphical, geochronologic, chemostratigraphical, magnetostratigraphical etc.) approaches, and to provide the international forum for scientific discussion and interchange on all aspects of the Permian, but specifically on refined intercontinental and regional correlations.

Fit within IUGS Science Policy: The objectives of the Subcommittee involve two main aspects of IUGS policy: 1) The development of an internationally agreed chronostratigraphic scale with units defined by GSSPs where appropriate and related to a hierarchy of units to maximize relative time resolution within the Permian System; and 2) the establishment of framework and

systems to encourage international collaboration in understanding the evolution of the Earth and life during the Permian Period.

3. ORGANISATION - interface with other international projects / groups

3a. Officers for 2020-2024 period:

Prof. Lucia Angiolini (SPS Chair)

Dipartimento di Scienze della Terra "A. Desio". Via Mangiagalli 34, 20133 Milano, Italy, E-mail: lucia.angiolini@unimi.it

Prof. Michael H. Stephenson (SPS Vice-chair)

British Geological Survey. Keyworth, Nottingham NG12 5GG, and Stephenson Geoscience Consulting, Keyworth, Nottingham, NG12 5HU, United Kingdom, E-mail: mikepalyno@me.com

Prof. Yichun Zhang (SPS Secretary)

State Key laboratory of Palaeobiology and Stratigraphy. Nanjing Institute of Geology and Palaeontology, 39 East Beijing Road, Nanjing, Jiangsu 210008, P.R. China, E-mail: yczhang@nigpas.ac.cn

4. EXTENT OF NATIONAL/REGIONAL/GLOBAL SUPPORT FROM SOURCES OTHER THAN IUGS

Shuzhong Shen and Michael Stephenson are investigating the possibility of support for SPS through the Deep-time Digital Earth (DDE) Big Science Program of IUGS focused on informatics support for biostratigraphic data management and palaeogeographic reconstructions. Lucia Angiolini was funded by an Italian national project to perform field activity in the Kungurian base GSSP candidate at Rockland, Nevada (Fund: MURST-PRIN 2017RX9XXXY, project 'Biota resilience to global change: biomineralization of planktic and benthic calcifiers in the past, present and future')

5. CHIEF ACCOMPLISHMENTS IN 2022 (including any relevant publications arising from ICS working groups)

- The proposal for the Global Stratotype Section and Point (GSSP) for the base-Artinskian Stage (Lower Permian) was ratified by the IUGS Executive Committee on 2 February 2022.

- The manuscript "Proposal for the Global Stratotype Section and Point (GSSP) for the base-Artinskian Stage (Lower Permian)" was sent to *Episodes* on 22 February 2022 (EPISODES-D-22-00018) and received a positive review.

- Five new voting members were selected based on their extensive experience in Permian stratigraphy (Annette Goetz, Germany; Sam Lee, School of Earth, Australia; Ana Karina Scomazzon, Brazil; Elisabeth Weldon, Australia; Dongxun Yuan, China).

- A new Working Group was organized "Gondwana to Euramerica correlations" with the aim of solving the difficulty of correlating between Gondwana and Euramerica.

- The Permian Time Scale was kept updated <https://permian.stratigraphy.org/gssps> and two issues of *Permophiles* were published (SPS Newsletters *Permophiles* 72 and 73).

- Two webinars have been organized (<https://permian.stratigraphy.org/interest>)

6. SUMMARY OF EXPENDITURE IN 2022

The amount received from ICS was spent for literature compilation, Dal'ny Tulkas GSSP manuscript for Episodes preparation, Standard Pro Annual ZOOM license for SPS, geochemical analyses on samples (Sr analyses) from Rockland section (Nevada), and support to the new Working Group "Gondwana to Euramerica correlations" to produce a photo-gallery of most important taxa for correlation.

Due to the Ukraine-Russian war, it was not possible to do field work in Dal'ny Tulkas and Mechetlino as scheduled. A field-trip to the Rockland section (Nevada), base Kungurian GSSP candidate, was performed by Lucia Angiolini and Charles Henderson from 14 to 23 October 2022. The expenses of Lucia Angiolini were mostly supported by an Italian National Research Fund and only subordinately by ICS funds.

7. SUMMARY OF INCOME IN 2022

An amount of Euros 4287,89 euros was allocated from ICS on July 2022.

8. BUDGET REQUESTED FROM ICS IN 2023***

We apply for 4800 US\$ from ICS for SPS activities in 2023. This will be mainly for the activities to establish the base-Kungurian GSSP at Rockland, Nevada and to organize a field trip in the area, and to support the participation to the STRATI 2023 Congress in Lille.

9. WORK PLAN, CRITICAL MILESTONES, ANTICIPATED RESULTS AND COMMUNICATIONS TO BE ACHIEVED NEXT YEAR:

- We plan to have the proposal of the base Kungurian GSSP proposal published in *Permophiles* and voted by SPS voting members.

- We plan to organize several webinars.

- We plan to support the activity of the new working group on Gondwana Correlation.

10. KEY OBJECTIVES AND WORK PLAN FOR THE PERIOD 2020-2024

- Establish the Artinskian and Kungurian GSSPs.

- Revise the Permian timescale where it needs to be improved (Guadalupian stages, replacement GSSP section of the base-Lopingian).

- Establish a robust palaeogeographic frameworks for the Permian and focus on N-S correlations.

- Propose DDE-sponsored informatics support for biostratigraphic data management and palaeogeographic reconstructions.

- Organize webinars to increase the size, diversity and international coverage of the Permian Community

- Publish at least two *Permophiles* issues each year.

APPENDIX [Names and Addresses of Current Officers and Voting Members]

Prof. Lucia Angiolini (SPS Chair)

Dipartimento di Scienze della Terra "A. Desio"
Via Mangiagalli 34, 20133, Milano, Italy

E-mail: lucia.angiolini@unimi.it

Dr. Alexander Biakov

Northeast Interdisciplinary Scientific Research Institute
Far East Branch, Russian Academy of Sciences,
Portovaya ul. 16, Magadan, 685000 Russia
E-mail: abiakov@mail.ru

Dr. Valery Chernykh

Institute of Geology and Geochemistry
Urals Branch of Russian Academy of Science
Pochtovy per 7, Ekaterinburg 620154 Russia
E-mail: vtschernich@mail.ru

Dr. Annette Goetz

Landesamt für Bergbau, Energie und Geologie
Stilleweg 2, 30655 Hannover, Germany
E-mail: Annette.Goetz@lbeg.niedersachsen.de

Dr. Valeriy K. Golubev

Borissiak Paleontological Institute, Russian Academy of Sciences
Profsoyuznaya str. 123, Moscow, 117997 Russia
E-mail: vg@paleo.ru

Prof. Charles M. Henderson

Dept. of Geoscience, University of Calgary
Calgary, Alberta, Canada T2N1N4
E-mail: cmhender@ucalgary.ca

Dr. Sam Lee

School of Earth, Atmospheric and Life Sciences,
University of Wollongong, Northfields Ave,
Wollongong, NSW 2522, Australia
E-mail: lsam@uow.edu.au

Prof. Spencer G. Lucas

New Mexico Museum of Natural History and Science
1801 Mountain Road N. W., Albuquerque, New Mexico 87104-
1375 USA
E-mail: spencer.lucas@state.nm.us

Prof. Ausonio Ronchi

Dipartimento di Scienze della Terra e dell'Ambiente
Università di Pavia - Via Ferrata 1, 27100 PV, ITALY
voce +39-0382-985856
E-mail: ausonio.ronchi@unipv.it

Dr. Tamra A. Schiappa

Department of Geography, Geology and the Environment
Slippery Rock University, Slippery Rock, PA 16057 USA
E-mail: tamra.schiappa@sru.edu

Prof. Mark D. Schmitz

Isotope Geology Laboratory
Department of Geosciences
Boise State University, 1910 University Drive
Boise, ID 83725-1535, USA
E-mail: markschmitz@boisestate.edu

Prof. Joerg W. Schneider

Freiberg University of Mining and Technology
Institute of Geology, Dept. of Palaeontology,
Bernhard-von-Cotta-Str.2, Freiberg, D-09596, Germany
E-mail: Joerg.Schneider@geo.tu-freiberg.de

Prof. Ana Karina Scomazzon

Universidade Federal do Rio Grande do Sul
Instituto de Geociências
Departamento de Paleontologia e Estratigrafia
LACONF - Laboratório de Conodontes e Foraminíferos
Porto Alegre, RS, Brazil
E-mail: akscomazzon@ufrgs.br

Prof. Shuzhong Shen

School of Earth Sciences and Engineering
Nanjing University, 163 Xianlin Avenue,
Nanjing, Jiangsu 210023, P.R. China
E-mail: szshen@nju.edu.cn

Prof. Michael H. Stephenson (SPS Vice-Chair)

British Geological Survey, Kingsley Dunham Centre
Keyworth, Nottingham NG12 5GG
United Kingdom
E-mail: mhste@bgs.ac.uk

Prof. Katsumi Ueno

Department of Earth System Science
Fukuoka University, Fukuoka 814-0180 JAPAN
E-mail: katsumi@fukuoka-u.ac.jp

Dr. Elisabeth Weldon

School of Life and Environmental Sciences, Faculty of Science
Engineering & Built Environment, Deakin University
Locked Bag 20000, Geelong, VIC 3220
+61 3 92517191
E-mail: l.weldon@deakin.edu.au

Dr. Dongxun Yuan

School of Resources and Geosciences
China University of Mining and Technology
1 Daxue Road, Xuzhou, Jiangsu 221116, P.R. China
E-mail: dxyuan@cumt.edu.cn

Prof. Yichun Zhang (SPS Secretary)

Nanjing Institute of Geology and Palaeontology
39 East Beijing Road, Nanjing, Jiangsu 210008, China
E-mail: yczhang@nigpas.ac.cn

Working group leaders

- 1) Artinskian-base and Kungurian-base GSSP Working Group;
Chair-Valery Chernykh.
- 2) Correlation between marine and continental Guadalupian
Working Group; Chair-Charles Henderson.
- 3) Correlation between marine and continental Carboniferous-
Permian Transition Working Group; Chair-Joerg Schneider.
- 4) Gondwana to Euramerica correlations Working Group;
Chair-Mike Stephenson.

Honorary Members

Prof. Giuseppe Cassinis

Dipartimento di Scienze della Terra e dell'Ambiente
Università di Pavia
Via Ferrata 1, 27100 PV, Italy
E-mail: cassinis@unipv.it

Dr. Boris I. Chuvashov

Institute of Geology and Geochemistry Urals Branch of
Russian Academy of Science
Pochtovy per 7
Ekaterinburg 620154 Russia
E-mail: chuvashov@igg.uran.ru

Prof. Ernst Ya. Leven

Geological Institute
Russian Academy of Sciences
Pyjevskiy 7
Moscow 109017 Russia
E-mail: erleven@yandex.ru

Dr. Galina Kotlyar

All-Russian Geological Research Institute
Sredny pr. 74
St. Petersburg 199206 Russia
E-mail: Galina_Kotlyar@vsegei.ru

Henderson's Harangue #11

Charles M. Henderson

Department of Geoscience, University of Calgary, Calgary,
Alberta, Canada T2N 1N4

Closing the Circle

As an attempt to stimulate debate or perhaps simply because something smells fishy, I deliver my eleventh harangue. In Italian, it would be "L'arringa di Henderson" (the double "r" is important).

As I get closer to the end of my career, a prospect that seems both terrifying and exciting, it is satisfying that at least one idea has come full circle. I defended my PhD dissertation on December 8, 1988 and was excited to relate my discovery of *Sweetognathus whitei* in some rocks called the 'unnamed formations' on Raanes Peninsula of Ellesmere Island. My colleague Benoit Beauchamp and I later named these rocks the Raanes and Great Bear Cape formations and *Sw. whitei* occurred in the lower part of the Great Bear Cape Formation. This became a datum for the base of the Artinskian, which allowed correlation with many other regions including the Ural Mountain succession of Russia. Through the fine research of Mark Schmitz the age of this datum is now known to be 290.1 or 290.5 Ma. I have been fortunate to travel to many interesting places, but perhaps one of the most interesting was a trip to Bolivia. The high elevation of La Paz and Lake Titicaca took by breath away. We later travelled across the Andes and dropped down to increasing levels of oxygen. Here the Apillapampa section with its fossiliferous limestone and interbedded volcanic tuffs would become key to understanding Lower Permian correlations including in the western USA; Henderson and Read in this issue of *Permophiles* show some of these correlation changes. The section will be important to link correlations with Gondwana successions as discussed by a new working group in recent issues of *Permophiles*. Following the tedious task of processing samples I discovered numerous conodonts, many of which belonged to species of *Sweetognathus*, a genus and lineage I thought I understood. At the same time Mark Schmitz was determining at Boise the geochronologic ages of zircons from those tuffs. I remember getting together with him when we both

had results. He asked me "based on your conodonts at this level what age would you like". This seemed like a great opportunity to truly show the power of conodonts! I said "well they display characters that suggest we are near the base-Artinskian with *Sw. whitei* and maybe still in the upper part of Sakmarian with *Sw. binodosus* so I would like something around 290 to 291 Ma". Mark replied "how about closer to 297 Ma". I responded "no, that is not what I would like". Some of these ages have leaked out in publications without calibration documentation, but it is true that Mark and I still have a paper to get out – ideally one that combines his geochronology with my conodont taxonomy. At the time however I wasn't as ready as I had hoped. I needed to find a scientific explanation for this discrepancy. I could suggest that the geochronology was wrong, but Mark had several ages and they followed the correct order. Furthermore, the process that sees uranium become lead is a chemical process with well-known parameters that don't change beyond an ever diminishing level of uncertainty. Chemical sciences, unlike biological sciences, yield predictable and immutable results. Biological sciences, and especially the ancient variety called paleobiology, yield results that are much more subjective and certainly subject to interpretations that differ among specialists. So I pondered this question for a long time. Around the same time, Spencer Lucas asked me to produce a summary chapter on Permian Conodont Biostratigraphy for his book with Shuzhong Shen (The Permian Time Scale; GSL SP 450). I worked on this paper during a time when my wife was recovering from leukemia via a stem-cell transplant – an extraordinary biological/medical advancement. I stepped down in 2015 from my position as Head of the Department of Geoscience at the University of Calgary and was given special leave to assist with her recovery. The recovery was difficult but successful, which brings joy to my heart each day! I spent many late evenings getting lost in the Permian after Elizabeth was asleep – this was my release from the scary world I was living in. A key paper was one by Scott Ritter (1986) who illustrated many forms of *Sweetognathus* from western USA. One of his new species *Sweetognathus inornatus* was much maligned. It was suggested by some that his forms were only juveniles of *Sw. whitei* and therefore a junior synonym of the latter species. Scott also illustrated a variety of morphotypes of *Sw. whitei*. I remember 'focusing' with bleary eyes on those images one night,

as I had many times before, when it suddenly hit me “there are two *Sw. whitei* species – there must be two lineages”. I didn’t get much sleep that evening! It is an insignificant discovery in the history of the world, but it is significant for a few determined Permian workers. I then set about defending my idea with presentations at GSA annual meetings. I told people that Heinz Kozur had suggested to me that there was something different between the holotype from Wyoming and the forms that others, including Valery Chernykh, called *Sw. whitei*, but Heinz didn’t know what it was. In those talks I showed how they differed and even employed a hockey metaphor describing the “blue team and the red team” (USA vs. Russia). I published the 2018 summary paper on Permian Conodont Biostratigraphy, but still there was considerable reluctance to accept this idea. It took a while, but now it is settled, I think. My MSc student Wyatt Petryshen did some mathematical magic to high-resolution 3D scans that demonstrated parallel evolutionary trajectories within at least two lineages of *Sweetognathus* (Petryshen et al., 2020). And, as I had predicted, an ash bed correlated with a level yielding *Sweetognathus whitei* from the uppermost part of the Taiyuan Formation (Gao et al., 2005) in southern North China provided an Asselian age of 295.65 Ma (Yang et al., 2020). It is interesting that the circle was opened and closed by geochronology; geochronology of Bolivian samples forced a rethink and the rethink was proven by geochronology of north China samples. Now when I look at Scott’s paper I think the holotype of *Sw. inornatus* is a senior synonym of *Sw. binodosus*. Hey Scott, do you want to write that paper or perhaps collaborate on that paper? Scott’s paratypes represent other species including *Sw. posterus* (see Beauchamp et al., 2022 and Henderson and Read in this issue).

If you have read recent issues of *Permophiles* and my harangues you will know that the Artinskian “*Sw. whitei*” is now referred to as *Sw. asymmetricus*. You would also know that a GSSP proposal for the base-Artinskian was ratified by IUGS February 1st 2022 and then suspended by IUGS March 1st 2022 because of the Russian-Ukraine war. This also means that we must cease the intended development of the base-Kungurian GSSP at the Mechetlino section in Russia. In another ICS development it was decided to adopt a new stratigraphic concept, the Standard Auxiliary Boundary Stratotype (SABS) to “provide a complementary expression of the boundary interval without the designation of a specific point” (Head et al., 2022). A report on our recent field research (October 2022) in northern Nevada appears elsewhere in this issue of *Permophiles* (see Angiolini et al.). This report points out a plan for the Carlin Canyon succession to become a SABS for the late Asselian to early Artinskian interval including Asselian-Sakmarian and Sakmarian-Artinskian boundaries. The Carlin Canyon section provides a complementary expression of the ratified base-Sakmarian GSSP at Usolka and the suspended base-Artinskian GSSP at Dalny Tulkas. The index fossils are the same and the sedimentary deposits are similar at Carlin Canyon (Beauchamp et al., 2022). The boundaries will be correlated, but it is important to note that a SABS is the boundary interval and not the point. Head et al. (2022) point out that “no such points can replicate the precise level defined by a GSSP either conceptually or in practice”.

There are some researchers who suggest that the GSSP process is flawed because you cannot really define a point that is applicable globally. I would argue that it is easy to define a point in a section – the hard part is getting agreement regarding the correlatability of that point. Once an agreement has been achieved that point defines the boundary only at the GSSP section. Everywhere else we have to correlate the point, which leads to a level of uncertainty, similar to that expressed routinely for geochronologic ages. We do this by doing the science, by employing every stratigraphic tool that we can including isotope geochemistry, magnetostratigraphy, sequence stratigraphy, and biostratigraphy of multiple fossil groups. Quantitative biostratigraphic techniques like Unitary Associations cannot be used to correlate a point because they define intervals, however Unitary Associations could be applicable to correlating a SABS boundary interval. In my view, the best aspect of the GSSP process is that it provides us with a goal. A GSSP or SABS decision allows us to test correlation in other sections – it allows us to continue to do the science to complete the goal - an International Geologic Time Scale so that we can better understand the history of this planet.

So some of you might (or not) be saying “that is a nice story, but where is the harangue”. The harangue is that I think it was a little too hard to convince my colleagues that the first occurrences of *Sweetognathus whitei* and *Sweetognathus asymmetricus* were separated by 5 million years. Some are reluctant to change previously established correlations. But a lot can happen in 5 million years – we need no better demonstration than to consider all of the events of the past 2.58 million years with multiple glacial and interglacial ages during the Pleistocene and Holocene. In order to truly close this circle we need to better understand these five million years because they do involve some major events of the late Paleozoic Ice Age. Are the correlations correct? What are the ages of loess deposits? How has the biostratigraphy of insects within this interval been correlated with the marine record? Does this affect the constraints on climate modeling for this interval? Have we done the science as well as possible?

References

- Beauchamp, B., Henderson, C.M., Dehari, E., Waldbott von Bassenheim, D., Elliot, S. and Calvo Gonzalez, D., 2022. Carbonate Sedimentology and Conodont Biostratigraphy of Late Pennsylvanian-Early Permian stratigraphic sequences, Carlin Canyon, Nevada: new insights into the tectonic and oceanographic significance of an iconic succession of the Basin and Range. In Henderson, C.M., Ritter, S. and Snyder, W.S. (eds.), Late Paleozoic and Early Mesozoic Tectonostratigraphy and Biostratigraphy of western Pangea, Special Publication 113: SEPM (Society for Sedimentary Geology), Broken Arrow, Oklahoma, p. 34–71.
- Gao, F., Ding, H. and Wan, X., 2005. Taxonomic revision of conodont *Sweetognathus* species in the uppermost Taiyuan Formation, Yuhuai Basin and its significance. *Acta Micropalaeontologica Sinica*, v. 22, n. 4, p. 370–382 (in Chinese with English abstract).
- Head, M.J., Aubry, M.P., Piller, W.E., and Walker, M., 2022. The Standard Auxiliary Boundary Stratotype: a proposed replacement for the Auxiliary Stratotype Point in supporting

- a Global boundary Stratotype Section and Point (GSSP). Episodes, online doi:10.18814/epiugs/2022/022012.
- Henderson, C.M., 2018. Permian conodont biostratigraphy. In Lucas, S.G. and Shen S.Z. (eds.), The Permian Timescale. Geological Society, London, Special Publication, v. 450, p. 119–142.
- Petryshen, W., Henderson, C.M., de Baets, K. and Jarochowska, E., 2020. Evidence of parallel evolution in the dental elements of *Sweetognathus* conodonts. Proceedings of the Royal Society B, v. 287, 20201922.
- Ritter, S. M., 1986. Taxonomic revision and phylogeny of post-early crisis *bisselli-whitei* Zone conodonts with comments on Late Paleozoic diversity. Geologica et Palaeontologica, v. 20, p. 139–165.
- Yang, J.H., Cawood, P.A., Montanez, I.P., Condon, D.J., Du, Y.S., Yan, J.X., Yan, S.Q., and Yuan, D.X., 2020, Enhanced continental weathering and large igneous province induced climate warming at the Permo-Carboniferous transition. Earth and Planetary Science Letters, v. 534, 116074.

Redefinition of the Global Stratotype Section and Point (GSSP) and new Standard Auxiliary Boundary Stratotype (SABS) for the base of Wuchiapingian Stage (Lopingian Series, Permian) in South China

Shu-zhong Shen*

State Key Laboratory for Mineral Deposits Research, School of Earth Sciences and Engineering and Frontiers Science Center for Critical Earth Material Cycling, Nanjing University, Nanjing 210023, China. Corresponding author
E-mail: szshen@nju.edu.cn

Dong-xun Yuan

School of Resources and Geosciences, China University of Mining and Technology, Xuzhou 221116, China

Yi-chun Zhang

State Key Laboratory of Palaeobiology and Stratigraphy, Nanjing Institute of Geology and Palaeontology, Chinese Academy of Sciences, Nanjing 210008, China

Charles, M. Henderson

Department of Geoscience, University of Calgary, Calgary, AB T2N 1N4, Canada

Quan-feng Zheng, Hua Zhang

State Key Laboratory of Palaeobiology and Stratigraphy, Nanjing Institute of Geology and Palaeontology, Chinese Academy of Sciences, Nanjing 210008, China

Min Zhang

Chinese Academy of Sciences (CAS) Key Laboratory of Earth

and Planetary Physics, Institute of Geology and Geophysics, Chinese Academy of Sciences, Beijing 100029, China

Yu Dai

Guangxi Institute of Regional Geological Survey, 6 Huanchengnaner Road, Guilin, Guangxi 541003, China

Hai-peng Xu, Wen-qian Wang

State Key Laboratory for Mineral Deposits Research, School of Earth Sciences and Engineering and Frontiers Science Center for Critical Earth Material Cycling, Nanjing University, Nanjing 210023, China

Qian Li

Guangxi Institute of Regional Geological Survey, 6 Huanchengnaner Road, Guilin, Guangxi 541003, China

Yue Wang

State Key Laboratory of Palaeobiology and Stratigraphy, Nanjing Institute of Geology and Palaeontology, Chinese Academy of Sciences, Nanjing 210008, China

Xiang-dong Wang

State Key Laboratory for Mineral Deposits Research, School of Earth Sciences and Engineering and Frontiers Science Center for Critical Earth Material Cycling, Nanjing University, Nanjing 210023, China

Jahandar Ramezani

Department of Earth, Atmospheric and Planetary Sciences, Massachusetts Institute of Technology, Cambridge, MA 02139, USA

Douglas H. Erwin

Department of Paleobiology, MRC-121, National Museum of Natural History, Washington, D.C. 20013-7012, USA

Lucia Angiolini

Dipartimento di Scienze della Terra “Ardito Desio”, Università degli Studi di Milano, Via Mangiagalli 34, I-20133 Milano

Fei-fei Zhang, Zhang-shuai Hou

State Key Laboratory for Mineral Deposits Research, School of Earth Sciences and Engineering and Frontiers Science Center for Critical Earth Material Cycling, Nanjing University, Nanjing 210023, China

Xi-yang Zhang

Key Laboratory of Ocean and Marginal Sea Geology, South China Sea, Institute of Oceanology, Innovation Academy of South China Sea Ecology and Environmental Engineering, Chinese Academy of Sciences, Guangzhou 510301, Guangdong Province, China

Shu-han Zhang

State Key Laboratory for Mineral Deposits Research, School of Earth Sciences and Engineering and Frontiers Science Center for Critical Earth Material Cycling, Nanjing University, Nanjing 210023, China

Yong-xin Pan

Chinese Academy of Sciences (CAS) Key Laboratory of Earth and Planetary Physics, Institute of Geology and Geophysics, Chinese Academy of Sciences, Beijing 100029, China

Michael Stephenson

British Geological Survey, Keyworth, Nottingham NG12 5GG, UK

Shi-long Mei

Alberta Geological Survey, 98 Avenue Edmonton, Alberta Canada T6B 2X3

Abstract

The Global Stratotype Section and Point (GSSP) of the Guadalupian/Lopingian (also the Capitanian/Wuchiapingian) boundary (GLB) was formally ratified at the Penglaitan section in the Laibin area, Guangxi Province in South China in 2005. However, the riverside GSSP section at Penglaitan and its auxiliary section at Tieqiao have been permanently flooded since 2020 due to a hydroelectric dam built 80 km downstream. Thus, the original stratotype point at Penglaitan no longer satisfies the requirements of a GSSP due to inaccessibility. In order to solve this issue, we excavated a new section along the bank of Hongshui River at a place ~10 m higher than the original GSSP at Penglaitan. Since the new section is short and still flooded in much of the year, we herein propose the Fengshan section near the Liuzhou City of Guangxi Province as a new Standard Auxiliary Boundary Stratotype (SABS) to support the GSSP for the base of the Wuchiapingian Stage. The new section at Penglaitan confirmed the conodont succession of the *Jinogondolella granti*, *Clarkina postbitteri* and *C. dukouensis* zones in ascending order. The Fengshan section also contains an excellent conodont succession from the *Jinogondolella prexuanhanensis* Zone in the upper Capitanian to the *Clarkina guangyuanensis* Zone in the lower Wuchiapingian, which is completely comparable with that of the Penglaitan section. Based on a restudy of the new stratotype section at Penglaitan and the SABS at Fengshan, we found that the evolution from *Jinogondolella granti* to *Clarkina postbitteri* is a continuum as transitional forms between these two species, mostly identified as *C. postbitteri hongshuiensis*, are present in both sections. The two subspecies of *C. postbitteri* (*C. postbitteri hongshuiensis* and *C. postbitteri postbitteri*) - on which the GLB was previously defined - were not resolved with our new samples so it was decided to refer key taxa to transitional specimens and *C. postbitteri*. The revised GSSP is moved laterally and defined at the base of Bed n6L in the newly exposed Penglaitan section. This point can be recognized and correlated at the new section by the first appearance datum (FAD) of the conodont *C. postbitteri* sensu lato within the lineage

Jinogondolella granti → *Clarkina postbitteri* → *C. dukouensis*. This point may be slightly lower (10-20 cm) from the previous GSSP level because of the irregular bedding surfaces and broader taxonomic identification of *C. postbitteri*. This level correlates to a level 30cm below the top of Unit 26 at the Fengshan section, which is proposed as a Standard Auxiliary Boundary Stratotype. It represents a major evolutionary turnover in conodont faunas from *Jinogondolella* to *Clarkina* and marks the end-Guadalupian extinction event which can be well recognized and correlated globally. At present, the previously published U-Pb date of 259.51 ± 0.21 Ma from a volcanic tuff from the uppermost part of the Emeishan basalts in Guizhou is adopted for the GLB age. Carbonate $\delta^{13}C_{carb}$ chemostratigraphy of the GLB interval at the Fengshan section exhibits a different trend from that of other sections, but several large excursions between 3 and 5‰ are present across the interval. Carbonate $^{87}Sr/^{86}Sr$ ratio is 0.707244 at the GLB, which is higher than what marks the beginning of the rising trend after the Capitanian minimum 0.707069, probably due to some diagenetic effects. Remarkably, the Fengshan section contains six normal and six reverse geomagnetic polarity zones in the uppermost Capitanian and three in the lowest Wuchiapingian.

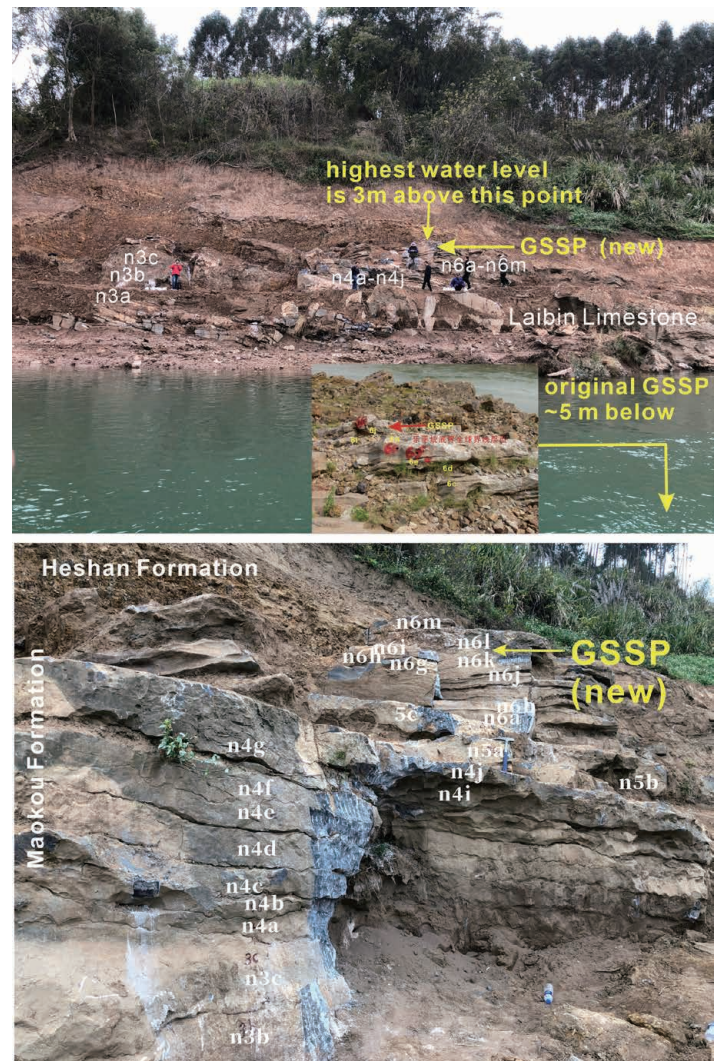


Fig. 1. Photos showing the normal water level of the Hongshui River and the new section with the newly defined GSSP. All bed numbers are prefixed with "n" to differentiate from those of the original GSSP section under water.

1. Introduction

The Lopingian Epoch is the last epoch of the Permian Period of the Paleozoic Era and has been widely documented as one of the most critical intervals in terms of biological and geological evolution of the Earth (Erwin, 2006). The base of the Lopingian Series (also the top of the Guadalupian) recorded one of the largest marine regressions of the Phanerozoic (Haq and Schutter, 2008). Massive volcanism associated with the Emeishan igneous province (He et al., 2007; Chen and Xu, 2019) and a pre-Lopingian biotic crisis (Jin, 1993; Jin et al., 1994) or end-Guadalupian mass extinction (Stanley and Yang, 1994; Shen and Shi, 2009; Wignall et al., 2009) characterize this boundary, although the magnitude of this extinction has been downgraded recently (Clapham et al., 2009; Fan et al., 2020; Shen et al., 2020). The Global Stratotype Section and Point (GSSP) was originally defined by the first appearance datum (FAD) of the conodont *Clarkina postbitteri postbitteri* within the lineage *Jinodondolella granti* → *Clarkina postbitteri hongshuiensis* → *C. postbitteri postbitteri* → *C. dukouensis* at the base of Bed 6k of the Penglaitan section in the Laibin area of Guangxi Province (Jin et al., 2006). This base-Lopingian GSSP was formally ratified on September 3, 2005 by the International Commission on Stratigraphy (ICS) of the International Union of Geological Sciences (IUGS). It has been well protected by the local Laibin

Government of Guangxi Province and two monuments were established after the GSSP was formally ratified.

The GSSP section (23°41'43", 109°19'16") (Fig. 1A) outcropped along the southern bank of the Hongshui River at Penglaitan, about 13 km southeast to the Laibin City in Guangxi and was easily accessible in most seasons of the year except during the summer flooding. The Hongshui River is one of the main tributaries of the Pearl River in the Guangxi Province of South China. A dam and a hydro power station for protecting tens of millions of people from periodic flooding and for generating electricity was constructed 80 km downstream from the GSSP section during the past six years. Filling the dam reservoir elevated the water level in the Hongshui River by ~15 m and caused both the Penglaitan GSSP section and its auxiliary Tieqiao section near the Laibin City to be submerged permanently since 2020.

In order to remedy the accessibility problem, an international team was organized six years ago to work on the base-Lopingian GSSP and searching for a replacement section. On the one hand, two boreholes were drilled intersecting the middle Wuchiapingian to the middle Guadalupian at the Penglaitan section and a square metre trench at the original GSSP section was cut. The rock slice across the main GLB interval, which is about 50 m long, has been moved to a storage museum on the Penglai Islet near the Penglaitan section. On the other hand, the team searched for a

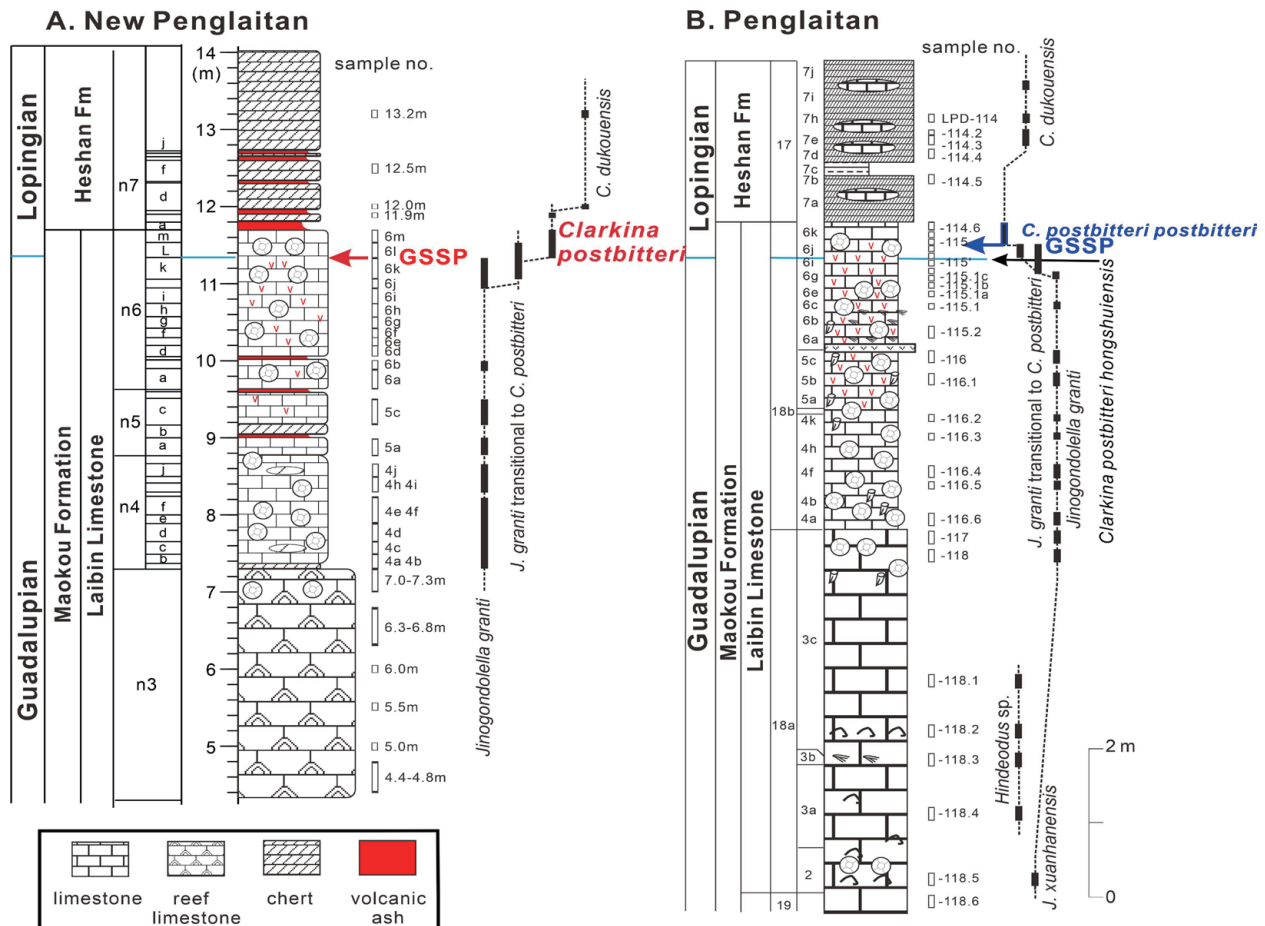


Fig. 2. Correlation of conodont ranges across the Guadalupian-Lopingian boundary interval between the original and new Penglaitan sections. A, new GSSP section; B, original GSSP section (after Jin et al., 2006)

new replacement section for the Penglaitan GSSP section since the dam had been planned a decade earlier. In this paper, we provide a detailed report for the new section at Penglaitan for the GSSP and document a Standard Auxiliary Boundary Stratotype (SABS) (Head et al., 2022) for the base of the Wuchiapingian Stage (also the base of the Lopingian Series) at Fengshan, Liuzhou City in Guangxi, South China. We call for discussions for the redefined GSSP section and SABS proposed in this paper.

2. New GSSP section and revised definition for the Guadalupian/Lopingian boundary at Penglaitan

2.1. New section at Penglaitan

The river banks at Penglaitan were heavily covered by quaternary alluvium and vegetation before the GSSP was flooded. In order to explore the presence of additional GLB strata beneath the surface, we excavated the river bank in a place about 10 m above the original GSSP. An excellent short section with the GLB interval was found (Figs. 1, 2). The new outcrop contains the stratigraphic interval from Units 2-6 of the Laibin Limestone of the uppermost Maokou Formation to the lowest part of Unit 7 of the basal Heshan Formation. Large samples for conodonts were collected repeatedly from the Laibin Limestone and basal part of the Heshan Formation. The Laibin Limestone at the new section is mainly composed of massive crinoid limestone, and bedding planes are hard to be traced laterally from the original GSSP point. This might be related to differential weathering. Our studies indicate that Bed n6k contains some specimens of *Jinogondolella granti* (Figs. 3.1, 3.2) and the Bed n6L to Bed n6m contains *Clarkina postbitteri* and transitional forms between *Jinogondolella granti* and *Clarkina postbitteri*, which are more or less comparable with *C. postbitteri hongshuiensis* (e.g., Figs. 3.9-3.19). The population contains transitional forms from the morphotypes with relatively straight platform, obtusely pointed posterior margin, relatively low blade and discrete denticles on the blade (e.g., Figs. 3.11-13, 16) and the other morphotype with a wide and slightly anteriorly arched platform with a high blade and fused denticles (e.g., Figs. 3.10, 3.17-19). The former morphotype is relatively small or immature, therefore, possesses some characters succeeded from *Jinogondolella granti*; the later morphotype is relatively large and has more characters of *Clarkina postbitteri*. Thus, the lineage from *Jinogondolella granti*→*Clarkina postbitteri*→*C. dukouensis* is recovered at the new GSSP section in association with transitional forms between *Jinogondolella granti* and *Clarkina postbitteri*. The original GSSP was recognized and correlated by the FAD of the conodont *C. postbitteri postbitteri* within the lineage *Jinogondolella granti*→*Clarkina postbitteri hongshuiensis*→*C. postbitteri postbitteri*→*C. dukouensis* (Jin et al., 2006). However, transitional forms existed in the topmost part of *Jinogondolella granti* Zone and throughout the *Clarkina postbitteri* Zone, and the two subspecies could not be resolved stratigraphically at the new section in terms of sample population approach, which is about 10 m higher topographically than the original GSSP (Fig. 1). We leave this issue for another conodont paper to discuss. The new section is still flooded during much of the year. We therefore recommend that the GSSP for the base of the Wuchiapingian Stage is to be maintained at Penglaitan and propose the

Fengshan section as a SABS for the base of the Lopingian (also Wuchiapingian). The new GSSP section at Penglaitan and the SABS section at Fengshan are described in Appendices 1 and 2 respectively, and will be practically used for future studies of the GLB.

2.2. Revised definition of the Guadalupian-Lopingian boundary

The base-Lopingian GSSP at Penglaitan was defined at a point at the base of Bed 6k of the Laibin Limestone, which was deposited during a major lowstand associated with a widespread regression recognizable globally (Jin et al., 2006; Yuan et al., 2017). Based on the discussions above, we suggest that this GSSP is slightly modified to correspond to the base of Bed n6L at the new section at Penglaitan which can be recognized and correlated by the FAD of *Clarkina postbitteri* within the lineage *Jinogondolella granti*→*Clarkina postbitteri*→*C. dukouensis* (Figs. 1, 2) (Jin et al., 2001b). In South China, a widespread unconformity caused by the Dongwu uplift at the GLB (Hu, 1994; Hou et al., 2020) is present and marked by the Wangpo Shale and is commonly associated with a reddish limonite bed. Continuous GLB intervals with complete conodont succession are very rare and have only been documented from the Penglaitan and Tieqiao sections in the Laibin area, and the Fengshan section in the Liuzhou area of Guangxi, the Douling area in Chenzhou, Hunan Province (Mei et al., 1994b, 1998; Shen and Zhang, 2008). Therefore, there was considerable debate regarding the conodont lineage and the definition for the GLB (Jin, 2000; Wang, 2000, 2001; Jin et al., 2001a; Kozur and Wang, 2002; Henderson et al., 2002; Wardlaw and Henderson, 2002). Jin et al. (2001b) proposed two positions for the base-Lopingian GSSP: Option A was the lowest occurrence of the conodont *C. postbitteri* in Bed 6i upper; and Option B was the lowest occurrence of *C. dukouensis* at Bed 7e at the Penglaitan section (Fig. 2B). Option A is excellent as it represents the FAD of the conodont genus *Clarkina* globally and it has been proven that this position represents a major evolutionary changeover and the end-Guadalupian mass extinction level within the conodont lineage from the Guadalupian *Jinogondolella* to the Lopingian *Clarkina* (Henderson et al., 2002). However, this position was previously opposed by some conodont specialists who raised the questions about the ancestor of *C. postbitteri* and whether or not there is a small gap or diastem (at the bedding plane) between Beds 6i lower and 6i upper because no transitional morphotypes between *Jinogondolella granti* and its successive species *Clarkina postbitteri* were found at Penglaitan (Wang, 2000, 2001; Kozur and Wang, 2002). As a result, two subspecies of *C. postbitteri*, *C. postbitteri hongshuiensis* and *C. postbitteri postbitteri*, were separated and described (Henderson et al., 2002). The base-Lopingian GSSP was largely defined at a transitional interval between *Jinogondolella granti* and *Clarkina postbitteri* using the FAD of the conodont *C. postbitteri postbitteri* within the lineage *Jinogondolella granti*→*Clarkina postbitteri hongshuiensis*→*C. postbitteri postbitteri*→*C. dukouensis* (Henderson et al., 2002; Jin et al., 2006), but was actually recognized and correlated by the FAD of *Clarkina postbitteri* (s.l.).

Since the two subspecies to define the base-Lopingian GSSP

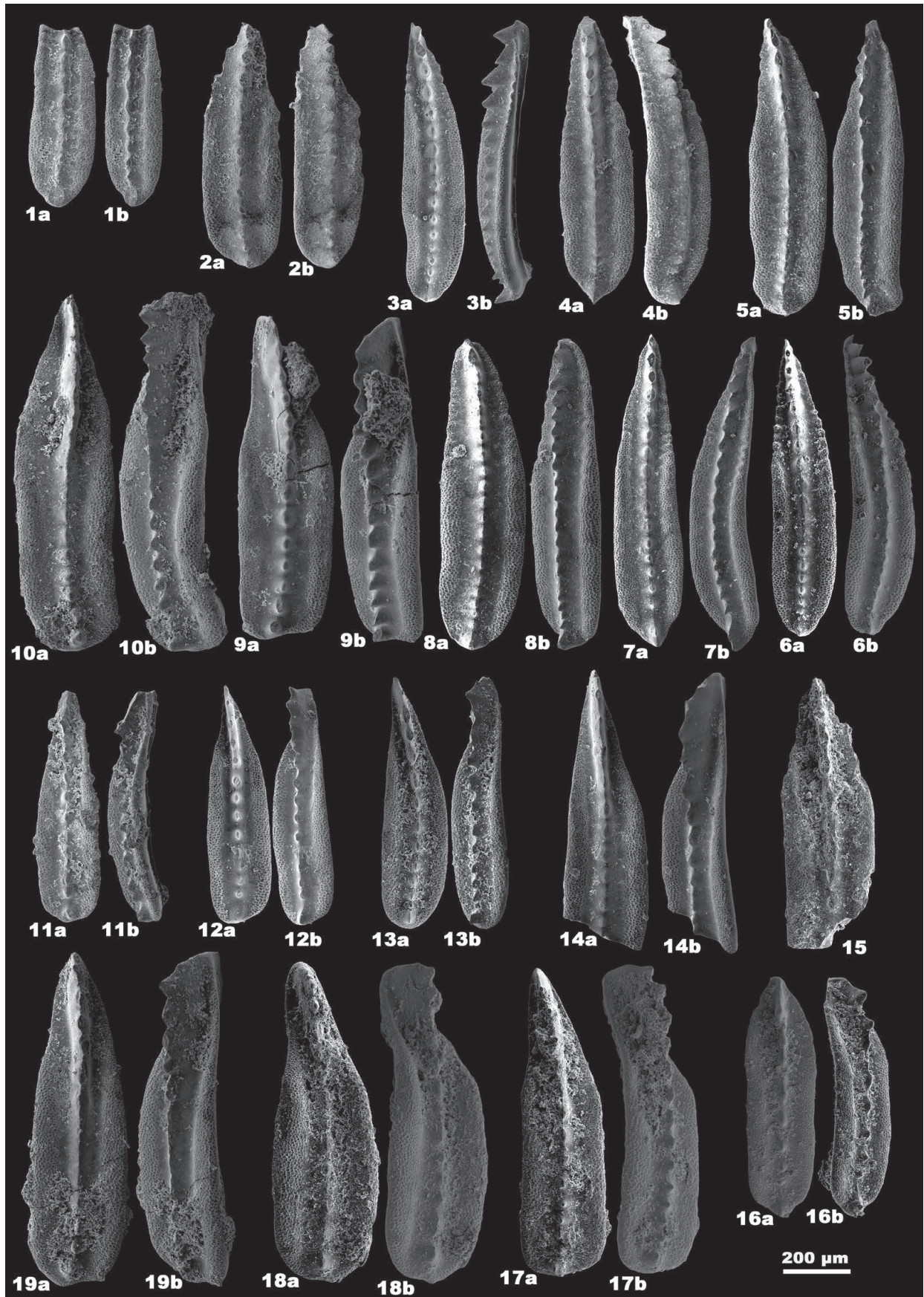


Fig. 3. Key conodonts from the new GSSP section at Penglaitan. 1-8. *Jinogondolella granti*, 1, 2 from Sample n6k, 3, 4, 6-8 from Sample n5a, 5 from Sample n6j; 9-19. *Clarkina postbitteri*, 9-14, 19 from Sample n6m, 15-18 from Sample n6L-n6m.

cannot be resolved in stratigraphic order in the new Penglaitan section, we herein revert to the first definition of Jin et al. (2001b) and propose that the GSSP to be defined by the FAD of *Clarkina postbitteri* at the base of Bed n6L at the new Penglaitan section ("n" is prefixed for all bed numbers of the new section to differentiate from the original GSSP bed numbers). The main reasons for this modification are as follows: 1) The modified definition represents a turning point in the evolutionary change of the Permian conodonts from the Guadalupian *Jinogondolella* to the Lopingian *Clarkina* and the end-Guadalupian mass extinction interval, and the FAD of *C. postbitteri* has been practically used for identifying the GLB since the GSSP was formally defined. The two subspecies of *C. postbitteri* (*C. postbitteri hongshuiensis* and *C. postbitteri postbitteri*) are more or less transitional (Henderson et al., 2002; Jin et al., 2006). In addition, undisputed specimens of *C. postbitteri hongshuiensis* have rarely been found elsewhere outside Penglaitan. Although *C. postbitteri hongshuiensis* has been reported from West Texas (Lambert et al., 2002), Panthalassa (Nishikane et al., 2011), South China (Sun and Xia, 2006; Zhang et al., 2008) and Oman (Baud et al., 2012), most of those records have since been revised and included in other species (Yuan et al., 2017; Shen et al., 2020). 2) *Clarkina postbitteri* coexists with *Jinogondolella granti* in the lower part of the *Clarkina postbitteri* Zone at both the Fengshan (see below) and the new Penglaitan sections. Some transitional forms with a relatively narrow platform and nearly parallel lateral margins between *Jinogondolella granti* and *Clarkina postbitteri postbitteri* exist in the *C. postbitteri* population at the new Penglaitan section (Figs. 3.9-3.19) (e.g., Yuan et al., 2017, figs. 4.10, 4.11). Thus, based on the stratigraphy and conodont successions (Henderson et al., 2002), the clear ancestor of *C. postbitteri* is determined to be *Jinogondolella granti* at the Penglaitan sections in South China (Henderson et al., 2002; Jin et al., 2006; Yuan et al., 2017) and the ancestor-based objection to the usage of *Clarkina postbitteri* is no longer valid. The base-Lopingian GSSP at Penglaitan was ratified nearly two decades ago and so far, there has been no record of *C. postbitteri* having any other lineages. 3) The FAD of *C. postbitteri* occurs at a major sequence boundary at a lowstand representing a significant global and mass extinction interval at the end of the Guadalupian, therefore, it can be widely applied to different regions (Mei et al., 1999; Mei and Henderson, 2001; Shen and Shi, 2009). 4) The interval represented by the entire *C. postbitteri* Zone is narrow (less than 1 m) and a further separation of the two subspecies is difficult both taxonomically and stratigraphically everywhere else in the world.

2.3. Geochronology for the Guadalupian/Lopingian boundary

Tuffaceous beds have been documented from the bioclastic limestones of the GLB interval at the Penglaitan GSSP (e.g., Jin et al., 2001b; Jin et al., 2006). Zhong et al. (2013) studied six of these beds and concluded that they were claystones of clastic origin, as opposed to volcanic ash beds, and not suitable for geochronology. Their conclusions were based on a) mineralogy and bulk geochemistry of the rocks suggesting a clastic origin from both mafic and felsic provenances and, b) analyses of separated zircons by the LA-ICPMS (microbeam) technique showing a wide range of U-Pb ages indicative of detrital zircon.

Nevertheless, three of the analyzed samples yielded major peaks in their zircon ages at ~260 Ma to ~269 Ma, which considering the large uncertainties of the analytical technique (average of ± 5 Myr), tend to fall within the expected age range of the upper Guadalupian and lower Lopingian. Therefore, the possibility of acquiring meaningful depositional ages by careful zircon screening and suitable analytical methods must not be ruled out. In the newly excavated section at Penglaitan, more pronounced and well-bedded 'ash beds' have been found (Fig. 2). Samples from these beds have been collected for high-precision U-Pb geochronology by the chemical abrasion thermal ionization mass spectrometry (CA-ID-TIMS) method to be carried out at MIT.

In the absence of radioisotopic age data directly tied to the GLB marine biostratigraphy at any location, geochronology from the Emeishan large igneous province and associated volcanic rocks in Southwest China and northern Vietnam have been used as a proxy for the GLB age. With the rare exception of direct $^{40}\text{Ar}/^{39}\text{Ar}$ geochronology from basalts (Li et al., 2018), the majority of high-precision age constraints on Emeishan come from U-Pb zircon geochronology of intrusive rocks (Shellnutt et al., 2012), interlayered ignimbrites (Zhong et al., 2014), overlying rhyolites (Shellnutt et al., 2020; Huang et al., 2022) and basalt in situ paleosol horizons (red boles, Huang et al., 2022). Tuff beds from sedimentary succession above and below the Emeishan basalts have also yielded U-Pb zircon ages (Yang et al., 2018), which place maximum and minimum age limits on the Emeishan magmatism. The bulk of reported CA-ID-TIMS geochronology constrains the Emeishan magmatism in between 259.69 ± 0.72 Ma (Ji et al., 2009) and 256.91 ± 0.77 Ma (Huang et al., 2022).

The age of GLB was initially estimated at ~259.1 Ma by Shen et al. (2010). Later, the CA-ID-TIMS U-Pb age of 259.51 ± 0.21 Ma from the uppermost tuff of the Puan volcanic sequence in the eastern Emeishan large igneous province by Yang et al. (2018) was considered the best age estimate for the GLB (Ramezani and Bowring, 2018; Shen et al., 2020; Wu et al., 2020). The latter has been adopted for the age of the GLB in the latest international Permian Timescale (Shen et al., 2020), pending direct geochronology from the new Penglaitan section

3. A proposal for the Fengshan section as a Standard Auxiliary Boundary Stratotype (SABS)

Since the new Penglaitan section for the GSSP is short and flooded during much of the year, we herein propose the Fengshan section as a Standard Auxiliary Boundary Stratotype to support the GSSP of the base of the Wuchiapingian (also the base of the Lopingian Series).

3.1. Location and general stratigraphy of the Fengshan section

In addition to the excavation of the river bank at Penglaitan, other potential replacement and auxiliary sections have been intensively searched for during the last six years. The Fengshan section located in a low mountain area (GPS: $24^{\circ}31'05''$, $109^{\circ}17'01''$) near Fengshan Town has been extensively studied (Fig. 4A). This section is 30 km northwest to Liuzhou City and 93.3 km north to the Penglaitan GSSP section (Fig. 4). Liuzhou City is the largest industrial city of Guangxi Province. The

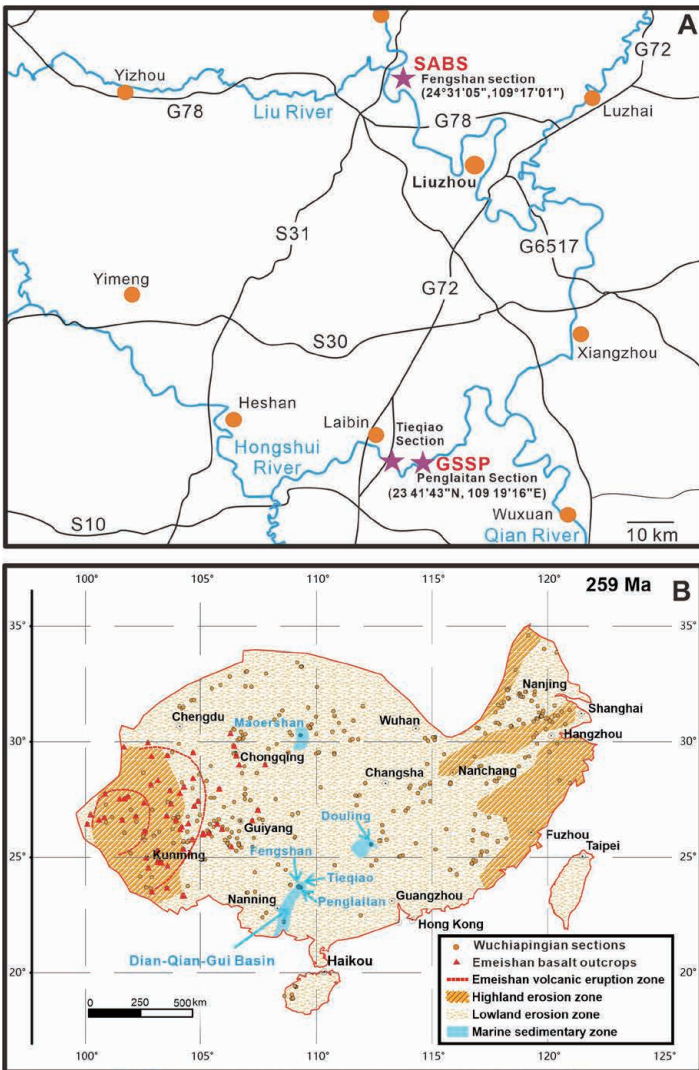


Fig. 4. Map of Guangxi Province, South China showing the studied sections (A) and paleoenvironmental reconstruction map of the South China block during the Guadalupian/Lopingian boundary (after Hou et al., 2020) showing the locations of the Penglaitan, Tieqiao and Fengshan sections (B).

Sanyuan Expressway passes by the Fengshan Town with multiple exits. A simple highway is available from the Fengshan Town to the section. Conodont samples were collected previously to study the base-Lopingian GSSP at the Fengshan section and the conodont *Clarkina postbitteri* was briefly reported (Mei et al., 1994b, 1998).

The Permian strata are well developed in the Fengshan area and mainly distributed in the Fengshan syncline with the central part of Lower Cretaceous purple sandy mudstone containing gypsum deposits (Fig. 5). The Permian System is fully comparable with that in the Laibin area. It comprises the Mapping, Chihhsia, Maokou, Heshan and Talung formations in ascending order. The Mapping Formation is composed of pale thick-bedded limestone containing abundant fusulines, and ranges from the Bashkirian (Carboniferous) to late Sakmarian or early Artinskian (Shen et al., 2019). The Chihhsia Formation is composed of a coal-bearing Liangshan Member in the basal part and a main dark thick-bedded limestone member with chert nodules. The main limestone member of the Chihhsia Formation contains

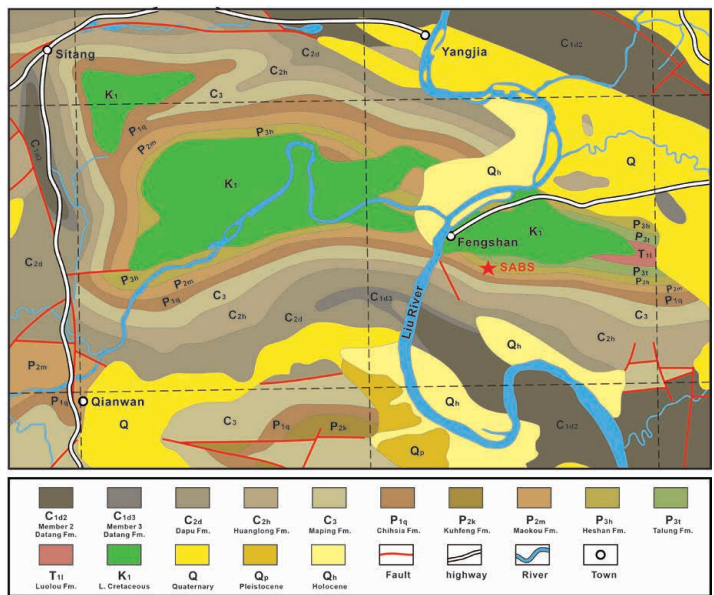


Fig. 5. Geological map showing the distribution of Permian strata and the location of the SABS in the Fengshan area.

abundant fusulines, rugose corals and brachiopods and mainly represents the Kungurian in South China. This formation is the most widely distributed Permian limestone basically covering the entire South China Block and it contains the same marine faunas. The overlying Maokou Formation represents the Guadalupian Series in South China and it mainly consists of pale thick-bedded limestone containing abundant fusulines and conodonts. This formation is conformably overlain by the thin- to medium-bedded dark limestone with cherty nodules of the Heshan Formation, which is occasionally interbedded with coal beds in the studied area (Figs. 5, 6). The Guadalupian-Lopingian transition is continuous because the Fengshan section was situated in the Dian-Qian-Gui basin during the end-Guadalupian lowstand (Fig. 4B). The Heshan Formation is generally equivalent to the Wuchiaping Formation of carbonate facies and the Lungtan Formation of the coal-bearing clastic facies in South China. The uppermost Talung Formation is mainly composed of thin-bedded fragile siliceous rocks and volcanogenic tuffaceous sandstones containing abundant ammonoids, which is mostly equivalent to the Changhsing Formation of carbonate facies in South China.

3.2. Biostratigraphy of the Fengshan section

The Fengshan section contains abundant conodonts, fusulines, brachiopods and crinoid fragments. Rare bryozoans and rugose corals have been also observed (Fig. 7).

3.2.1. Conodont zonation

Conodonts from the GLB interval at both Penglaitan and Fengshan are dominated by *Jinogondolella* in the Guadalupian and *Clarkina* in the Lopingian. Transitional morphotypes between *Jinogondolella* and *Clarkina* are present in the topmost part of the Laibin Limestone of the Maokou Formation. *Sweetognathus fengshanensis*, *Iranognathus* sp. and *Hindeodus* sp. have been commonly found. *Clarkina postbitteri* as the marker of the boundary interval from the Fengshan section has been reported in the top 0.55 m of Bed 18 of Mei et al. (1994b) and Mei et al.

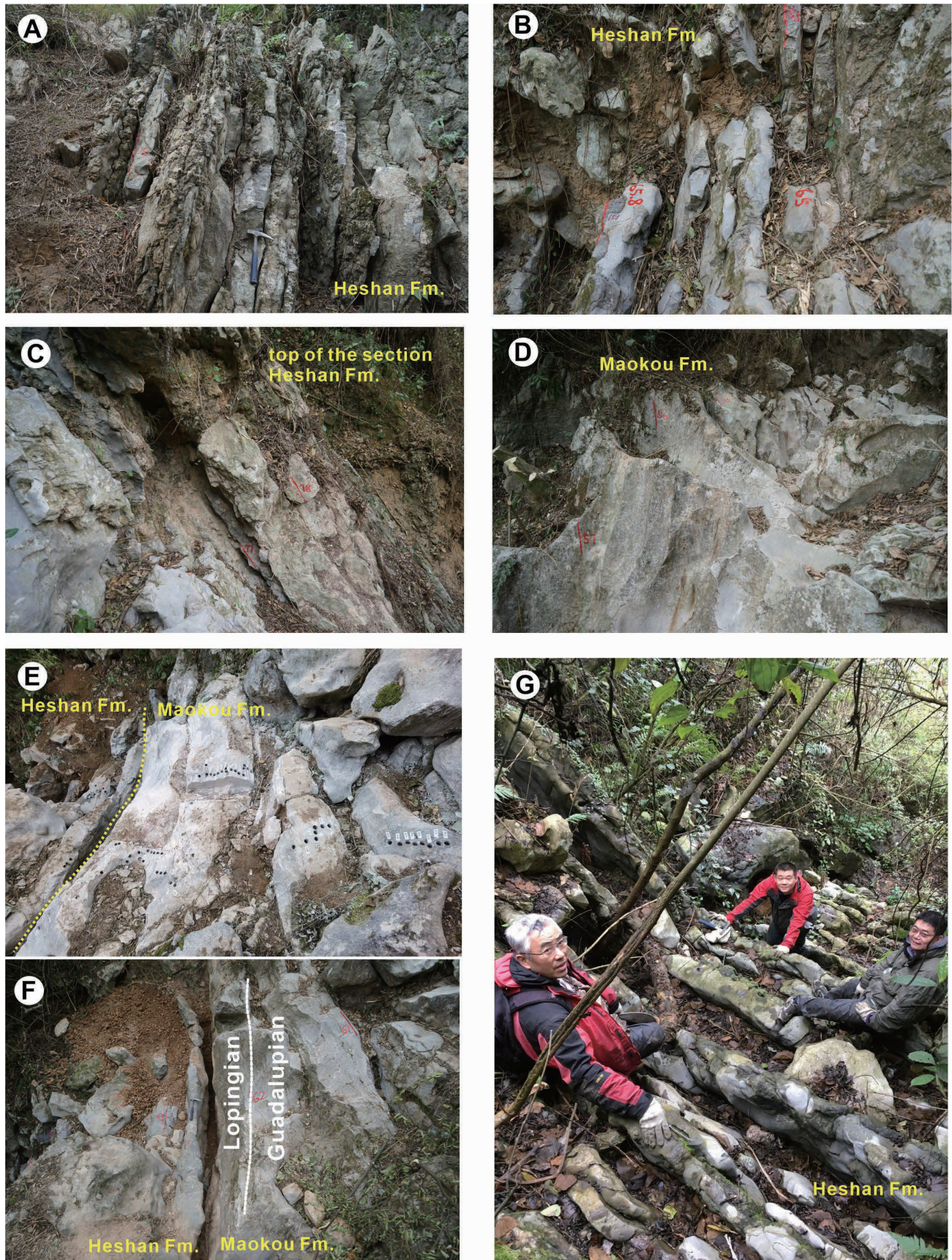


Fig. 6. Outcrops of the Fengshan section (SABS) showing the lithology of the Maokou and Heshan formations. A, B, C. Heshan Formation at the upper part of the section. D. massive limestone of the Maokou Formation. E, F. the lithologic boundary between the Maokou and the Heshan formations and the Guadalupian/Lopingian boundary at the SABS. G. the basal part of the Heshan Formation.

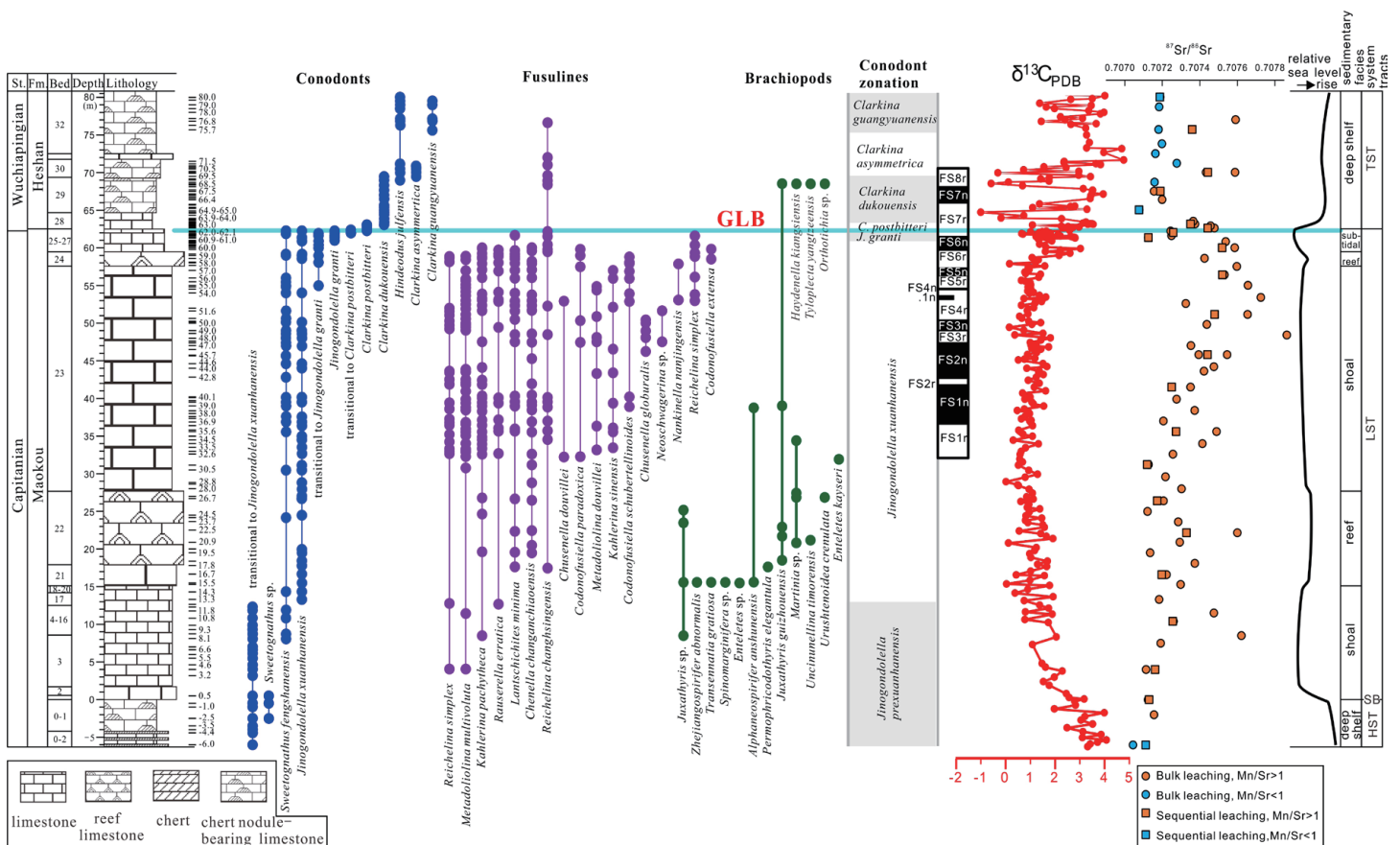


Fig. 7. Stratigraphic range chart of conodont, fusuline and brachiopod fossils and $\delta^{13}C_{carb}$ and $^{87}Sr/^{86}Sr$ ratio profile of the Fengshan section (SABS)

(1998). The complete conodont succession used for defining the base-Lopingian GSSP at Penglaitan can be found in the Fengshan section as well (Figs. 7-9).

Jinogondolella prexuanhanensis Zone (-6 m – 13.3 m): This zone is not fully revealed at the measured section (Unit 0-2 to a part of Unit 17) and starts by the first occurrence of the zonal species. All the specimens are basically transitional morphotypes from *J. prexuanhanensis* to *J. xuanhanensis*. *Sweetognathus fengshanensis* is rarely found in this zone (Figs. 7, 10).

Jinogondolella xuanhanensis Zone (13.3 m – 61 m): This zone is dominated by the zonal species only, but many of the specimens are fragmentary. *Sweetognathus fengshanensis* can be found commonly in the zone. Transitional morphotypes from *Jinogondolella prexuanhanensis* to *J. xuanhanensis* are observed from the underlying 13.3 m. In the upper part of the zone, transitional morphotypes from *J. xuanhanensis* to *J. granti* are found between Units 23-24 (27.7 m – 59.5 m). This zone has been widely reported from the Penglaitan section and many other sections in the world (Mei et al., 1998; Wardlaw, 2000; Lambert et al., 2002; Zhang et al., 2008) (Figs. 7, 10).

Jinogondolella granti Zone (61.0 m – 62.0 m): This zone is found from Unit 25 and the most part of Unit 26 (61 m-62 m) at the Fengshan section. *J. xuanhanensis* and transitional morphotypes from *J. xuanhanensis* to *J. granti* are also commonly found in this zone. *J. granti* ranges into the overlying *Clarkina postbitteri* Zone. Several *Sweetognathus fengshanensis* and *Hindeodus* sp. are also present in this zone (Figs. 7, 11).

Clarkina postbitteri Zone (62.0 m – 63.05 m). This zone ranges across the lithologic boundary between the uppermost part (Unit 26) of the Maokou Formation and the basal part (Unit 27 and Unit 28) of the Heshan Formation. It is marked by the first occurrence of *Clarkina postbitteri*. Rare specimens of *Jinogondolella xuanhanensis* and *J. granti* continue to be present in this zone. *Sweetognathus fengshanensis* and *Hindeodus* sp. are also found. The specimens of *Clarkina postbitteri* from the uppermost part of the Maokou Formation have slightly more elongate outline and straight platform, which suggest the transitional morphotypes to *Jinogondolella granti* (e.g., Yuan et al., 2017, figs. 4.10, 4.11), therefore, more or less like *Clarkina postbitteri hongshuiensis* of Henderson et al. (2002) (e.g., Fig. 11.8). The zonal species ranges into the overlying *Clarkina dukouensis* Zone in the basal part of the Heshan Formation (Figs. 7, 11).

Clarkina dukouensis Zone (63.05 m – 69.5 m): This zone is mainly present in dark thin- to medium-bedded limestone in the lower part of the Heshan Formation. It is widely reported from the basal part of the Wuchiapingian Stage in South China and Iran, which was deposited during the initial stage of the widespread transgression in the Lopingian in South China. In the basal part, *Clarkina postbitteri* is yet present. *Iranognathus* sp., *Hindeodus* sp. are also found from this zone. Some questionable specimens similar to *Clarkina asymmetrica* are found in the middle part of the zone (Figs. 7, 12).

Clarkina asymmetrica Zone (69.5 m – 75.7 m): This zone is

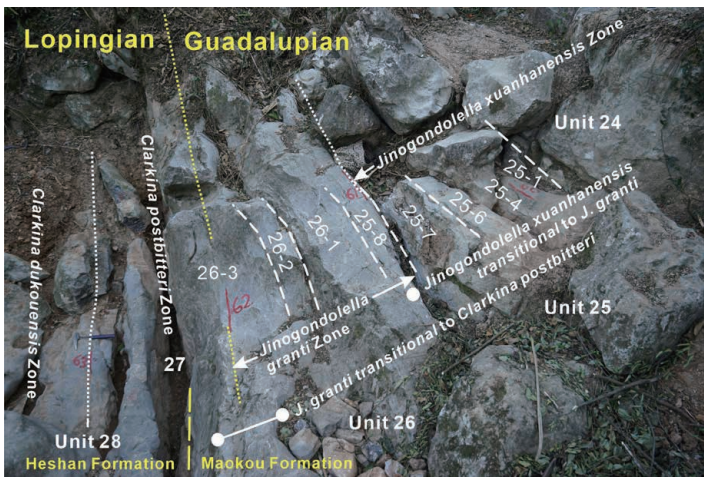


Fig. 8. The Guadalupian-Lopingian boundary interval and detailed fossil zones at the Fengshan section.

marked by the first occurrence and then dominated by the zonal species. *Hindeodus julfensis* is commonly found in this zone too. In the uppermost part, some questionable specimens of *Clarkina guangyuanensis* are present. The uppermost 4.2 m (71.5 m – 75.7 m) has no samples, therefore, is tentatively assigned to this zone below the first occurrence of reliable *C. guangyuanensis* at 75.7 m (Figs. 7, 12).

Clarkina guangyuanensis Zone (75.7 m – 80.0 m): This is the topmost zone at the measured section at Fengshan. It is dominated by the zonal species. *Merrilina divergens*, *Hindeodus julfensis* are occasionally found in this zone. In the upper part (79-80 m), several questionable incomplete specimens similar to *Clarkina liangshanensis* or *C. transcaucasica* are found (Figs. 7, 12).

3.2.2. Fusuline zonation

In the Fengshan section, the Maokou Formation comprises thin- to thick-bedded limestone of deep shelf facies in the lower part containing the fusuline *Neoschwagerina craticulifera* Zone and the *Colania majulensis* Zone. This part is exposed on the mountains near the Fengshan section. The measured upper part of the Maokou Formation is composed of thick-bedded to massive sponge-bryozoan-algae bioherm limestone of platform margin facies, which is the counterpart of the Laibin Limestone at Penglaitan. The Maokouan fusulines occur in the thick-bedded bioclastic limestone very abundantly and reach about 30% of the total composition of the rock. This part probably contains two fusuline zones, the *Metadoliolina multivoluta* Zone in the lower and the *Lantschichites minima* Zone in the upper. *Codonofusiella* is very abundant in the uppermost part of the Maokou Formation

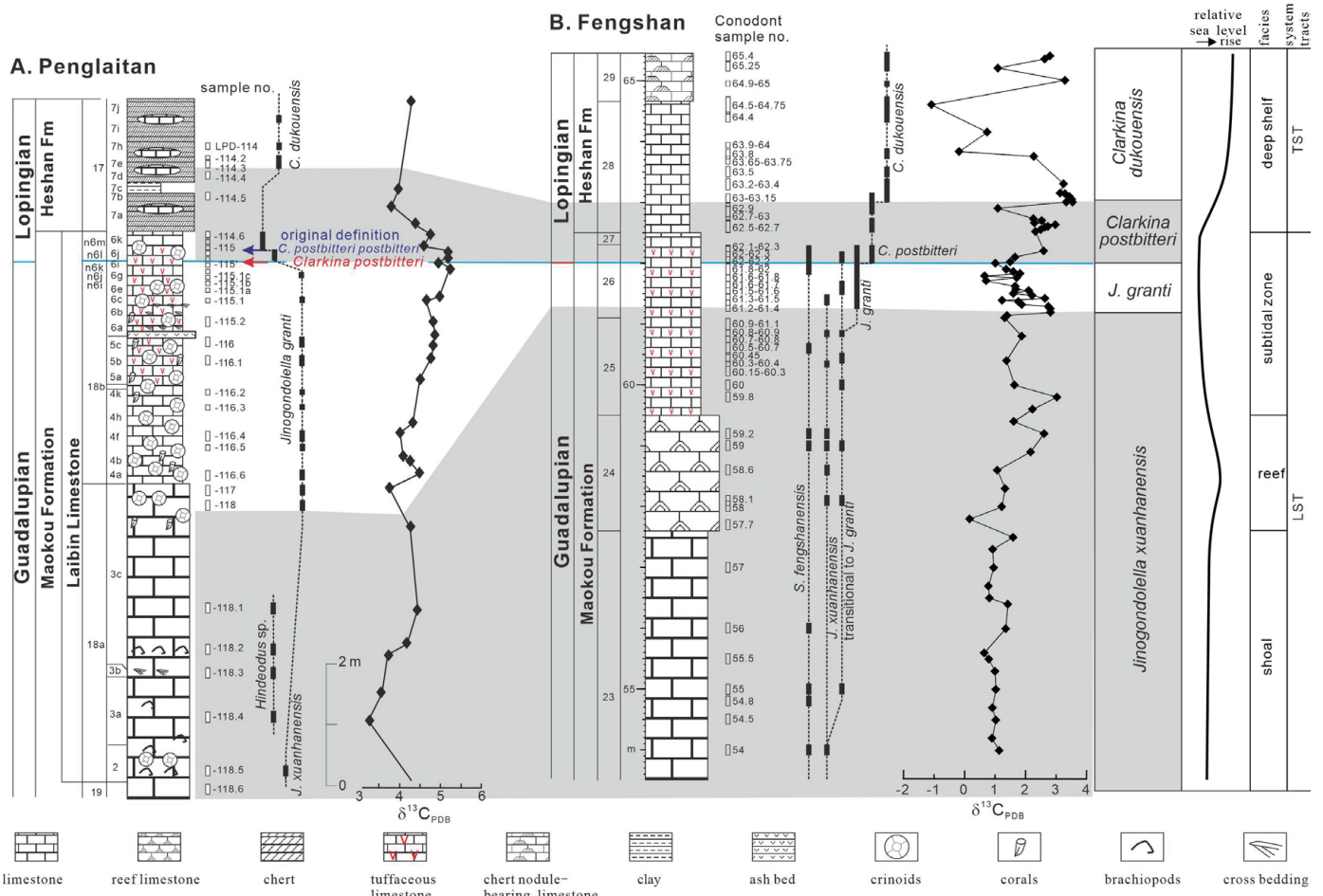


Fig. 9. Correlation of fossil zones, chemostratigraphy and sedimentary settings across the Guadalupian-Lopingian boundary interval between the Penglaitan and Fengshan sections. Bed numbers with a prefix “n” are from the new section at Penglaitan. Original defined and modified GSSP are shown in the Penglaitan section.



Fig. 10. Key conodonts from the upper part of the Maokou Formation at the Fengshan section. 1-4. *Jinogondolella prexuanhanensis* transitional to *J. xuanhanensis*, from Sample 12.7 m; 5-12. *Jinogondolella xuanhanensis*, 5 from Sample 14.3 m; 6 from Sample 17.8 m; 7 from Sample 19.5 m; 8 from Sample 34.5 m; 9 from Sample 39.5 m; 10 from Sample 44.6 m; 11 from Sample 47 m; 12 from Sample 50.2 m. 13-16. *Sweetognathus fengshanensis*, 13 from Sample 11.8 m; 14 from Sample 14.3 m; 15, 16 from Sample 40.2 m.



Fig. 11. Key conodonts from the GLB interval at the Fengshan section. 1. *Jinogondolella xuanhanensis* transitional to *J. granti*, from Sample 55 m. 2-4. *Jinogondolella granti*, from Sample 61.9 m. 5, 6. *Jinogondolella* sp., from Sample 62.0-62.3 m. 7-9. *Clarkina postbitteri*, from Sample 62.0-62.3 m. 10-14. *Clarkina postbitteri*, from Sample 62.9 m.



Fig. 12. Key conodonts from the lower part of the Heshan Formation of the Fengshan section (SABS). 1-4. *Clarkina dukouensis*, 1 from Sample 64.5-64.75 m; 2 from Sample 68.7 m; 3 from Sample 64.9-65.0 m; 4 from Sample 69.0 m. 5-7. *Clarkina asymmetrica*, 5 from Sample 69.5 m; 6 from Sample 70.5 m; 7 from Sample 70.0 m. 8-10. *Clarkina guangyuanensis*, from Sample 2017-26.5 m.

at the Fengshan section. The overlying Heshan Formation is mainly composed of dark thin-bedded limestone with chert beds of deep-shelf facies in the lower part and algae limestone of platform facies in the upper part and contains rare fusulines. Only one species, *Rechelina changhsingensis*, ranges from the Maokou Formation into the Heshan Formation. The widely distributed *Codonofusiella* fauna in the Wuchiapingian in South China is not found in the lowest part of Heshan Formation. The following fusuline zones can be recognized.

Metadoliolina multivoluta Zone (4 m – 17.8 m): This zone is in the massive bioclastic limestones in the upper part of the Maokou Formation (equivalent to the Laibin Limestone) at the Fengshan section. It is dominated by *Metadoliolina multivoluta*, *M. douvillei* and *M. delicata*. *Neoschwagerinids* are rare and only two specimens of *Neoschwagerina* sp. were found in the middle part of the zone. *Chusenella globularis* and *C. douvillei* are common. (Fig. 13).

Lantschichites minima Zone (17.8 m – 61.9 m): *Lantschichites minima* first occurs at 17.8 m in the upper part of Maokou Formation and marks the base of this zone, but it gains a dominant composition from this level until the GLB. Large *Metadoliolina* species continue to be present in the *Lantschichites minima* Zone. The disappearances of large fusulines at 58.9 m in the latest Guadalupian probably marked the profound environmental deterioration globally. Above this level, only small fusulines continue to be present. *Lantschichites minima* is commonly associated with some *Codonofusiella* species such as *C. extensa*, *C. schubertellinoides* and *C. paradoxica*. This zone is most abundant in the topmost part of the Capitanian Stage and it has been occasionally reported from the lowest part of the Wuchiapingian at the Penglaitan section in the Laibin area (Wang et al., 2020). In other regions of South China, the *Lantschichites minima* Zone is either missing or absent (Fig. 14).

3.2.3. Brachiopods

Brachiopods are also abundant in the interval between 8.8 m and 39 m at the Fengshan section. The brachiopod fauna is characterized by a mixed character between the upper Guadalupian and Lopingian elements (Fig. 15). In fact, the appearance of typical Lopingian brachiopod species in the Capitanian has been observed not only in sections of South China (Shen and Shi, 2009), but also in Iran (Crippa and Angiolini, 2012) and the Mediterranean region (Verna et al., 2010). The typical middle-upper Capitanian brachiopod *Urushtenoidea crenulata* is found at 27 m and a local Lengwuan (=Capitanian) species *Zhejiangospirifer abnormalis* is present at 15.5 m. *Urushtenoidea crenulata* has been widely reported from the upper part of the Capitanian and never reported from the Lopingian anywhere in the world (Shen et al., 2003; Shen and Zhang, 2008; Shen, 2018). On the other hand, some very abundant species in the Wuchiapingian in South China, Iran, Transcaucasia (Kotljar et al., 1983; Garbelli et al., 2014; Shen, 2018) including *Transennatia gratiosa*, *Permophricodothyris elegantula* and *Juxathyris guizhouensis*, are present in this interval. Therefore, this brachiopod fauna obviously indicates that the horizon is close to the latest Capitanian which is fully comparable with that of the Penglaitan section (Shen and Shi, 2009). These are typical

lower-middle Wuchiapingian taxa, which are found abundantly also in Tethyan sections (Angiolini and Carabelli, 2010; Ghaderi et al., 2014; Viaretti et al., 2022).

3.3. Chemostratigraphy

3.3.1 $\delta^{13}\text{C}_{\text{carb}}$ and $\delta^{18}\text{O}_{\text{carb}}$

Carbonate carbon isotope ($\delta^{13}\text{C}_{\text{carb}}$ and $\delta^{18}\text{O}_{\text{carb}}$) based on bulk samples were analyzed in order to establish the $\delta^{13}\text{C}_{\text{carb}}$ chemostratigraphy (Fig. 7). 269 bulk samples were analyzed for the 80.3 m interval across the GLB at the Fengshan section. $\delta^{13}\text{C}_{\text{carb}}$ values are between -1.09‰ and +4.76‰ with an average +1.68‰ for the whole section. The values in the basal 4.5 m (-6 m to -1.5 m) are between +2.47‰ and +4.07‰ in the section, then declined to ~+1‰ at the base of the *Jinogondolella xuanhanensis* Zone. $\delta^{13}\text{C}_{\text{carb}}$ values remain around ~+1‰ throughout the *J. xuanhanensis* Zone until 58.3 m, then frequently fluctuated between -1.09‰ and +4.76‰ across the GLB interval. At least five negative and positive excursions are present within the interval from 58.3 m to 73 m (Figs. 7, 9). $\delta^{13}\text{C}_{\text{carb}}$ values rapidly increased from +0.16‰ at 57.3 m to +3.02‰ at 59.8 m at the base of the *J. granti* Zone. Then, $\delta^{13}\text{C}_{\text{carb}}$ values declined with two minor negative excursions of ~2‰ in the *J. granti* Zone. $\delta^{13}\text{C}_{\text{carb}}$ values bounced back to +3.53‰ at the top of *Clarkina postbitteri* Zone, followed by another negative excursion of 4.62‰ with the lowest value -1.09‰ at 64.6 m in lower part of the *C. dukouensis* Zone. Above this negative excursion, two more negative carbon excursions with a magnitude 4‰ respectively in the uppermost part of *C. dukouensis* Zone and the basal part of *C. asymmetrica* Zone are present. After that, $\delta^{13}\text{C}_{\text{carb}}$ values fluctuated between +1.44‰ and +4.67‰ (Fig. 7).

$\delta^{18}\text{O}_{\text{carb}}$ values from all bulk samples are between -9.2‰ and -4.94‰ with an average -6.69‰, therefore a diagenetic effect may be present. Moreover, the large multiple fluctuations in $\delta^{18}\text{O}_{\text{carb}}$ values around the GLB are obviously different from all other coeval sections (Fig. 7).

3.3.2 $^{87}\text{Sr}/^{86}\text{Sr}$ ratio

The strontium isotope ratio ($^{87}\text{Sr}/^{86}\text{Sr}$) has been widely used to date marine sediments and fossils to achieve a temporal correlation among different regions. The non-parametrical Locally Weighted Scatterplot Smoother (LOWESS) Version 5 established with a statistical regression was widely used to interpolate the strontium isotope ratios of temporally undetermined marine sediments (McArthur et al., 2012) and it has been updated by McArthur et al. (2020). The Capitanian Stage is characterized by the Capitanian minimum with the lowest value of $^{87}\text{Sr}/^{86}\text{Sr}$ ratio between 0.7068-0.7070 in the Phanerozoic, therefore, it has been regarded as a very useful tool for correlation (Korte et al., 2006; Kani et al., 2013; Kani et al., 2018; Wang et al., 2018; Kani and Isozaki, 2021; Wang et al., 2021).

In order to investigate $^{87}\text{Sr}/^{86}\text{Sr}$ chemostratigraphy at the Fengshan section, 63 whole rock samples were collected (Fig. 7).

About 10 mg of the powders were weighed for $^{87}\text{Sr}/^{86}\text{Sr}$ analyses, and a weak acid (0.2 N HAc) leaching method was used to dissolve the powders. We also tried a sequential-leaching method followed Bellefroid et al. (2018) to obtain the least-altered seawater Sr isotopic signal (Appendix 3). Sr was

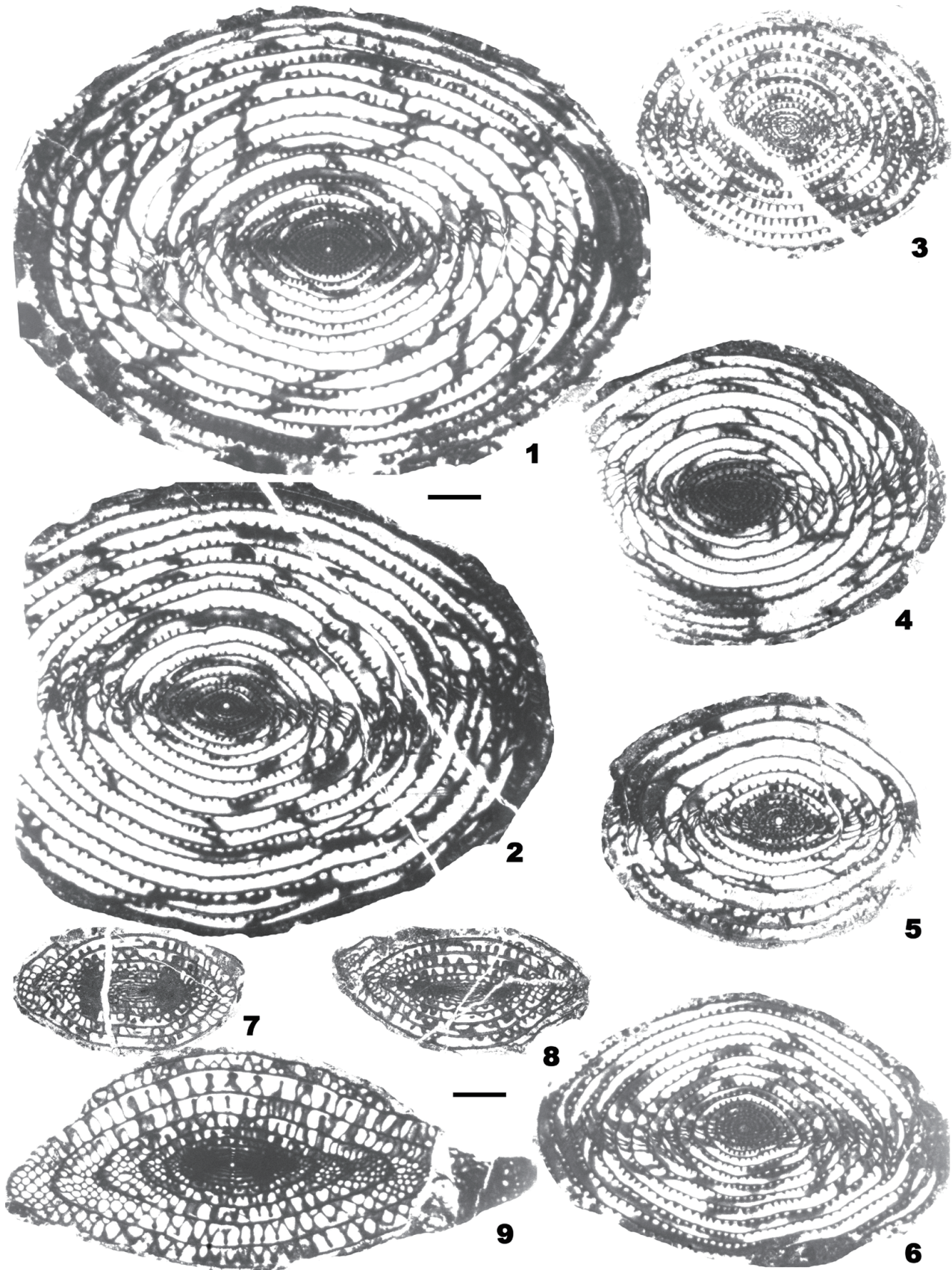


Fig. 13. Fusulines from the uppermost part of the Maokou Formation of the Fengshan section (SABS). 1, 2. *Metadoliolina multivoluta* (Sheng, 1963). 1, 176682, axial section; 2, 176691, axial section. 3. *Metadoliolina douvillei* (Gubler, 1935), 176692, subaxial section. 4-6. *Metadoliolina delicata* (Yang, 1978). 4, 176688, axial section; 5, 176681, axial section; 6, 176690, axial section. 7, 8. *Chusenella douvillei* (Colani, 1924). 7, 176646, subaxial section; 8, 176683, subaxial section. 9. *Chusenella globularis* (Gubler, 1935), 176689, axial section. Scale bar=1 mm.

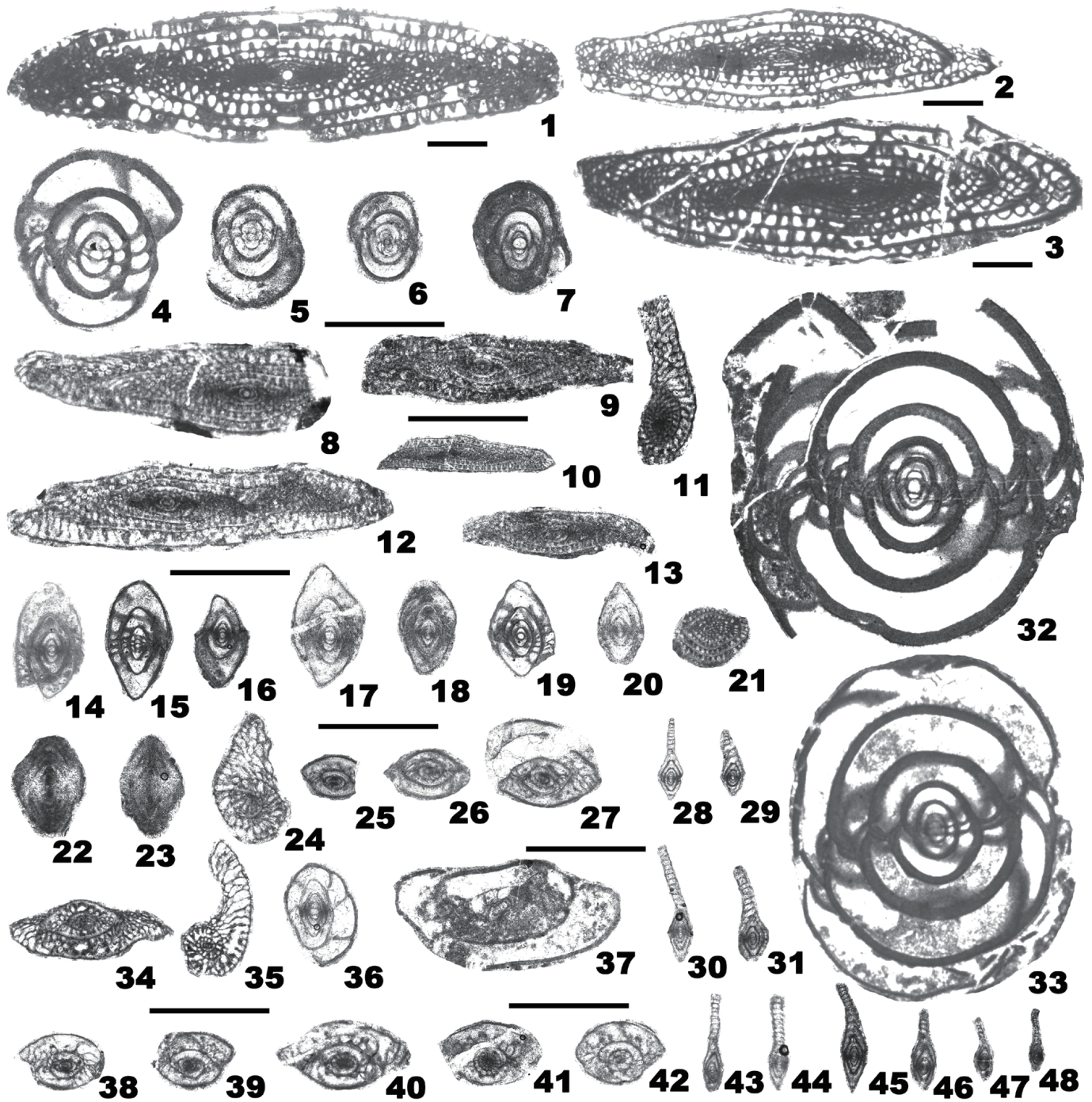


Fig. 14. Fusulines from the GLB interval of the Fengshan section. 1-3. *Schwagerina serrata* Ding, 1978. 1, 176685, axial section; 2, 176687, subaxial section; 3, 176684, axial section. 4-7. *Kahlerina pachythea* Kochansky-Devide and Ramovs, 1955. 4, 176668, subaxial section; 5, 176645, subaxial section; 6, 176643, axial section; 7, 176641, axial section. 8-13. *Lantschichites minima* (Chen, 1956). 8, 176639, axial section; 9, 176644, axial section; 10, 176640, subaxial section; 11, 176660, transverse section; 12, 176654, axial section; 13. 176637, subaxial section. 14-20. *Chenella changanchiaoensis* (Sheng and Wang, 1962). 14, 176667, axial section; 15, 176665, axial section; 16, 176658, axial section; 17, 176652, axial section; 18, 176653, axial section; 19, 176647, axial section; 20, 176657, axial section. 21. *Neoschwagerina* sp., 176677, oblique section. 22, 23. *Nankinella nanjingensis* Zhou and Zhang, 1984. 22, 176642, subaxial section; 23, 176655, subaxial section. 24-27. *Codonofusiella paradoxica* Dunbar and Skinner, 1937. 24, 176673, transverse section; 25, 176676, axial section; 26, 176675, axial section; 27, 176674, axial section. 28-31. *Reichelina simplex* Sheng, 1955. 28, 176662, axial section; 29, 176663, axial section; 30, 176636, axial section; 31, 176649, axial section. 32, 33. *Kahlerina sinensis* Sheng, 1963. 32, 176650, axial section; 33, 176686, axial section. 34, 35. *Codonofusiella extensa* Skinner and Wilde, 1955. 34, 176661, subaxial section; 35, 176664, transverse section. 36, 37. *Rauserella erratica* Dunbar, 1944. 36, 176656, transverse section; 37, 176638, subaxial section. 38-42. *Codonofusiella schubertellinoides* Sheng, 1956. 38, 176672, subaxial section; 39, 176670, subaxial section; 40, 176669, subaxial section; 41, 176659, axial section; 42. 176651, oblique section. 43-48. *Reichelina changhsingensis* Sheng and Chang, 1958. 43, 176679, subaxial section; 44, 176678, subaxial section; 45, 176671, axial section; 46, 176666, subaxial section; 47, 176680, axial section; 48. 176648, axial section.

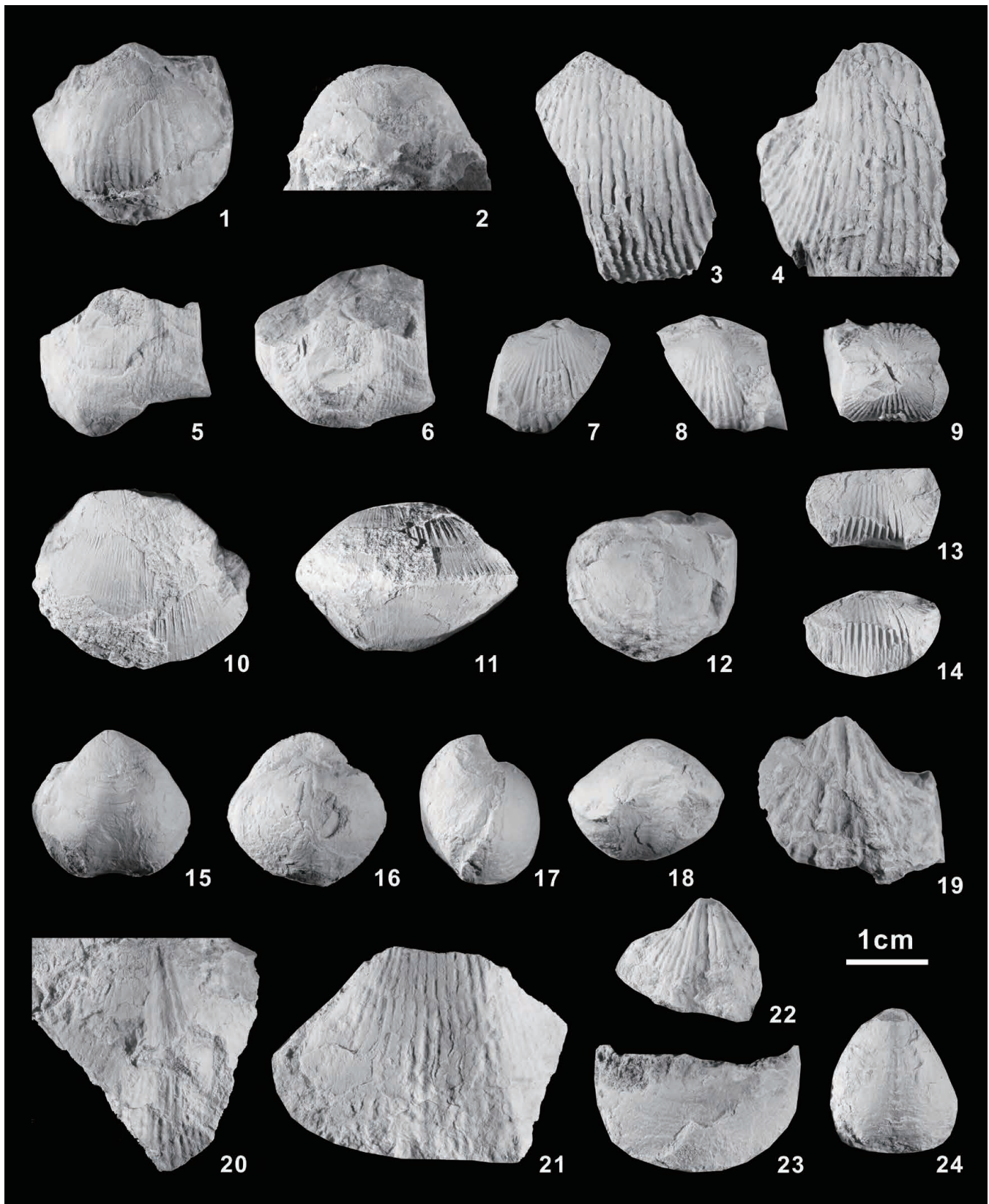


Fig. 15. Brachiopod fossils from the Fengshan section (SABS). 1, 2. *Haydenella kiangsiensis* (Kayser, 1883). ventral and posterior views, 68.3 m. 3, 4. *Tylopecta yangtzeensis* (Frech, 1911). 3, 4, ventral views, 68.3 m. 5, 6. *Transennatia gratiosa* (Waagen, 1884). ventral and posterior views, 15.5 m. 7-9. *Urushtenoidea crenulata* (Ting, 1962). ventral, dorsal and posterior views of a conjoined shell, 27 m. 10, 11. *Orthotichia* sp. dorsal and anterior views, 68.3 m. 12. *Enteletes kayseri* Waagen, 1883. lateral view, 32 m. 13, 14. *Uncinunellina timorensis* (Beyrich, 1864). ventral and anterior views, 20.7 m. 15-18. *Juxathyris guizhouensis* (Liao, 1980). ventral, dorsal, lateral and anterior views of a conjoined shell, 68.3 m. 19. *Zhejiangospirifer abnormalis* Liang, 1990. ventral view, 15.3 m. 20-22. *Alphaneospirifer anshunensis* (Liao, 1980), ventral view, 39 m; ventral view, 39 m; ventral view, 15.5 m. 23. *Permophricodothyris elegantula* (Waagen, 1883). ventral view of anterior portion of ventral valve, 17.8 m. 24. *Martinia* sp. ventral view, 23 m.

extracted by cation exchange resin, and the isotopic composition was measured by Neptune-MC-ICP-MS at Nanjing Institute of Geology and Palaeontology (NIGP), Chinese Academy of Sciences. The contents of the trace elements Mg, Fe, Mn, and Sr and the main element Ca were also analyzed to test whether these samples were altered by subsequent diagenesis or not (Appendix 3 for methodology). Major and trace elements of samples were analyzed on an Agilent 710 ICP-OES

The results show that two leaching methods yield similar Sr isotopic trends (Fig. 7). Based on the samples with Mn/Sr < 1, a cutoff widely used for identifying diagenetic alteration (Bellefroid et al., 2018; Wang et al., 2018), the $^{87}\text{Sr}/^{86}\text{Sr}$ ratios in the Fengshan section varied from 0.707043 to 0.707276. Due to the high Mn/Sr ratios around GLB, most of the analyzed samples were considered not to represent the open marine seawater $^{87}\text{Sr}/^{86}\text{Sr}$ ratios, thus the minimum of $^{87}\text{Sr}/^{86}\text{Sr}$ ratios, a unique stratigraphic marker for the Capitanian (Liu et al., 2013; Korte and Ullmann, 2016; Li et al., 2021; Wang et al., 2021), was not detected in this study (Fig. 7). However, two values in the basal part of the section and nine samples in the basal part of the Heshan Formation around 0.7070-0.7072 (blue points in Fig. 7) are very close to the Capitanian minimum.

To investigate the reasons producing the profound offset between the Fengshan section and global data is beyond the scope of the present paper. Many reasons such as the intensity of continental weathering, volcanism, diagenetic effect and different leaching methods may lead to variations in $^{87}\text{Sr}/^{86}\text{Sr}$. Since the average $^{87}\text{Sr}/^{86}\text{Sr}$ ratio at the Fengshan section is much higher than that of the Penglaitan section and many samples yield Mn/Sr > 1, global factors such as continental weathering, volcanism etc. can be excluded. Depositional water depth may be another reason to affect the results of $^{87}\text{Sr}/^{86}\text{Sr}$ ratio. However, facies analysis indicates that the GLB interval at the Fengshan and Penglaitan sections are both characterized by shallow shoal and bioherm settings (see Section 10). Thus, it seems that diagenetic alternation of the samples at Fengshan is the most likely reason to produce higher $^{87}\text{Sr}/^{86}\text{Sr}$ ratios.

3.4. Magnetostratigraphy

Magnetic polarity zones can serve as a very useful tool for global correlation in both marine and terrestrial sequences. Magnetostratigraphic investigation was carried out by Manfred Menning and Shuzhong Shen in the Laibin area during 1994. They collected 640 oriented cylinders from the Chihsia, Maokou and basal part of the Heshan formations at the Tieqiao section and from the GLB interval at the Penglaitan section. Partial or total remagnetization complicates the magnetostratigraphic research (Menning et al., 1996) and so far no result has been published. More than 150 paleomagnetic samples were collected from the new Penglaitan section. Unfortunately, a preliminary test suggests that most of those samples suffered subsequent remagnetization. To establish a magnetostratigraphical framework, high-resolution samples across the GLB at the Fengshan section have been collected as well (Fig. 6E). A new high-resolution magnetostratigraphic sequence (ca. 260.85 – 258.75 Ma) on the Fengshan section in South China is established. Below the GLB, the magnetic polarity sequences are characterized by a

mixed interval consisting of six normal (FS1n-FS6n) and six reverse (FS1r-FS6r) magnetozones. In the early Lopingian three magnetozones (FS7r, FS7n, and FS8r) are recognized. The GLB is in the reversed polarity interval (FS7r) (Zhang et al., in preparation). The *Jinogondolella granti* Zone is within the upper part of normal magnetozone FS6n and the reverse magnetozone FS7r, the *Clarkina postbitteri* Zone is within FS7r, which is 0.75cm above the boundary between FS6n and FS7r. The *C. dukouensis* Zone is across three polarity zones from FS7r to FS8r.

Generally, the Carboniferous to early Guadalupian belongs to the reverse polarity Kiaman Superchron; whereas, the interval from the mid-Guadalupian and above belongs to Permian-Triassic mixed polarity Illawarra Superchron. Its boundary is marked by the first normal polarity zone called Illawarra Reversal largely in the Wordian (Hounslow and Balabanov, 2018). The Capitanian is normal polarity dominated (Jin et al., 2000; Steiner, 2006; Hounslow and Balabanov, 2018), but detailed polarity zones and their biostratigraphic and geochronologic constrains are unclear so far. The Fengshan section, for the first time, provided a high-resolution magnetostratigraphical timescale and will have great potential for correlation across the GLB between the marine and terrestrial sequences (Zhang et al., in preparation).

3.5. Lithofacies and sequence stratigraphy

The Fengshan section is composed of an 87 m-thick carbonate sequence with diverse and abundant fossils (Figs. 7, 16). The lowest 5.3 m (Unit 0) consists mainly of dark grey, thin- to medium-bedded packstone, wackestone and lime mudstone. The upper part is rich in chert nodules, and the lower part contains abundant thin- to medium-bedded chert. Fossils in limestones are dominated by sponge spicules and minor calcispheres. Bioclasts in chert nodules and bedded cherts are dominated by benthic fossils, such as crinoids and gastropods. The lithofacies and biofacies indicate that Unit 0 was deposited in a deep shelf environment below the storm-wave base, representing the final highstand stage before the global end-Guadalupian regression.

Overlying the basal deep-shelf facies is a set of light grey, medium- to thick-bedded bioclastic grainstone (Units 1 to 2) (Fig. 16A), intercalated by packstone, wackestone, and rudstone. Fossils in this interval are dominated by abraded debris of shallow benthos, such as crinoids, brachiopods, gastropods, foraminifers, bryozoans, calcareous sponges, and *Tubiphytes*. At the base of this interval, the sedimentary environment changed from the deep shelf settings to shallow shoal settings, marking a rapid shallowing representing the onset of the great end-Guadalupian regression event. Therefore, this surface corresponds to a significant drop of relative sea level and represents a type 1 sequence boundary

Units 21 and 22 comprise mainly light grey or dark reddish grey, thick- to very thick-bedded sponge bafflestone (Fig. 16B), and minor rudstone. Calcareous sponges, mainly sphinctozoan and inozoan sponges, dominate the baffling fauna. The spaces between baffling sponges are filled mainly by lime muds, with minor calcite-spar-filling voids. Some gastropods and crinoid debris are present sporadically in the lime mud. The lithofacies and biofacies demonstrated that this interval represents low- to moderate-energy reef facies formed below the FWB, representing

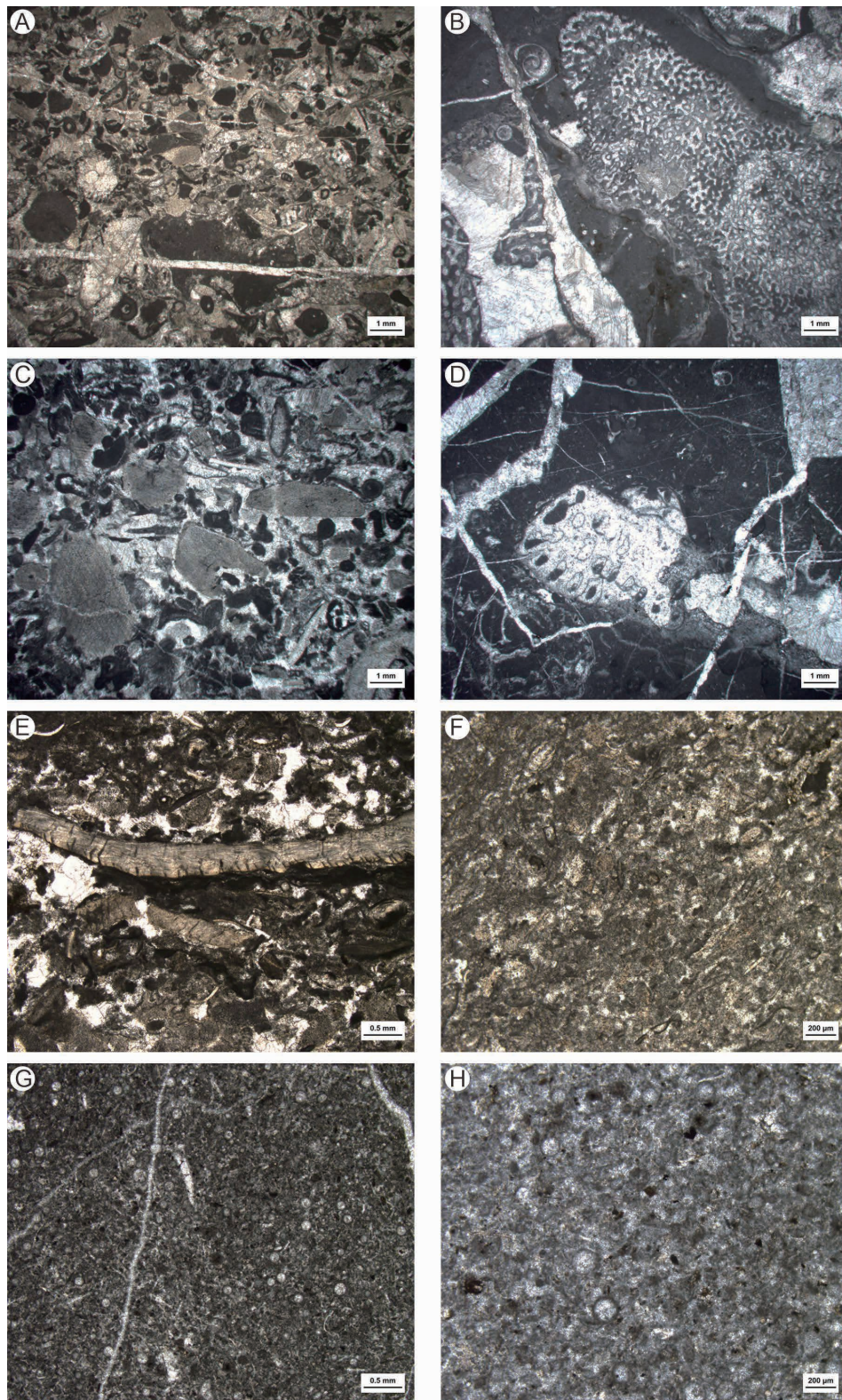


Fig. 16. Sedimentary microfacies of the Maokou and Heshan formations of the Fengshan section (SABS). A. shoal facies, bioclastic grainstone containing abundant crinoid debris and Tubiphytes, Unit 3 (4.75 m). B. reef facies, sponge bafflestone showing the dominance of calcareous sponge and minor gastropods in lime mud matrices, Unit 22 (21.5 m). C. shoal facies, crinoid-bioclaster grainstone consisting of abundant crinoid debris, foraminifers, and micritic bioclasts, Unit 23 (50.6 m). D. reef facies, sponge bafflestone showing the calcareous sponge-dominant fossil group and the lime mud-rich matrix, Unit 24 (57.7 m). E. subtidal zone facies, bioclastic grainstone consisting mainly of abraded debris of crinoids, ostracods, and brachiopods, Unit 26 (61.2 m). F. subtidal zone facies, bioclastic packstone containing abraded debris of crinoids, ostracods, small foraminifers, and micritic bioclasts, Unit 26 (62 m). G. deep shelf facies, fecal pellet-calcisphere wackestone showing common calcispheres and worn fecal pellets, as well as some ostracods, Unit 28 (64 m). H. deep shelf facies. Calcisphere-bioclaster packstone composed mainly of calcispheres and micritic fossil debris, Unit 29 (65.3 m).

a minor higher-order transgression during the long-term end-Guadalupian lowstand stage of the relative sea level.

The reef limestone of Unit 22 is overlain by a thick succession (29.9 m) of light grey to greyish white, thick- to very thick-bedded, bioclastic packstone, grainstone, and rudstone (Unit 23) (Fig. 16C), with a 1.9 m-thick sponge bafflestone on the top (Unit 24) (Fig. 16D). Fossils are dominated by crinoid skeletons, small foraminifers, fusulines, and brachiopods, bryozoans, and calcareous sponges. Similar to the interval of Units 1 to 20, Units 23 and 24 represent mainly the high-energy, agitated bioclastic shoal or open marine platform facies above the FWB (Unit 23) with a minor transgression in the topmost part (Unit 24).

The topmost 3 m of the Maokou Formation is composed of light grey to dark grey, thin- to medium-bedded or nodular, bioclastic grainstone/packstone/wackestone (Fig. 16E, F). Grains are dominated by heavily abraded skeletons of crinoids, brachiopods, ostracods, and foraminifers. Greyish-green clay minerals altered from volcanic ash are common in this interval. The lithofacies and biofacies suggest that this interval formed in a high- to moderate-energy subtidal zone above the FWB, representing the shallowest part of the topmost Maokou Formation. This interval corresponds to the uppermost lowstand system tract during the end-Guadalupian regression in association with the Emeishan volcanism in South China.

The basal Heshan Formation comprises dark grey to greyish black, thin- to medium-bedded wackestone and lime mudstone with packstone interbeds (Fig. 16G, H). Fossils are dominated by calcispheres, sponge spicules, and minor thin-shelled bivalves, ostracods, echinoderms, and fecal pellets. All these features indicate that this interval was deposited in a deep shelf environment below the storm-wave base, representing a rapid transgression after the global end-Guadalupian regression.

4. Correlation between the SABS and GSSP section

The Fengshan SABS section is basically consistent with the GSSP section at Penglaitan in terms of conodont and fusuline biostratigraphy and sedimentary sequence (Figs. 7, 9). Thus, it is an ideal SABS to support the base-Lopingian GSSP. Future studies around GLB may mainly rely on the Fengshan section because it has a long well-exposed succession and will not be flooded.

The conodont succession around the GLB including the *Jinogondolella prexuanhanensis*, *J. xuanhanensis*, *J. granti*, *Clarkina postbitteri* (including *C. postbitteri hongshuiensis*, *C. postbitteri postbitteri* and transitional morphotypes), *C. dukouensis*, *C. asymmetrica* and *C. guangyuanensis* zones in ascending order is fully recovered at the Fengshan section. Thus, they are completely correlative with those at the Penglaitan and Tieqiao sections in the Laibin area (Figs. 7, 9).

Fusulines dominated by *Lantschichites minima* and some small *Codonofusiella* in the uppermost part of the Maokou Formation are also comparable with those at Penglaitan and Tieqiao sections. In the Tieqiao section similar assemblages have been found in the topmost part of Maokou Formation which include *Metadoliolina douvillei*, *M. spherioidea*, *Lepidolina parasuschanica*, *Schwagerina pseudocompacta*, *Chusenella zhonghuaensis*, *Kahlerina sinensis*, *Lantschichites minima* and

Chenella changanchiaoensis. *Yabeina* and *Lepidolina* have not been found at the Fengshan section. In the Tieqiao section, the third fusuline assemblages contain both *Yabeina gubleri* and *Metadoliolina douvillei* (Shen et al., 2007). A slight difference is that the basal part of the Heshan Formation at Penglaitan and Tieqiao is characterized by the *Codonofusiella kueichowensis* Zone, but representative elements of this zone have not been found at the Fengshan section. *Codonofusiella* species are abundant in the topmost part of the Guadalupian and *Reichelina changhsingensis* ranges across the GLB at the Fengshan section. In addition, *Lantschichites minima* ranges into the basal part of the Wuchiapingian at Penglaitan (Wang et al., 2020), but it is restricted to the Maokou Formation at Fengshan.

Lithologically, the thick-bedded Laibin Limestone in the topmost part of the Maokou Formation at Penglaitan and Tieqiao in the Laibin area, which represents a lowstand system tract deposited continuously on the slope setting in the GLB interval, is also well developed at the Fengshan section. A minor difference is that the equivalent massive Laibin Limestone at Fengshan contains relatively less crinoid fragments and more abundant fusulines and foraminifers, and it is characterized by the sponge-bryozoan-algae bioherm facies. The topmost part of the Laibin Limestone at Penglaitan contains greenish tuffaceous ashes in the coarse crinoid bioclastic limestone (Fig. 9A), which directly indicate a temporal link with the last stage of the Emeishan large igneous province in southwest China. These ashes have been also observed at the Fengshan section (Fig. 9B).

Furthermore, high-resolution magnetic polarity zones are established at the Fengshan section. This magnetostratigraphy will provide a basis for the correlation between marine and terrestrial sequences around the GLB. $\delta^{13}\text{C}_{\text{carb}}$ values across the GLB at the Penglaitan show a gradual increase from +3.7‰ in the base of *Jinogondolella granti* Zone to +5.06‰ in the basal part of *Clarkina postbitteri* Zone, followed by a decline of ~2‰ in the upper part of *C. dukouensis*. The broad interval with relatively low values in the *Jinogondolella xuanhanensis* Zone and the generally increasing $\delta^{13}\text{C}_{\text{carb}}$ trends in the uppermost part of the *J. xuanhanensis* Zone are largely comparable between the Penglaitan and Fengshan sections (Fig. 9) (Shen et al., 2020). However, obvious differences are also present. The Penglaitan section has higher $\delta^{13}\text{C}_{\text{carb}}$ values and does not have multiple excursions across the GLB. All the $\delta^{13}\text{C}_{\text{carb}}$ chemostratigraphical signals need to be investigated if they suffered diagenesis because previous reports of those $\delta^{13}\text{C}_{\text{carb}}$ excursions are in different horizons and quite variable in magnitude and time (Isozaki et al., 2007; Wignall et al., 2009; Bond et al., 2010; Chen et al., 2011; Nishikane et al., 2011; Liu et al., 2013; Shen et al., 2013).

5. Correlation with other regions

5.1 Other areas in South China

The conodont succession established from the Fengshan, Penglaitan and Tieqiao sections can be mostly recognized in many other sections in South China. However, the *Jinogondolella granti* and *Clarkina postbitteri* zones in the GLB interval are largely unidentifiable and represented by a distinct unconformity indicated by black Wangpo Shale, a purple limonite bed and greenish volcanic ash with no conodonts (Mei and Wardlaw,

1996; Yuan et al., 2017, 2019; Hou et al., 2020). The underlying *Jinogondolella xuanhanensis* Zone and the overlying *Clarkina dukouensis* Zone can be widely identified in most areas of South China, suggesting sea water withdrawal in South China in the latest *Jinogondolella xuanhanensis* Zone and returned in the *Clarkina dukouensis* Zone although at different times in different sections (Hou et al., 2020).

Sun and Xia (2006) recognized some *Clarkina postbitteri hongshuiensis* in the Dachongling section in Pingxiang, Guangxi. However, they are difficult to identify because the figured specimens are broken and unclear. Zhang et al. (2008) recognized the *C. postbitteri postbitteri* Subzone in the Maoershan section, Hubei, South China. However, most illustrated specimens appear to have serrations (e.g., Zhang et al., 2008, pl. 2, fig. 4), which is a character of *Jinogondolella*. Other specimens may be assignable to *Clarkina leveni* (e.g., Zhang et al., 2008, pl. 3, fig. 10). Shen and Zhang (2008) recognized this zone in the uppermost part of the Douling Formation in Chenzhou, Hunan. Thus, this zone has only been recognized in a few localities of South China.

5.2 North America

The Guadalupian Series and its three component stages are represented by the sequence in the Guadalupe and Glass Mountains areas and it is overlain by the evaporite deposits of the Ochoan Series in North America. Most of the conodont zones of the Capitanian Stage including the *Jinogondolella postserrata*, *J. shannoni*, *J. altudaensis*, *J. prexuanhanensis* and *J. xuanhanensis* zones can be recognized in both South China and North America, providing a good correlation basis for the Capitanian Stage between South China and North America (Mei et al., 1994a; Wardlaw et al., 1999; Shen et al., 2020). However, the conodont zones above the *J. prexuanhanensis* zone are controversial between North America and South China (Mei et al., 1998; Wang, 2000, 2001; Henderson et al., 2002; Kozur and Wang, 2002; Lambert et al., 2002) and they all show some disagreement over the FAD of *Clarkina postbitteri*, its identification and evolutionary lineage. Rare specimens of *Jinogondolella granti* and *Clarkina postbitteri hongshuiensis* were reported from the Reef Trial Member of the Bell Canyon Formation in the Guadalupe Mountains National Park in West Texas (Lambert et al., 2002; Lambert et al., 2010; Wardlaw and Nestell, 2010; Bell et al., 2015). Based on the latest study on the Guadalupian conodonts from West Texas and South China, these specimens were re-assigned to *Jinogondolella altudaensis* which is the most common species in this member (Yuan et al., 2017; Shen et al., 2020). Wardlaw and Nestell (2010) illustrated two specimens as *Clarkina postbitteri hongshuiensis* from the Apache Mountains, West Texas. They coexist with very abundant *Jinogondolella altudaensis* in the same samples. These two specimens still have a broad platform, dense denticles, and a very small cusp, which are the characters typical within the sample population of *J. altudaensis*. Thus, Yuan et al. (2017) did not regard them as *Clarkina postbitteri hongshuiensis* and reassigned these two specimens to *Jinogondolella altudaensis* based on a sample population approach. The strata above the *J. altudaensis* at the Apache Mountains are represented by the evaporite deposits of the Castile Formation (Yuan et al., 2017; Shen et al., 2020).

Thus, the topmost zone in West Texas is near the *Jinogondolella prexuanhanensis* Zone, and no transitional population from *J. altudaensis* to *Clarkina postbitteri hongshuiensis* has been found and there are at least three more conodont zones (the *Jinogondolella prexuanhanensis*, *J. xuanhanensis* and *J. granti* zones) between the *J. altudaensis* Zone and the *Clarkina postbitteri* Zone in South China. Therefore, the evolutionary relationship between *Jinogondolella altudaensis* and *Clarkina postbitteri hongshuiensis* cannot be demonstrated based on the West Texas specimens.

Problems for the GLB correlation between South China and North America were also raised by ammonoids (Zhou, 2017). Six Permian ammonoid zones were recognized in South China and the upper three zones are correlative with those from the Permian of Las Delicias, Coahuila, Mexico and west Texas, USA (Zhou, 2017), of which the uppermost *Eoaxoceras spinosai-Difuntites furnishi* Zone from the 3rd Member of the Shaiwa Formation in Ziyun, Guizhou Province has been regarded as the counterpart of the *Eoaxoceras spinosai-Difuntites* Zone of the upper Capitanian in Coahuila, Mexico and west Texas, USA (Miller, 1944; Wardlaw, 2000). Thus, ammonoids provide direct correlation between the uppermost Capitanian and the lower part of the 3rd Member of the Shaiwa Formation in Guizhou, South China (Zhou, 2017, fig. 9). However, Zhou (2017) assigned the *Eoaxoceras spinosai-Difuntites furnishi* Zone in the 3rd Member of the Shaiwa Formation to the Wuchiapingian of South China because this zone is found between the 4th Member of the Shaiwa Formation containing the conodonts *Clarkina cf. guangyuanensis* and *C. subcarinata*, and the *Waagenoceras* Zone in the Chongtuo Member below, which contains *Jinogondolella aserrata* and *J. postserrata* (Hao et al., 1999; Wang et al., 2016). Thus, Zhou (2017) claimed that the south Chinese Wuchiapingian Stage partly overlaps with the uppermost Guadalupian in Coahuila, Mexico and west Texas, USA. However, a re-examination suggests that none of the conodonts illustrated by Hao et al. (1999) from the 4th Member have been correctly identified. The single specimen assigned to "*Clarkina subcarinata*" only has a lower view, which is not identifiable. Even if those conodonts were of Wuchiapingian or Changhsingian in age, it does not indicate that the underlying 3rd Member is of Lopingian in age. On the contrary, the same latest Guadalupian ammonoid zone between the 3rd Member of the Shaiwa Formation and the uppermost Capitanian in Coahuila, Mexico and west Texas, USA suggests that the 3rd Member of the Shaiwa Formation is latest Capitanian in age. This correlation is supported by a subsequent conodont study in which the Guadalupian *Sweetognathus inornatus* and *Sw. paraguizhouensis* (both may be assignable to *Sw. subsymmetricus*) were reported from the 3rd Member of the Shaiwa Formation (Ji et al., 2009) in Ziyun, Guizhou, South China (Shen et al., 2019).

Chemostratigraphy across the GLB interval has been previously intensively studied in order to unravel the causes of the end-Guadalupian biological crisis and environmental changes (Isozaki et al., 2007; Wignall et al., 2009; Bond et al., 2010; Saitoh et al., 2013; Shen et al., 2013). The different chemostratigraphical signals may have some potential to be used for the correlation around the GLB. However, so far many data

are controversial due to different reasons.

5.3. Iran

The Permian and Lower Triassic succession in central Iran was first classified into 12 units, among which Units 1-7 belong to the Permian and Units 8-12 to the Lower and Middle Triassic. Units 1-3 were assigned to Surmaq Formation, which is largely lower and middle Guadalupian. The overlying Abadeh Formation consists of Units 4a, 4b and 5 of mainly black shale and thin-bedded limestone (Iranian-Japanese-Research-Group, 1981; Taraz et al., 1981). Traditionally, the GLB in the Abadeh area was placed at the base of Unit 6, that is, the base of the Hambast Formation, marked by the brachiopod *Araxilevis* Bed followed by the ammonoid *Araxoceras tectum* Zone and the conodont *Clarkina leveni* Zone. A distinct lithologic boundary between Units 5 and 6 is well recognized in the outcrop at Abadeh, central Iran. The small and specialized fusuline *Codonofusiella* is abundant in Unit 5. A re-examination of the conodonts collected by Walter Sweet suggests that the base of the Hambast Formation contains the conodont *Clarkina dukouensis* and possibly *C. postbitteri* in the basal part of Unit 6 (Shen and Mei, 2010). Subsequent collecting of the conodont and geochemical samples suggests that the upper part of Unit 5 already contains *Clarkina* and some minor, but distinct $\delta^{13}\text{C}_{\text{carb}}$ fluctuations are present in the upper part of Unit 5 in association with the beginning of the rising trend of $^{87}\text{Sr}/^{86}\text{Sr}$ ratio (Liu et al., 2013). This GLB is also well recognized at the base of the Julfa Beds in the Kuh-e-Ali Bashi area of northwest Iran (Shen and Mei, 2010).

5.4. Oman

Middle Permian to Lower Triassic rocks are exposed at Buday'ah in the Oman Mountains, Oman. The Buday'ah Formation ranges from the Guadalupian to Lower Triassic. The GLB interval may be developed in the basal part of the section. Unit 1 consists of pillow basalt that provided a base for the Permian-Triassic sedimentary succession above. These volcanic and sedimentary rocks formed in a deep oceanic setting along the southern margin of the Neotethys. Unit 2 is a dm-1.2 m thick pelagic red ammonoid-bearing limestone, which is overlain by the radiolarian-bearing cherts. The Wordian-Capitanian ammonoid *Timorites* sp. and *Waagenoceras* cf. *mojsisovicsiis* were reported in the basal part of this unit. In the topmost part of this unit, *Clarkina postbitteri hongshuiensis* was found and illustrated (Baud et al., 2012). However, a careful re-examination of these conodonts shows that they have relatively dense, more stout denticles, more straight platform and some of them (e.g., Baud et al., 2012, fig. 10-14, 16, 19) have weak serrations, therefore, these conodonts have some characters of *Jinogondolella*, but the horizon should be very close to the GLB based on the overlying Wuchiapingian radiolarians *Pseudoalbaillella fusiformis* and *Follicucullus ventricosus*.

6. Accessibility and protection

The new Penglaitan GSSP section is about 10 m higher than the original GSSP level and is still flooded periodically during the high water season of the Hongshui River. The SABS at Fengshan is located in a small valley in a low mountain area near

Fengshan Town with direct paved road access. A simple highway is available directly to the section. The section is easily accessible by any vehicle, and it will be fully protected by the local government after it is ratified as the SABS. Heavy vegetation on either sides of the creek will be cleared and a dedicated access road will be built along the section, and a monument will be erected. Sample collecting for research purposes will be guaranteed.

7. Appendices: Descriptions of the studied sections

7.1. Appendix 1: Description of the new GSSP section at Penglaitan (Figs. 1, 2)

Heshan Formation

Unit n7, Black thin- to medium-bedded chert with multiple volcanic ash beds, 3.3 m (11.7 m – 14.0 m)

Bed n7j, black medium-bedded chert, yielding conodont *Clarkina dukouensis*, 1.28 m (12.72 m – 14.0 m).

Bed n7i, volcanic ash, 2 cm (12.70 m – 12.72 m).

Bed n7h, brownish chert, 6 cm (12.64 m – 12.70 m).

Bed n7g, greenish volcanic ash, 4 cm (12.60 m – 12.64 m).

Bed n7f, dark grey medium-bedded chert with limestone lenses, 28 cm (12.32 m-12.60 m).

Bed n7e, greenish volcanic ash, 2 cm (12.3 m – 12.32 m).

Bed n7d, dark grey medium-bedded chert, fragile, yielding conodont *Clarkina dukouensis*, 35 cm (11.95 m – 12.3 m).

Bed n7c, greenish volcanic ash, 5 cm (11.90 m – 11.95 m).

Bed n7b, black thin-bedded chert with limestone lenses, fragile, yielding abundant conodont *Clarkina postbitteri*, 10cm (11.80 m-11.90 m).

Bed n7a, greenish volcanic ash bed, 10 cm (11.70 m – 11.80 m).

—————conformity—————

Maokou Formation (Laibin Limestone)

Unit n6, coarse dark grey medium-bedded crinoid limestone containing tuffaceous materials, 2.07 m (9.63 m – 11.70 m).

Bed n6m, coarse dark grey medium-bedded crinoid limestone, yielding conodont *Clarkina postbitteri* and transitional forms to *Jinogondolella granti*. 15 cm (11.56 m – 11.70 m).

Bed n6L, coarse dark grey medium-bedded crinoid limestone, yielding conodont *Clarkina postbitteri* and *Jinogondolella granti*, 20 cm (11.35 m – 11.56 m). The base of this bed has been defined as the new GSSP at Penglaitan.

Bed n6k, coarse dark grey medium-bedded crinoid limestone containing tuffaceous materials, yielding abundant conodont *Jinogondolella granti* and the solitary corals *Cania*, 29 cm (11.06 m – 11.35 m).

Bed n6j, coarse dark grey medium-bedded crinoid limestone containing tuffaceous materials and the conodont *Jinogondolella granti*, 11 cm (10.95 m – 11.06 m).

Bed n6i, coarse dark grey medium-bedded crinoid limestone containing tuffaceous materials, 20 cm (10.75 m – 10.95 m).

Bed n6h, coarse dark grey medium-bedded crinoid limestone containing tuffaceous materials, 16 cm (10.59 m – 10.75 m).

Bed n6g, coarse dark grey medium-bedded crinoid limestone containing tuffaceous materials, 22 cm (10.43 m – 10.59 m).

Bed n6f, coarse dark grey medium-bedded crinoid limestone containing tuffaceous materials, 12 cm (10.31 m – 10.43 m).

Bed n6e, coarse dark grey medium-bedded crinoid limestone containing tuffaceous materials, 11 cm, (10.20 m – 10.31 m).

Bed n6d, dark grey medium-bedded crinoid limestone, 14 cm, (10.06 m – 10.20 m)

Bed n6c, ash bed, 6 cm, (10.0 m – 10.06 m).

Bed n6b, dark grey thick-bedded limestone with cross-bedding, yielding the conodont *Jinogondolella granti*, 10 cm, (9.90 m – 10.0 m).

Bed n6a, Dark grey thick-bedded crinoid limestone with cross-bedding, 27 cm (9.63 m – 9.90 m).

Unit n5. Medium-bedded limestone with tuffaceous materials, 85 cm (8.78 m–9.63 m)

Bed n5e, ash bed, 3 cm (9.60 m– 9.63 m).

Bed n5d, dark grey medium-bedded limestone containing abundant tuffaceous materials, 8 cm (9.52 m – 9.60 m).

Bed n5c, dark grey medium-bedded limestone containing volcanic materials, limestone breccia, abundant brachiopods, corals *Cania* and the conodont *Jinogondolella granti*, 35 cm (9.18 m – 9.53 m).

Bed n5b, dark cherty limestone with 3 cm ash bed at the base, containing brachiopods *Spinomarginifera lopingensis*, 18 cm (9.0 m – 9.18 m).

Bed n5a, dark grey medium-bedded limestone containing the brachiopod *Spinomarginifera lopingensis*, the conodont *Jinogondolella granti*, ammonoids and corals, 22 cm (8.78 m – 9.0 m).

Unit n4. Dark grey medium-bedded crinoid limestone, 1.48 m (7.3 m – 8.78 m).

Bed n4k, dark grey thin-bedded crinoid limestone, 11 cm (8.67 m – 8.78 m).

Bed n4j, dark grey thick-bedded crinoid limestone with thin cherty bands, containing abundant nautiloids and conodont *Jinogondolella granti*, 15 cm (8.52 m – 8.67 m).

Bed n4i, dark grey thick-bedded crinoid limestone, containing abundant conodont *Jinogondolella granti*, 11 cm (8.41 m – 8.52 m)

Bed n4h, dark grey medium-bedded or lenticular crinoid limestone, containing abundant conodont *Jinogondolella granti*, 11 cm (8.30 m – 8.41 m)

Bed n4g, dark grey medium-bedded or lenticular crinoid limestone, 5 cm (8.25 m – 8.30 m)

Bed n4f, dark grey medium-bedded crinoid limestone, containing abundant conodont *Jinogondolella granti*, 25 cm (8.0 m – 8.25 m)

Bed n4e, dark grey medium-bedded crinoid limestone, containing abundant conodont *Jinogondolella granti*, 13 cm (7.87 m – 8.0 m)

Bed n4d, dark grey medium-bedded crinoid limestone, containing abundant conodont *Jinogondolella granti*, 12 cm (7.65 m – 7.87 m)

Bed n4c, dark grey medium-bedded crinoid limestone, containing abundant conodont *Jinogondolella granti*, 14 cm (7.51 m – 7.65 m)

Bed n4b, dark grey medium-bedded limestone, containing some reddish breccia and abundant crinoid fragments and abundant conodont *Jinogondolella granti*, bedding plane corrugated, 13 cm (7.38 m – 7.51 m)

Bed n4a, dark grey medium-bedded limestone with cherty bands, containing abundant crinoids and conodont *Jinogondolella granti*, 8 cm (7.30 m – 7.38 m)

Unit n3. Pale grey thick-bedded limestone containing abundant brachiopods including *Spinomarginifera lopingensis*, 2.95 m (4.35 m – 7.30 m)

Unit n2. Greyish thin- to medium-bedded limestone with chert bands along the bedding plane, 0.94 cm (3.41 m – 4.35 m)

Unit n1, mostly covered

7.2. Appendix 2: Description of the SABS at Fengshan (Fig. 4)

The section is measured 80 m-thick and every metre is marked with paint on the outcrop. Limestone beds are dominant and 32 lithological units have been identified, with some units subdivided into several subunits. Samples of conodonts, fusulines and brachiopods and other fossils were collected from this section. More than 130 samples with an average weight between 5-20 kg have been collected from each limestone bed across the GLB.

Lower part of Lopingian Heshan Formation (18.3 m thick in total)

Unit 32. Dark grey to greyish, thin- to medium-bedded, bioclastic wackestone and lime mudstone, intercalated with thin-bedded bioclastic packstone, yielding conodont *Clarkina guangyuanensis*, *Hindeodus julfensis*, *H. sp.*, *Merrilina divergens*; and fusuline *Reichelina changhsingensis*. 8.3 m (72.5 m – 80.8 m)

Unit 31. Pale grey to greyish thick-bedded rudstone and floatstone containing fusuline *Reichelina changhsingensis*. 0.75 m (71.75 m – 72.5 m).

Unit 30. Dark to pale grey, thin- to medium-bedded, bioclastic packstone or wackestone with cherty nodules and bands. Containing conodont *Clarkina asymmertica*, *Hindeodus julfensis*, *H. sp.*; and fusuline *Reichelina changhsingensis*. 2.4 m (69.35 m – 71.75 m)

Unit 29. Dark grey to greyish, thin- to medium-bedded bioclastic packstone, wackestone and lime mudstone with cherty-nodules, yielding conodont *Clarkina dukouensis*, *Hindeodus julfensis*, *H. sp.*, *Iranognathus sp.*; and fusuline *Reichelina changhsingensis*. 4.7 m (64.65 m – 69.35 m)

Unit 28. Dark grey to greyish, medium-bedded wackestone and lime mudstone, yielding conodont *Clarkina postbitteri*, *C. dukouensis*, *Hindeodus sp.* and *Iranognathus sp.* 2.15 m (62.5 m – 64.65 m). This unit has been further subdivided into 9 subunits.

28-9. Dark grey, thin- to medium-bedded, bioclastic wackestone-lime mudstone, yielding the conodont *Clarkina dukouensis*. 0.3 m (64.35 m – 64.65 m);

28-8. Dark grey, thin- to medium-bedded, bioclastic packstone-wackestone, yielding the conodonts *Clarkina dukouensis*, *Iranognathus sp.*, *Hindeodus sp.* 0.94 m (63.41 m – 64.35 m);

28-7. Dark grey, medium-bedded, bioclastic wackestone-lime mudstone, yielding the conodonts *Clarkina dukouensis*, *Hindeodus sp.* 0.2 m (63.21 m – 63.41 m);

28-6. Dark grey, lenticular, bioclastic packstone-wackestone. 0.05 m (63.16 m – 63.21 m);

28-5. Dark grey, medium-bedded, bioclastic wackestone-lime mudstone, yielding the conodonts *Clarkina dukouensis*, *C.*

postbitteri, *Hindeodus* sp. 0.18 m (62.98 m – 63.16 m);

28-4. Dark grey, lenticular, bioclastic packstone-wackestone. 0.04 m (62.94 m – 62.98 m);

28-3. Dark grey, medium-bedded, bioclastic wackestone-lime mudstone, yielding the conodonts *Clarkina postbitteri*, *Hindeodus* sp. 0.11 m (62.83 m – 62.94 m);

28-2. Dark grey, lenticular, bioclastic packstone-wackestone. 0.08 m (62.75 m – 62.83 m);

28-1. Dark grey, medium-bedded, bioclastic wackestone-lime mudstone, yielding the conodonts *Clarkina postbitteri*, *Hindeodus* sp., *Iranognathus* sp. 0.25 m (62.5 m – 62.75 m);

Unit 27. Grey medium-bedded bioclastic grainstone, pinching out laterally. 0.2 m (62.3 m – 62.5 m)

—————conformity—————

Upper part of Maokou Formation (68.8 m in total)

Unit 26. Grey to dark grey, bedded to nodular bioclastic packstone, wackestone and grainstone, yielding conodont *Clarkina postbitteri*, *Jinogondolella granti*, *J. xuanhanensis*, *Sweetognathus fengshanensis*, *Hindeodus* sp. and fusuline *Reichelina changhsingensis*, *R. simplex* and *Lantschichites minima*. 1.2 m (61.1 m – 62.3 m). This unit is subdivided into three subunits:

26-3. Grey to dark grey, nodular, bioclastic packstone-wackestone, yielding the conodont *Clarkina postbitteri*, *Jinogondolella granti*, *Sweetognathus fengshanensis*, *Hindeodus* sp. 0.5 m (61.8 m – 62.3 m). The Guadalupian/Lopingian boundary is correlated at 62.0m in this bed, 30cm below the top of Unit 26 (Fig. 8). The sample between 62.0 m – 62.3 m contains both *Clarkina postbitteri* and *Jinogondolella granti*, and some transitional forms between these two species.

26-2. Dark grey bioclastic grainstone-rudstone, yielding *Jinogondolella* sp. 0.1 m (61.7 m – 61.8 m);

26-1. Grey to dark grey, nodular, bioclastic packstone-wackestone, yielding the conodont *Jinogondolella granti*, transitional to *J. granti*, *J. xuanhanensis*, *Hindeodus* sp. 0.6 m (61.1 m – 61.7 m).

Unit 25. Pale grey, medium-bedded bioclastic wackestone, packstone and grainstone yielding conodont *Jinogondolella granti*, transitional to *J. granti*, *J. xuanhanensis*, *Hindeodus* sp.; fusuline *Chenella changanchiaoensis*, *Codonofusiella extensa*, *C. paradoxa*, *Kahlerina pachythea*, *Lantschichites minima*, *Rauserella erratica*, *Reichelina changhsingensis*, *R. simplex*. 1.6 m (59.5 m – 61.1 m). This unit is subdivided into 8 subunits.

25-8. Pale grey medium-bedded bioclastic grainstone-rudstone, yielding the conodonts *Jinogondolella granti*, *Hindeodus* sp. 0.2 m (60.90 m – 61.10 m);

25-7. Pale to dark grey, nodular, bioclastic packstone, wackestone or lime mudstone, yielding the conodonts *Jinogondolella xuanhanensis*, transitional to *Jinogondolella granti*. 0.25 m (60.65 m – 60.90 m);

25-6b. Pale grey medium-bedded bioclastic grainstone-rudstone, yielding the conodonts *Hindeodus* sp., transitional to *Jinogondolella granti*. 0.2 m (60.45 m – 60.65 m);

25-6a. Pale grey sponge-brachiopod floatstone. 0.1 m (60.35 m – 60.45 m);

25-5. Pale to dark grey, nodular, bioclastic wackestone-lime mudstone, yielding the conodont *Jinogondolella xuanhanensis*.

0.1 m (60.25 m – 60.35 m);

25-4. Pale to dark grey, nodular, bioclastic wackestone-lime mudstone, yielding the conodonts *Hindeodus* sp., transitional to *Jinogondolella granti*. 0.25 m (60.0 m – 60.25 m);

25-3. Grey to pale grey, medium-bedded, bioclastic wackestone, packstone or grainstone, yielding the conodont *Jinogondolella* sp. 0.3 m (59.7 m – 60.0 m);

25-2. Pale grey nodular bioclastic wackestone. 0.05 m (59.65 m – 59.7 m);

25-1. Pale grey, medium-bedded, bioclastic grainstone-rudstone. 0.15 m (59.5 m – 59.65 m).

Unit 24. Dark reddish, grey, thick-bedded and massive reef limestone yielding conodont *Jinogondolella xuanhanensis*, transitional to *J. granti*, *Sweetognathus fengshanensis*; and fusuline *Chenella changanchiaoensis*, *Codonofusiella schubertelloides*, *C. paradoxa*, *C. extensa*, *Kahlerina pachythea*, *Lantschichites minima*, *Reichelina simplex*, *Nankinella nanjingensis*, *Rauserella erratica*, *Schwagerina serrata*, *Metadoliolina multivoluta*, *M. douvillei*. 1.9 m (57.6 m – 59.5 m)

Unit 23. Pale grey to greyish, very thick-bedded, bioclastic packstone, grainstone and rudstone yielding conodont *Jinogondolella xuanhanensis*, transitional to *J. granti*, *Sweetognathus fengshanensis*, *Hindeodus* sp.; fusuline *Reichelina changhsingensis*, *R. simplex*, *Lantschichites minima*, *Kahlerina pachythea*, *K. sinensis*, *Codonofusiella paradoxa*, *C. schubertelloides*, *Chenella changanchiaoensis*, *Rauserella erratica*, *Metadoliolina multivoluta*, *M. douvillei*, *M. delicata*, *Schwagerina serrata*, *Nankinella nanjingensis*, *Chusenella douvillei*, *C. globularis*, *Neoschwagerina* sp.; and brachiopods *Alphaneospirifer pyramidiformis*, *Juxathyris guizhouensis*, *Enteleter kayseri*, *Martinia* sp. 29.9 m (27.7 m – 57.6 m)

Unit 22. Dark reddish grey, very thick-bedded, reef limestone yielding conodont *Jinogondolella xuanhanensis*, *Sweetognathus fengshanensis*, *Hindeodus* sp.; fusuline *Chenella changanchiaoensis*, *Lantschichites minima*, *Kahlerina pachythea*; and brachiopod *Urushtenoidea crenulata*, *Martinia* sp., *Juxathyris guizhouensis*, *Juxathyris* sp., *Uncinunellina timorensis*, *Permophricodothyris* sp. 9.8 m (17.9 m – 27.7 m)

Unit 21. Pale grey, very thick-bedded, bioclastic and lithoclastic rudstone containing conodont *Jinogondolella xuanhanensis*; and fusuline *Lantschichites minima*, *Reichelina changhsingensis*, *Rauserella erratica* and brachiopods *Permophricodothyris elegantula*, *Alphaneospirifer* sp., *Juxathyris* sp., *Spinomarginifera* sp., *Enteleter* sp., *Zhejiangospirifer abnormalis*. 2.8 m (15.1 m – 17.9 m)

Unit 20. Pale to dark grey, nodular, bioclastic wackestone-lime mudstone. 0.25 m (14.85 m – 15.1 m)

Unit 19. Pale grey medium-bedded bioclastic grainstone. 0.3 m (14.55 m – 14.85 m)

Unit 18. Grey to dark grey, nodular, bioclastic packstone, wackestone and lime mudstone yielding conodont *Sweetognathus fengshanensis* and *Jinogondolella xuanhanensis*. 0.3 m (14.25 m – 14.55 m)

Unit 17. Pale grey, medium- to very thick-bedded, bioclastic grainstone yielding conodont *Jinogondolella xuanhanensis* and fusuline *Schwagerina serrata*. 1.55 m (12.7 m – 14.25 m)

Unit 16. Pale to dark grey, nodular, bioclastic wackestone and lime mudstone yielding conodont transitional to *Jinogondolella xuanhanensis*. 0.15 m (12.55 m – 12.7 m)

Unit 15. Pale grey, thin-bedded, bioclastic grainstone. 0.1 m (12.45 m–12.55 m)

Unit 14. Pale to dark grey, nodular, bioclastic packstone, wackestone and lime mudstone yielding conodont transitional to *Jinogondolella xuanhanensis*. 0.2 m (12.25 m – 12.45 m)

Unit 13. Pale grey, medium- to thick-bedded, bioclastic grainstone. 0.3 m (11.95 m – 12.25 m)

Unit 12. Grey to pale grey, nodular, bioclastic wackestone and lime mudstone yielding conodont *Sweetognathus fengshanensis*, transitional to *Jinogondolella xuanhanensis*. 0.25 m (11.7 m – 11.95 m)

Unit 11. Pale grey, medium- to thick-bedded, bioclastic grainstone yielding fusuline *Metadoliolina multivoluta*, *M. douvillei*. 0.8 m (10.9 m – 11.7 m)

Unit 10. Grey to pale grey, bioclastic wackestone, lime mudstone and rudstone yielding conodont *Sweetognathus fengshanensis*, transitional to *Jinogondolella xuanhanensis*. 0.15 m (10.75 m – 10.9 m)

Unit 9. Pale grey, medium- to thick-bedded, bioclastic grainstone. 0.35 m (10.4 m – 10.75 m)

Unit 8. Grey to dark grey, nodular, bioclastic packstone, wackestone and lime mudstone. 0.2 m (10.2 m – 10.4 m)

Unit 7. Pale grey, medium- to thick-bedded, bioclastic grainstone yielding conodont transitional to *Jinogondolella xuanhanensis*. 0.7 m (9.5 m – 10.2 m)

Unit 6. Grey to dark grey, nodular, bioclastic wackestone and lime mudstone. 0.1 m (9.4 m – 9.5 m)

Unit 5. Pale grey, medium- to thick-bedded, bioclastic grainstone yielding conodont *Sweetognathus fengshanensis*, transitional to *Jinogondolella xuanhanensis*. 0.7 m (8.7 m – 9.4 m)

Unit 4. Dark grey nodular bioclastic wackestone. 0.05 m (8.65 m – 8.7 m)

Unit 3. Pale grey to greyish, thin- to thick-bedded, bioclastic wackestone, packstone and grainstone yielding conodont *Sweetognathus fengshanensis*, transitional to *Jinogondolella xuanhanensis*; and fusuline *Schwagerina serrata*, *Metadoliolina multivoluta*, *Kahlerina pachythea*. 6.95 m (1.7 m – 8.65 m)

Unit 2. Pale grey to greyish, medium- to thick-bedded, bioclast, lithoclast rudstone. 1.15 m (0.55 m – 1.7 m)

Unit 1. Pale grey, thick-bedded, bioclast, lithoclast rudstone yielding conodont *Sweetognathus* sp., transitional to *Jinogondolella xuanhanensis*. 0.55 m (0 m – 0.55 m)

Unit 0-1. Dark grey, thin- to medium-bedded, bioclastic wackestone containing cherty nodules yielding conodont *Sweetognathus* sp. and transitional to *Jinogondolella xuanhanensis*. 4.2 m (-4.2 m – 0 m)

Unit 0-2. Dark grey, thin- to medium-bedded, bioclastic wackestone and packstone alternating with dark to dark grey, thin-bedded cherts yielding conodonts: transitional to *Jinogondolella xuanhanensis*. 2.1 m (-4.2 m – -6.3 m)

7.3. Appendix 3: Methodology for measuring $^{87}\text{Sr}/^{86}\text{Sr}$ ratio

About 10 mg of the powders were weighed, and 10 ml of 0.2

N HAc was added to dissolve the carbonate powders at room temperature for 3 hours. After centrifugation, the supernatants were decanted to Teflon beakers and dried at 120°C; then were re-dissolved in double distilled HNO₃ for three times. Finally, the dried samples were dissolved in 6 ml 7 M HNO₃. A total of sixty-three samples were leached by this method (Fig. 7).

We also tried a sequential-leaching method followed that of Bellefroid et al. (2018) to obtain the least-altered seawater Sr isotopic signal. By comparing the lithology of our samples to Bellefroid et al. (2018), we selected the third leachate (S3 in their study) to analyze the $^{87}\text{Sr}/^{86}\text{Sr}$ ratios. About 50 mg powders were weighed and the samples were pre-leached using 7 ml of 1 N ammonium acetate (N1) (Montañez et al., 1996; Bailey et al., 2000), to remove weakly clay-adsorbed ions. Pre-leached samples were dissolved in three successive steps of 8 ml 0.04 M acetic acid (S1 to S3). For each step, samples were reacted for 15 min in an ultrasonic bath and then centrifuged. The third leachate fraction was transferred to an acid-cleaned Teflon beaker, dried down and re-dissolved in double distilled HNO₃ for three times, after which the samples were dissolved in 7 N HNO₃ for column chemistry. Twenty-three samples were dissolved by sequential-leaching method (Fig. 7).

The Sr was extracted by cation exchange resin, and the purified samples were dried and redissolved in 3% HNO₃ for $^{87}\text{Sr}/^{86}\text{Sr}$ analyses. The isotopic composition was measured by Neptune-MC-ICP-MS at Nanjing Institute of Geology and Palaeontology (NIGP), Chinese Academy of Sciences. Standard sample NBS 987 was analyzed every five samples, returning an average value of 0.710271 ($\sigma = \pm 0.000005$, $n = 11$). The measured $^{87}\text{Sr}/^{86}\text{Sr}$ values were normalized to $^{86}\text{Sr}/^{88}\text{Sr}$ of 0.1194, and the standard errors for Sr isotope analyses are between 0.000004 and 0.000015. All the results were corrected to NBS 987 as 0.710248 (McArthur et al., 2001).

A split of 5 ml from each dissolved leachate was dried and then redissolved by 5% HNO₃ for major and trace element analysis on an Agilent 710 ICP-OES at NIGP. Calibration standards were made in-house using certified single element standards and were mixed to match typical carbonate concentration ranges. Geological standard samples JLs-1 (limestone) and JDo-1 (dolostone) were measured every ten samples as external reference standards. The precision of the analysis is better than 5%.

References

- Angiolini, L. and Carabelli, L., 2010. Upper Permian brachiopods from the Nesen formation, North Iran. *Special Paper in Palaeontology*, n. 84, p. 41–90.
- Bailey, T.R., McArthur, J.M., Prince, H. and Thirlwall, M.F., 2000. Dissolution methods for strontium isotope stratigraphy whole rock analysis. *Chemical Geology*, v. 167, p. 313–319.
- Baud, A., Richoz, S., Beauchamp, B., Cordey, F., Grasby, S., Henderson, C. M., Krystyn, L. and Nicora, A., 2012. The Buday'ah Formation, Sultanate of Oman: A Middle Permian to Early Triassic oceanic record of the Neotethys and the late Induan microsphere bloom. *Journal of Asian Earth Sciences*, v. 43, n. 1, p. 130–144.
- Bell, G.L.J., Hearst, J.M., Nestell, M.K., Nestell, G.P. and

- Lambert, L.L., 2015. Stratigraphic framework and biostratigraphic significance of the terminal Guadalupian Reef Trail Member, Bell Canyon Formation in the Patterson Hills, Type Guadalupian Area, Texas. *Stratigraphy*, v. 12, n. 2, p. 93–107.
- Bellefroid, E.J., Planavsky, N.J., Miller, N.R., Brand, U. and Wang, C., 2018. Case studies on the utility of sequential carbonate leaching for radiogenic strontium isotope analysis. *Chemical Geology*, v. 497, p. 88–99.
- Bond, D.P.G., Hilton, J., Wignall, P.B., Ali, J.R., Stevens, L.G., Sun, Y.D. and Lai, X.L., 2010. The Middle Permian (Capitanian) mass extinction on land and in the oceans. *Earth-Science Reviews*, v. 102, n. 1–2, p. 100–116.
- Chen, B., Joachimski, M.M., Sun, Y.D., Shen, S.Z. and Lai, X.L., 2011. Carbon and conodont apatite oxygen isotope records of Guadalupian–Lopingian boundary sections: Climatic or sea-level signal?. *Palaeogeography, Palaeoclimatology, Palaeoecology*, v. 311, n. 3–4, p. 145–153.
- Chen, J. and Xu, Y.G., 2019. Establishing the link between Permian volcanism and biodiversity changes: Insights from geochemical proxies. *Gondwana Research*, v. 75, p. 68–96.
- Clapham, M.E., Shen, S.Z. and Bottjer, D.J., 2009. The double mass extinction revisited: reassessing the severity, selectivity, and causes of the end-Guadalupian biotic crisis (Late Permian). *Paleobiology*, v. 35, n. 1, p. 32–50.
- Crippa, G. and Angiolini, L., 2012. Guadalupian (Permian) brachiopods from the Ruteh Limestone, North Iran. *Georabia*, v. 17, n. 1, p. 125–176.
- Erwin, D.H., 2006. *Extinction: How life on Earth nearly ended 250 million years ago*. Princeton University Press, New Jersey, 296pp.
- Fan, J.X., Shen, S.Z., Erwin, D.H., Sadler, P.M., MacLeod, N., Cheng, Q.M., Hou, X.D., Yang, J., Wang, X.D., Wang, Y., Zhang, H., Chen, X., Li, G.X., Zhang, Y.C., Shi, Y.K., Yuan, D.X., Chen, Q., Zhang, L.N., Li, C. and Zhao, Y.Y., 2020. A high-resolution summary of Cambrian to Early Triassic marine invertebrate biodiversity. *Science*, v. 367, n. 6475, p. 272–277.
- Garbelli, C., Angiolini, L., Shen, S.Z., Crippa, G., Yuan, D.X., Bahrammanesh, M., Abbasi, S. and Birjandi, M., 2014. Additional brachiopod findings from the Lopingian succession of the Ali Bashi Mountains, NW Iran. *Rivista Italiana di Paleontologia e Stratigrafia*, v. 120, n. 1, p. 119–126.
- Ghaderi, A., Garbelli, C., Angiolini, L., Ashouri, A.R., Korn, D., Rettori, R. and Gharaie, M.H.M., 2014. Faunal change near the end-Permian extinction: the brachiopods of the Ali Bashi Mountains, NW Iran. *Rivista Italiana di Paleontologia e Stratigrafia*, v. 120, n. 1, p. 27–59.
- Hao, W.C., Yao, J.X. and Liu, J.B., 1999. Permian conodonts from the Shaiwa section in Ziyun, Guizhou. In Yao, A., Ezaki, Y., Hao, W.C. and Wang, X.P. (eds.), *Biotic and Geological Developments of the Paleo-Tethys in China*, Beijing, Peking University Press, p. 73–79.
- Haq, B.U. and Schutter, S.R., 2008. A chronology of Paleozoic sea-level changes. *Science*, v. 322, n. 5898, p. 64–68.
- He, B., Xu, Y.G., Huang, X.L., Luo, Z.Y., Shi, Y.R., Yang, Q.J. and Yu, S.Y., 2007. Age and duration of the Emeishan flood volcanism, SW China: Geochemistry and SHRIMP zircon U-Pb dating of silicic ignimbrites, post-volcanic Xuanwei Formation and clay tuff at the Chaotian section. *Earth and Planetary Science Letters*, v. 255, n. 3–4, p. 306–323.
- Head, M.J., Aubry, M.P., Piller, W.E. and Walker, M., 2022. The Standard Auxiliary Boundary Stratotype: a proposed replacement for the Auxiliary Stratotype Point in supporting a Global boundary Stratotype Section and Point (GSSP). Episodes, in press.
- Henderson, C.M., Mei, S.L. and Wardlaw, B.R., 2002. New conodont definitions at the Guadalupian-Lopingian boundary. *Carboniferous and Permian of the world; XIV ICCP proceedings: Memoir Canadian Society of Petroleum Geologists*, v. 19, p. 725–735.
- Hou, Z.S., Fan, J.X., Henderson, C.M., Yuan, D.X., Shen, B.H., Wu, J., Wang, Y., Zheng, Q.F., Zhang, Y.C., Wu, Q. and Shen, S.Z., 2020. Dynamic palaeogeographic reconstructions of the Wuchiapingian Stage (Lopingian, Late Permian) for the South China Block. *Palaeogeography, Palaeoclimatology, Palaeoecology*, v. 546, p. 109667.
- Hounslow, M.W. and Balabanov, Y.P., 2018. A geomagnetic polarity timescale for the Permian, calibrated to stage boundaries. *Geological Society, London, Special Publications*, v. 450, n. 1, p. 61–103.
- Hu, S.Z., 1994. On the event of Dongwu Movement and its relation with Permian subdivision. *Journal of Stratigraphy*, v. 18, n. 4, p. 309–315.
- Huang, H., Huyskens, M.H., Yin, Q.Z., Cawood, P.A., Hou, M.C., Yang, J.H., Xiong, F.H., Du, Y.S. and Yang, C.C., 2022. Eruptive tempo of Emeishan large igneous province, southwestern China and northern Vietnam: Relations to biotic crises and paleoclimate changes around the Guadalupian-Lopingian boundary. *Geology*, v. 50, n. 9, p. 1083–1087.
- Iranian-Japanese-Research-Group, 1981. The Permian and Lower Triassic Systems in Abadeh region, central Iran. *Memoirs of the Faculty of Sciences, Kyoto University, Series of Geology and Mineralogy*, v. 47, n. 2, p. 61–133.
- Isozaki, Y., Kawahata, H. and Ota, A., 2007. A unique carbon isotope record across the Guadalupian–Lopingian (Middle–Upper Permian) boundary in mid-oceanic paleo-atoll carbonates: The high-productivity “Kamura event” and its collapse in Panthalassa. *Global and Planetary Change*, v. 55, n. 1–3, p. 21–38.
- Ji, X.X., Li, M. and Feng, H.Z., 2009. Middle Permian conodonts from the Shaiwa Group in Sidazhai area, Ziyun County, Guizhou. *Geological Review*, v. 55, n. 1, p. 113–120.
- Jin, Y.G., 1993. Pre-Lopingian benthos crisis. *Comptes Rendus XII ICC-P, Volume 2: Buenos Aires*, p. 269–278.
- Jin, Y.G., 2000. Conodont definition on the basal boundary of Lopingian stages: A report from the International Working Group on the Lopingian Series. *Permophiles*, n. 36, p. 37–40.
- Jin, Y.G., Zhang, J. and Shang, Q.H., 1994. Two phases of the end-Permian mass extinction. In Embry, A.F., Beauchamp, B. and Glass, D.J. (eds.), *Canadian Society of Petroleum Geologists, Memoir 17, Volume 17: Calgary, Canadian Society of Petroleum Geologists*, p. 813–822.
- Jin, Y.G., Shang, Q.H. and Cao, C.Q., 2000. Late Permian

- magnetostratigraphy and its global correlation. *Chinese Science Bulletin*, v. 45, n. 8, p. 698–705.
- Jin, Y.G., Henderson, C.M., Wardlaw, B.R. and Glenister, B.F., 2001a. A commentary on the proposal for the GSSP for the Guadalupian/Lopingian boundary. *Permophiles*, n. 38, p. 30–35.
- Jin, Y.G., Henderson, C.M., Wardlaw, B.R., Glenister, B.F., Mei, S.L., Shen, S.Z. and Wang, X.D., 2001b. Proposal for the global stratotype section and point (GSSP) for the Guadalupian-Lopingian boundary. *Permophiles*, n. 39, p. 32–42.
- Jin, Y.G., Shen, S.Z., Henderson, C.M., Wang, X.D., Wang, W., Wang, Y., Cao, C.Q. and Shang, Q.H., 2006. The Global Stratotype Section and Point (GSSP) for the boundary between the Capitanian and Wuchiapingian stage (Permian). *Episodes*, v. 29, n. 4, p. 253–262.
- Kani, T., Hisanabe, C. and Isozaki, Y., 2013. The Capitanian (Permian) minimum of $^{87}\text{Sr}/^{86}\text{Sr}$ ratio in the mid-Panthalassan paleo-atoll carbonates and its demise by the deglaciation and continental doming. *Gondwana Research*, v. 24, n. 1, p. 212–221.
- Kani, T., Isozaki, Y., Hayashi, R., Zakharov, Y. and Popov, A., 2018. Middle Permian (Capitanian) seawater $^{87}\text{Sr}/^{86}\text{Sr}$ minimum coincided with disappearance of tropical biota and reef collapse in NE Japan and Primorye (Far East Russia). *Palaeogeography, Palaeoclimatology, Palaeoecology*, v. 499, p. 13–21.
- Kani, T. and Isozaki, Y., 2021. The Capitanian Minimum: A Unique Sr Isotope Beacon of the Latest Paleozoic Seawater. *Frontiers in Earth Science*, v. 9, p. 662581.
- Korte, C. and Ullmann, C.V., 2016. Permian strontium isotope stratigraphy. In Lucas, S.G., and Shen, S.Z. (eds.), *The Permian Timescale*, The Geological Society of London, London, v. 450, p. 105–118.
- Korte, C., Jasper, T., Kozur, H.W. and Veizer, J., 2006. $\text{Sr}^{87}/\text{Sr}^{86}$ record of Permian seawater. *Palaeogeography Palaeoclimatology Palaeoecology*, v. 240, n. 1–2, p. 89–107.
- Kotljarskiy, G.V., Zakharov, Y.D., Koczyrkevich, B.V., Kropatcheva, G.S., Rostovcev, K.O., Chedija, I.O., Vuks, G.P. and Guseva, E.A., 1983. *Pozdnepermiskii Etap Evoliutsii Organicheskogo Mira, Dzhul'finskii i Dorashamskii Iarusy SSSR (Evolution of the latest Permian biota, Dzhulfian and Dorashamian regional stages in the USSR)*. Leningrad, Nauka, 200 pp.
- Kozur, H.W. and Wang, C.Y., 2002. Comments to the base of the Lopingian Series defined in the Penglaitan section. *Permophiles*, n. 40, p. 25–30.
- Lambert, L.L., Wardlaw, B.R., Nestell, M.K. and Nestell, G.P., 2002. Latest Guadalupian (Middle Permian) conodonts and foraminifers from West Texas. *Micropaleontology* v. 48, n. 4, p. 343–364.
- Lambert, L.L., Bell, G.L., Fronimos, J.A., Wardlaw, B.R. and Yisa, M.O., 2010. Conodont biostratigraphy of a more complete Reef Trail Member section near the type section, latest Guadalupian Series type region. *Micropaleontology*, v. 56, n. 1–2, p. 233–253.
- Li, Q., Yang, S., Azmy, K., Chen, H., Hou, M., Wang, Z., Xu, S., Yang, D., Zhang, X. and Chen, A., 2021. Strontium isotope evolution of Middle Permian seawater in the Sichuan Basin, South China: Possible causes and implications. *Palaeogeography, Palaeoclimatology, Palaeoecology*, v. 565, p. 110188.
- Li, Y.J., He, H.Y., Ivanov, A.V., Demonterova, E.I., Pan, Y.X., Deng, C.L., Zheng, D.W. and Zhu, R.X., 2018. $^{40}\text{Ar}/^{39}\text{Ar}$ age of the onset of high-Ti phase of the Emeishan volcanism strengthens the link with the end-Guadalupian mass extinction. *International Geology Review*, v. 60, n. 15, p. 1906–1917.
- Liu, X.C., Wang, W., Shen, S.Z., Gorgij, M.N., Ye, F.C., Zhang, Y.C., Furuyama, S., Kano, A. and Chen, X.Z., 2013. Late Guadalupian to Lopingian (Permian) carbon and strontium isotopic chemostratigraphy in the Abadeh section, central Iran. *Gondwana Research*, v. 24, n. 1, p. 222–232.
- McArthur, J.M., Howarth, R.J. and Bailey, T.R., 2001. Strontium isotope stratigraphy: LOWESS Version 3: Best fit to the marine Sr-isotope curve for 0–509 Ma and accompanying look-up table for deriving numerical age. *The Journal of Geology*, v. 109, n. 2, p. 155–170.
- McArthur, J.M., Howarth, R.J. and Shields, G.A., 2012. Strontium isotope stratigraphy. In Gradstein, F.M., Ogg, J.G., Schmitz, M.D., and Ogg, G.M. (eds.), *The Geological time scale 2012*, Volume vol. 2, Elsevier, Amsterdam, p. 127–144.
- McArthur, J.M., Howarth, R.J., Shields, G.A. and Zhou, Y., 2020. Strontium isotope stratigraphy. In Gradstein, F.M., Ogg, J.G., Schmitz, M.D., and Ogg, G.M. (eds.), *Geologic Time Scale 2020*, Volume 1, Elsevier, Amsterdam, p. 211–238.
- Mei, S.L. and Wardlaw, B.R., 1996. On the Permian "liangshanensis-bitteri" zone and the related problems In Wang, H.Z., and Wang, X.L. (eds.), *Centennial Memorial Volume of Professor Sun Yunzhu: Stratigraphy and Palaeontology*, China University of Geosciences Press, Wuhan, p. 130–140.
- Mei, S.L. and Henderson, C.M., 2001. Evolution of Permian conodont provincialism and its significance in global correlation and paleoclimate implication. *Palaeogeography, Palaeoclimatology, Palaeoecology*, v. 170, n. 3–4, p. 237–260.
- Mei, S.L., Jin, Y.G. and Wardlaw, B.R., 1994a. Succession of conodont zones from the Permian "Kuhfeng" Formation, Xuanhan, Sichuan and its implications in global correlation. *Acta Palaeontologica Sinica*, v. 33, n. 1, p. 1–23.
- Mei, S.L., Jin, Y.G. and Wardlaw, B.R., 1994b. Zonation of conodonts from the Maokouan-Wuchiapingian boundary strata, South China. In Jin, Y.G., Utting, J., and Wardlaw, B.R. (eds.), *Permian stratigraphy, environments and resources*, Nanjing University Press, Nanjing, *Palaeoworld*, v. 4, p. 225–233.
- Mei, S.L., Jin, Y.G. and Wardlaw, B.R., 1998. Conodont succession of the Guadalupian-Lopingian boundary strata in Laibin of Guangxi, China and West Texas, USA. In Jin, Y.G., Wardlaw, B.R., and Wang, Y. (eds.), *Permian stratigraphy, environments and resources*, Nanjing University Press, Nanjing, *Palaeoworld*, v. 9, p. 53–76.
- Mei, S.L., Shi, X.Y., Chen, X.F., Sun, K.Q. and Yan, J.X., 1999. Permian Cisuralian and Guadalupian sequence stratigraphy in south Guizhou and central Guangxi and its relation

- to conodont evolution. *Earth Science-Journal of China University of Geosciences*, v. 24, n. 1, p. 21–31.
- Menning, M., Jin, Y.G. and Shen, S.Z., 1996. The Illawarra Reversal (265 Ma) in the marine Permian, Guangxi, South China. In *Proceedings Abstracts to 30th International Geological Congress, Beijing*, v. 2, p. 9.
- Miller, A.K., 1944. Part IV Permian cephalopods. In King, R.E., Dunbar, C.O.J., Cloud, P.E., and Miller, A.K. (eds.), *Geology and Paleontology of the Permian Area Northwest of Las Delicias, Southwestern Coahuila, Mexico*. Geological Society of America Special Paper, Volume 52, p. 71–127.
- Montañez, I.P., Banner, J.L., Osleger, D.A., Borg, L.E. and Bosserman, P.J., 1996. Integrated Sr isotope variations and sea-level history of Middle to Upper Cambrian platform carbonates: Implications for the evolution of Cambrian seawater $^{87}\text{Sr}/^{86}\text{Sr}$. *Geology*, v. 24, n. 10, p. 917–920.
- Nishikane, Y., Kaiho, K., Takahashi, S., Henderson, C.M., Suzuki, N., and Kanno, M., 2011. The Guadalupian-Lopingian boundary (Permian) in a pelagic sequence from Panthalassa recognized by integrated conodont and radiolarian biostratigraphy, *Marine Micropaleontology*, v. 78, n. 3–4, p. 84–95.
- Ramezani, J. and Bowring, S.A., 2018. Advances in numerical calibration of the Permian timescale based on radioisotopic geochronology. Geological Society, London, Special Publications, v. 450, n. 1, p. 51–60.
- Saitoh, M., Isozaki, Y., Ueno, Y., Yoshida, N., Yao, J.X. and Ji, Z.S., 2013. Middle–Upper Permian carbon isotope stratigraphy at Chaotian, South China: Pre-extinction multiple upwelling of oxygen-depleted water onto continental shelf. *Journal of Asian Earth Sciences*, v. 67–68, p. 51–62.
- Shellnutt, J.G., Denyszyn, S.W. and Mundil, R., 2012. Precise age determination of mafic and felsic intrusive rocks from the Permian Emeishan large igneous province (SW China). *Gondwana Research*, v. 22, n. 1, p. 118–126.
- Shellnutt, J.G., Pham, T.T., Denyszyn, S.W., Yeh, M.W. and Tran, T.A., 2020. Magmatic duration of the Emeishan large igneous province: Insight from northern Vietnam. *Geology*, v. 48, n. 5, p. 457–461.
- Shen, S.Z., 2018. Global Permian brachiopod biostratigraphy: an overview. Geological Society, London, Special Publications, v. 450, n. 1, p. 289–320.
- Shen, S.Z. and Zhang, Y.C., 2008. Earliest Wuchiapingian (Lopingian, late Permian) brachiopods in southern Hunan, South China: implications for the pre-Lopingian crisis and onset of Lopingian recovery/radiation. *Journal of Paleontology*, v. 82, n. 5, p. 924–937.
- Shen, S.Z. and Shi, G.R., 2009. Latest Guadalupian brachiopods from the Guadalupian/Lopingian boundary GSSP section at Penglaitan in Laibin, Guangxi, South China and implications for the timing of the pre-Lopingian crisis. *Palaeoworld*, v. 18, n. 2–3, p. 152–161.
- Shen, S.Z., Sun, D.L. and Shi, G.R., 2003. A biogeographic mixed late Guadalupian (late Middle Permian) brachiopod fauna from an exotic limestone block at Xiukang in Lhaze county, Tibet. *Journal of Asian Earth Sciences*, v. 21, n. 10, p. 1125–1137.
- Shen, S.Z., Henderson, C.M., Bowring, S.A., Cao, C.Q., Wang, Y., Wang, W., Zhang, H., Zhang, Y.C. and Mu, L., 2010. High-resolution Lopingian (Late Permian) timescale of South China. *Geological Journal*, v. 45, n. 2–3, p. 122–134.
- Shen, S.Z. and Mei, S.L., 2010. Lopingian (Late Permian) high-resolution conodont biostratigraphy in Iran with comparison to South China zonation. *Geological Journal*, v. 45, n. 2–3, p. 135–161.
- Shen, S.Z., Wang, Y., Henderson, C.M., Cao, C.Q. and Wang, W., 2007. Biostratigraphy and lithofacies of the Permian System in the Laibin-Heshan area of Guangxi, South China. *Palaeoworld*, v. 16, n. 1–3, p. 120–139.
- Shen, S.Z., Cao, C.Q., Zhang, H., Bowring, S.A., Henderson, C.M., Payne, J.L., Davydov, V.I., Chen, B., Yuan, D.X., Zhang, Y.C., Wang, W. and Zheng, Q.F., 2013. High-resolution $\delta^{13}\text{C}_{\text{carb}}$ chemostratigraphy from latest Guadalupian through earliest Triassic in South China and Iran. *Earth and Planetary Science Letters*, v. 375, p. 156–165.
- Shen, S.Z., Zhang, H., Zhang, Y.C., Yuan, D.X., Chen, B., He, W.H., Mu, L., Lin, W., Wang, W.Q., Chen, J., Wu, Q., Cao, C.Q., Wang, Y. and Wang, X.D., 2019. Permian integrative stratigraphy and timescale of China. *Science in China Series D: Earth Sciences*, v. 62, n. 1, p. 154–188.
- Shen, S.Z., Yuan, D.X., Henderson, C.M., Wu, Q., Zhang, Y.C., Zhang, H., Mu, L., Ramezani, J., Wang, X.D., Lambert, L.L., Erwin, D.H., Hearst, J.M., Xiang, L., Chen, B., Fan, J.X., Wang, Y., Wang, W.Q., Qi, Y.P., Chen, J., Qie, W.K. and Wang, T.T., 2020. Progress, problems and prospects: An overview of the Guadalupian Series of South China and North America. *Earth-Science Reviews*, v. 211, p. 103412.
- Stanley, S.M. and Yang, X.N., 1994. A double mass extinction at the end of the Paleozoic Era. *Science*, v. 266, n. 5189, p. 1340–1344.
- Steiner, M.B., 2006. The magnetic polarity time scale across the Permian-Triassic boundary. In Lucas, S.G., Cassinis, G., and Schneider, J.W. (eds.), *Non-marine Permian biostratigraphy and biochronology*, The Geological Society, London, v. 265, p. 15–38.
- Sun, D.Y. and Xia, W.C., 2006. Identification of the Guadalupian-Lopingian boundary in the Permian in a bedded chert sequence, south China. *Palaeogeography, Palaeoclimatology, Palaeoecology*, v. 236, n. 3–4, p. 272–289.
- Taraz, H., Golshani, F., Nakazawa, K., Shimizu, D., Bando, Y., Ishii, K., Murata, M., Okimura, Y., Sakagami, S., Nakamura, K. and Tokuoka, T., 1981. The Permian and the Lower Triassic Systems in Abadeh Region, Central Iran. *Kyoto University, Faculty of Science (Geology and Mineralogy), Memoirs*, v. 47, n. 2, pp. 61–133.
- Verna, V., Angiolini, L., Chaouachi, C., Soussi, M., Henderson, C.M., Davydov, V.I., Nicora, A. and Bougdar, M., 2010. Guadalupian brachiopods from Djebel Tebaga de Medenine, South Tunisia. *Rivista Italiana di Paleontologia e Stratigrafia*, v. 116, n. 3, p. 309–349.
- Viaretti, M., Heward, A.P., Gementi, A. and Angiolini, L., 2022. Upper Cisuralian-lower Guadalupian brachiopods from the Qarari unit, Batain Plain, northeast Oman: Systematics, palaeoecology and correlation. *Rivista Italiana*

- di Paleontologia e Stratigrafia, v. 128, n. 3, p. 643–694.
- Wang, C.Y., 2000. The base of the Lopingian Series—restudy of the Penglaitan section. *Acta Micropalaeontologica Sinica*, v. 17, n. 1, p. 1–17.
- Wang, C.Y., 2001. Re-discussion of the base of the Lopingian Series. *Permophiles*, v. 38, p. 27–29.
- Wang, D.C., Jiang, H.S., Gu, S.Z. and Yan, J.X., 2016. Cisuralian–Guadalupian conodont sequence from the Shaiwa section, Ziyun, Guizhou, South China. *Palaeogeography, Palaeoclimatology, Palaeoecology*, v. 457, p. 1–22.
- Wang, W.Q., Garbelli, C., Zheng, Q.F., Chen, J., Liu, X.C., Wang, W. and Shen, S.Z., 2018. Permian $^{87}\text{Sr}/^{86}\text{Sr}$ chemostratigraphy from carbonate sequences in South China. *Palaeogeography, Palaeoclimatology, Palaeoecology*, v. 500, p. 84–94.
- Wang, W.Q., Katchinoff, J.A.R., Garbelli, C., Immenhauser, A., Zheng, Q.F., Zhang, Y.C., Yuan, D.X., Shi, Y.K., Wang, J.Y., Planavsky, N. and Shen, S.Z., 2021. Revisiting the Permian seawater $^{87}\text{Sr}/^{86}\text{Sr}$ record: New perspectives from brachiopod proxy data and stochastic oceanic box models. *Earth-Science Reviews*, v. 218, p. 103679.
- Wang, Y., Zhang, Y.C., Zheng, Q.F., Tian, X.S., Huang, X. and Luo, M., 2020. The early Wuchiapingian (late Permian) fusuline fauna from the Penglaitan Section, South China. *Papers in Paleontology*, v. 6, n. 3, p. 485–499.
- Wardlaw, B.R., 2000. Guadalupian conodont biostratigraphy of the Glass and Del Norte Mountains. In Wardlaw, B.R., Grant, R.E., and Rohr, D.M. (eds.), *The Guadalupian Symposium*, Smithsonian contributions to the Earth Sciences, Smithsonian Institution, Washington D.C., n. 32, p. 37–81.
- Wardlaw, B.R. and Henderson, C.M., 2002. Reply to Kozur and Wang's "Comments to the base of the Lopingian Series defined in the Penglaitan section. *Permophiles*, v. 40, p. 31–32.
- Wardlaw, B.R. and Nestell, M.K., 2010. Latest Middle Permian conodonts from the Apache Mountains, West Texas. *Micropaleontology*, v. 56, n. 1–2, p. 149–183.
- Wardlaw, B.R., Lamberti, L.L. and Mei, S.L., 1999. Succession of latest Guadalupian (Permian) conodont faunas from South China and West Texas. In: *Proceedings of the International Conference on Pangea and the Paleozoic-Mesozoic transition*, China University of Geosciences Press, Wuhan, p. 156.
- Wignall, P.B., Sun, Y.D., Bond, D.P.G., Izon, G., Newton, R.J., Veldre, S., Widdowson, M., Ali, J.R., Lai, X.L., Jiang, H.S., Cope, H. and Bottrell, S.H., 2009. Volcanism, mass extinction, and carbon isotope fluctuations in the Middle Permian of China. *Science*, v. 324, n. 5931, p. 1179–1182.
- Wu, Q., Ramezani, J., Zhang, H., Yuan, D.X., Erwin, D.H., Henderson, C.M., Lambert, L.L., Zhang, Y.C. and Shen, S.Z., 2020. High-precision U–Pb zircon age constraints on the Guadalupian in West Texas, USA. *Palaeogeography, Palaeoclimatology, Palaeoecology*, v. 548, p. 109668.
- Yang, J.H., Cawood, P.A., Du, Y.S., Condon, D.J., Yan, J.X., Liu, J.Z., Huang, Y. and Yuan, D.X., 2018. Early Wuchiapingian cooling linked to Emeishan basaltic weathering?. *Earth and Planetary Science Letters*, v. 492, p. 102–111.
- Yuan, D.X., Shen, S.Z. and Henderson, C.M., 2017. Revised Wuchiapingian conodont taxonomy and succession of South China. *Journal of Paleontology*, v. 91, n. 6, p. 1199–1219.
- Yuan, D.X., Shen, S.Z., Henderson, C.M., Chen, J., Zhang, H., Zheng, Q.F. and Wu, H.C., 2019. Integrative timescale for the Lopingian (Late Permian): A review and update from Shangsi, South China. *Earth-Science Reviews*, v. 188, p. 190–209.
- Zhang, L.L., Zhang, N. and Xia, W.C., 2008. Conodont succession in the Guadalupian–Lopingian boundary interval (Upper Permian) of the Maoershan section, Hubei Province, China. *Micropaleontology*, v. 53, n. 6, p. 433–446.
- Zhong, Y.T., He, B., Mundil, R. and Xu, Y.G., 2014. CA-TIMS zircon U–Pb dating of felsic ignimbrite from the Binchuan section: Implications for the termination age of Emeishan large igneous province, *Lithos*, v. 204, p. 14–19.
- Zhong, Y.T., He, B. and Xu, Y.G., 2013. Mineralogy and geochemistry of claystones from the Guadalupian–Lopingian boundary at Penglaitan, South China: Insights into the pre-Lopingian geological events. *Journal of Asian Earth Sciences*, v. 62, p. 438–462.
- Zhou, Z.R., 2017. Permian basal ammonoid sequence in Nanpanjiang area of South China—possible overlap between basal Guadalupian and platform-based Lopingian. *Journal of Paleontology*, *Memoir 74*, v. 91, p. 1–95.

The Once and Future Quest: the Kungurian GSSP candidate at Rockland Section and SABS at Carlin Canyon, Nevada

Lucia Angiolini

Dipartimento di Scienze della Terra “A. Desio”
Via Mangiagalli 34, 20133, Milano, Italy

Benoit Beauchamp

Department of Geoscience, University of Calgary
2500 University Drive NW Calgary, Alberta, Canada T2N 1N4

Luke Bratton

Department of Geoscience, University of Calgary
2500 University Drive NW Calgary, Alberta, Canada T2N 1N4

Bryana Fraser

Department of Geoscience, University of Calgary
2500 University Drive NW Calgary, Alberta, Canada T2N 1N4

Charles Henderson

Department of Geoscience, University of Calgary
2500 University Drive NW Calgary, Alberta, Canada T2N 1N4

Walt Snyder

Department of Geosciences, Boise State University
1910 University Drive, Boise ID 83725-1535 USA

Andrea Zanchi

Dipartimento di Scienze dell’Ambiente e della Terra
University of Milano-Bicocca, Milano, Italy



Fig. 1. Group photo in front of the Carlin Canyon C6 angular unconformity separating Mississippian and Lower Pennsylvanian strata below and Gzhelian to Lower Permian above. Lucia Angiolini holds a copy of the newly printed Special Publication 113. From left to right: Walter Snyder, Luke Bratton, Charles Henderson, Lucia Angiolini, Benoit Beauchamp, and Bryana Fraser.

Introduction

From October 14 to October 21, 2022, an international team composed of Lucia Angiolini (University of Milano, I), Andrea

Zanchi (University of Milano-Bicocca, I), Luke Bratton and Bryana Fraser (MSc students, University of Calgary, Canada), under the guidance of Benoit Beauchamp and Charles Henderson (University of Calgary) and Walt Snyder (Boise State University, USA) visited the Carboniferous to Lower Permian successions of Carlin Canyon (near Carlin, Nevada) and Rockland Section (near Wells, Nevada).

There were two main goals of this field trip. The first was to investigate the base-Kungurian GSSP candidate at Rockland (Henderson et al., 2012) and possible Standard Auxiliary Boundary Stratotype (SABS *sensu* Head et al., 2022 and formally recognized by ICS at the end of October 2022) at Carlin Canyon. As underlined in *Permophiles* #73 (Chair note at p. 3 and C. Henderson’s harangue at p. 6), SPS is following the IUGS statement of March 18, 2022 in reaction to the invasion of Ukraine by the Russian Federation. The sanctions mean that research on the base-Kungurian GSSP candidate at the Mechetlino section, Urals, Russia (Chernykh et al., 2012; Chernykh, 2020) cannot be continued. The geopolitical situation and the necessity to have permanent free access to a GSSP section have focussed SPS efforts to define the GSSP at the Rockland section, which records the same bioevent (*ie.* the FAD of *Neostreptognathodus pnevi*). The two sections are very

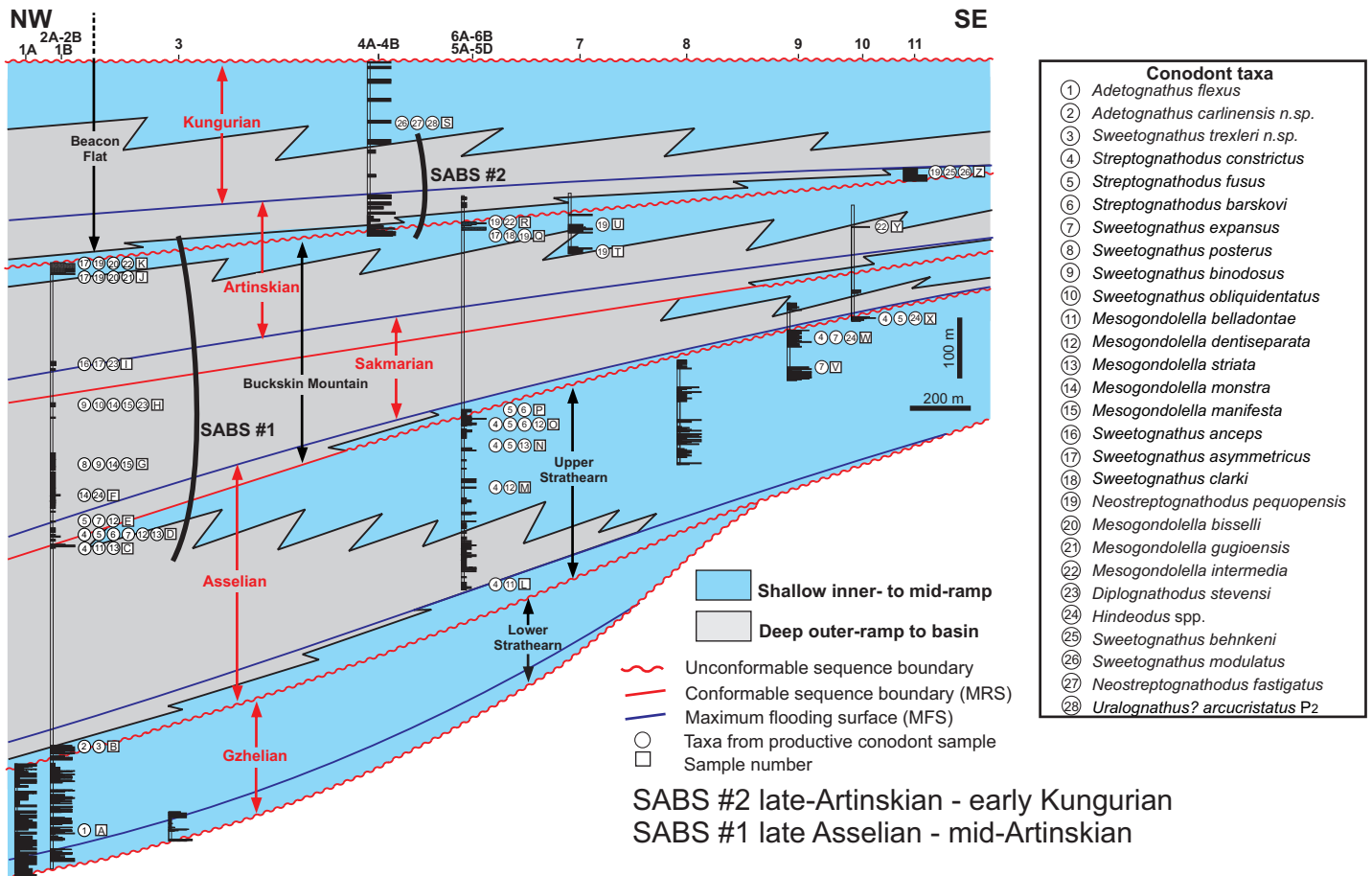


Fig. 2. Schematic cross-section of the Carlin Canyon region showing multiple progradational carbonate ramps and the position of potential Standard Auxiliary Boundary Stratotypes. SABS #1 includes upper Asselian to mid-Artinskian strata in an outer-ramp to basin setting with correlated base-Sakmarian and base-Artinskian boundaries. These boundaries at Carlin have been discussed in the Sakmarian and Artinskian GSSP proposals. Note that these boundaries coincide with the maximum flooding surfaces of 3rd order sequences. SABS #2 is a potential Standard Auxiliary Boundary Stratotype for the base-Kungurian, pending result of samples collected in October 2022. This figure is modified from Figure 8 in Beauchamp et al. (2022).



Fig. 3. A. Google Earth image of potential upper Asselian to mid-Artinskian SABS. The correlated base-Artinskian is located at 40°44.108"N; 116°00.270"W. B. The roadbed is a bedding plane (with thin sand cover) that represents the MFS of an upper Sakmarian-mid-Artinskian 3rd order sequence. The sample in white bags yielded about 200 platform specimens of *Sweetognathus* including *Sw. asymmetricus* and *Sw. anceps*. The RST can be seen in the background with mid to upper Artinskian and correlated Wolfcampian-Leonardian boundary near the horizon.

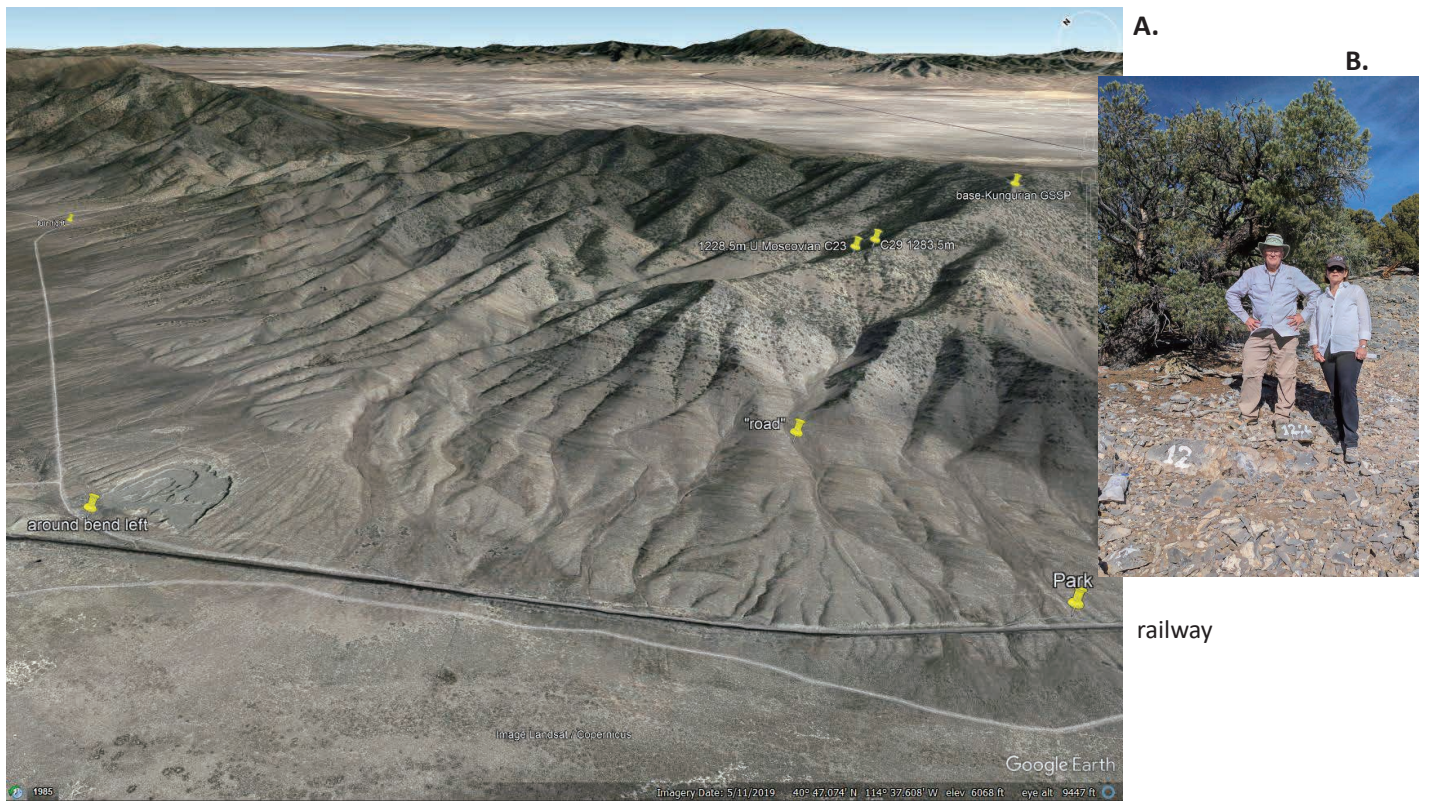


Fig. 4. A. Google Earth image of potential base-Kungurian GSSP at Rockland section, Nevada. The boundary sample is located at 40.77904°N; 114.60604°W. B. Lucia Angiolini and Charles Henderson on the base Kungurian GSSP candidate, Rockland section. Bed 12 includes the boundary with the FO of *Neostreptognathodus pnevi*.

comparable (Henderson et al., 2012).

The second goal was to consider the Carlin Canyon area as a potential SABS for the base-Sakmarian, base-Artinskian, and maybe also the base-Kungurian. The upper Asselian to upper Artinskian succession has been well studied in this area (Beauchamp et al., 2022). A new section was measured and sampled during this trip that should include the Artinskian-Kungurian boundary.

Carlin Canyon

Carlin Canyon represents a very interesting area to further investigate the potentiality of the Sakmarian, Artinskian and Kungurian successions of Nevada in terms of GSSP and SABS candidates.

Located near Carlin, famous for its gold ores (Carlin-type gold deposits) and for the Humboldt River route that pioneers followed in the 19th century (California Trail), the Upper Pennsylvanian to Kungurian succession of Carlin Canyon has been the subject of a very recently published exhaustive paper by Beauchamp et al. (2022).

Another feature of Carlin Canyon, well-known since the 20th century according to a nice quotation from McPhee (1981) and reproduced at the beginning of the introduction in Beauchamp et al. (2022), is a spectacular angular unconformity of Upper Pennsylvanian limestone resting on Mississippian to Lower Pennsylvanian sedimentary rocks (Fig. 1) – often called the C6 unconformity.

Of interest for the Sakmarian, Artinskian and Kungurian GSSP and SABS candidates are the Buckskin Mountain and Beacon Flat formations, which record three third-order transgressive–regressive sequences according to Beauchamp et al. (2022) (Fig. 2). The upper Asselian-upper Artinskian Buckskin Mountain Formation is composed of outer ramp to basinal calcareous shale and siltstone and lime mudstone, which are partially covered. In the upper part of the formation coarse bioclastic limestone with crinoids and fusulinids occurs. One sample from section 2A near the MFS (Fig. 3) of the second of the three T-R sequences [figs 6, 8 in Beauchamp et al. (2022)] yielded *Sweetognathus anceps* and *Sw. asymmetricus* and thus correlates with the lowermost Artinskian (Beauchamp et al., 2022). The Beacon Flat Formation comprises in the lower part poorly exposed cherty dolostone passing to fossiliferous cherty dolostone and limestone with echinoderms, brachiopods, bryozoans, and fusulinids forming resistant ledges. Considered to be late Artinskian to Kungurian in age, the unit was sampled for conodonts during the field trip along sections 4a-4b [figs 6, 8 in Beauchamp et al. (2022)]. If the conodont samples are productive, Carlin Canyon could be a good location for the base-Sakmarian, base-Artinskian and base-Kungurian SABS (Fig. 2).

The Rockland section

On October 19th, Charles Henderson, Lucia Angiolini and Luke Bratton visited the Rockland section. The site is freely accessible on Bureau of Land Management forestry land by 1 hour-drive along a gravel road departing from the I-80 highway near Wells, followed by an about 3 hours-long hike, climbing for 600 metres (Fig. 4). As written by C. Henderson in his

harangue in *Permophiles* #73: “...some effort and reasonable level of fitness is required to get to this site in the Basin and Range province of Nevada”. This is true, but once the site is reached at 40.77904°N and 114.60604°W, a continuous and very well outcropping section can be sampled freely. The beds are already numbered sequentially and include fusulinids, conodonts, crinoids and some brachiopods. As described by Henderson et al. (2012), at Rockland all Artinskian and Kungurian are exposed and the boundary interval is expanded in carbonate facies, mostly of outer ramp to slope setting (Fig. 4).

Chernykh et al. (2012) and Henderson et al. (2012) have already proved the wide correlation potential of the chosen point (*ie.* the FAD of *Neostreptognathodus pnavi*) from two distant regions. Another very interesting occurrence, reported by Henderson et al. (2012) at 28.5 m above the boundary interval in Rockland, is that of *Pamirina ex gr. darvasica*, which allows direct correlation with the Tethyan Scale and seems to suggest that the base-Kungurian falls within the upper Yakhtashian and that the base of the Bolorian is therefore higher in the Kungurian. This is in contrast with the correlation of the Tethyan Scale recently published in *Permophiles* #73 by Zhang et al. (2022), who suggested a much lower top (and possibly base) of the Bolorian with respect to previously published correlation schemes.

One limitation of Rockland section was the extrapolation to the GSSP level of the Sr isotopes. SPS funds were provided to Kate Tierney (University of Iowa) to analyze additional whole rock samples to complete the curve through the GSSP level. Luke Bratton will be running Sr isotopes on conodonts from this location and at Carlin as part of his MSc in order to test Sr correlation.

In addition, access and protection of the site must be guaranteed. The site is protected because it is on Bureau of Land Management land. Some effort is needed to improve access, mark the route with signs, and mark the GSSP site. Charles Henderson and Walt Snyder are in contact with the Chief Geologist of Nevada, BLM officials and the mining industry to address these issues.

Additional research in the area

Other topics were briefly investigated during the October



Fig. 5. Thrust-related fold in the Ely Group, Amphitheatre outcrop that predates deposition of the Strathearn Formation in this region.



Fig. 6. Panoramic view of the Humboldt River meander taken from Rattlesnake Ridge looking north toward the C6 angular unconformity.

made in the Serpukhovian Tonka Formation, upper Asselian Upper Strathearn Member and upper Asselian-lower Sakmarian lower part of the Buckskin Mountain Formation at Carlin Canyon. Another collection was made at the base of the Pequop Formation in Secret Canyon of Sakmarian age. Here, the upper Artinskian-Kungurian part of the succession was resampled for conodonts.

The brachiopod assemblages are not well known in the literature and will be described and used for paleoecological and paleoclimate studies.

A structural analysis was also undertaken in the Carlin Canyon area. Starting from the paper by Trexler et al. (2004), the pre-Pennsylvanian deformations have been analysed in terms of fault and fold analyses, confirming their direct relationships with a NW-SE contractional event occurred before the deposition of the Lower Strathearn Member unconformably resting on the deformed units of the Carboniferous Ely Group (Fig. 5). A subsequent tectonic event is responsible for the folding of the Lower and Upper Strathearn Formation and it is related to the formation of NNW-SSE tight folds involving the Pennsylvanian unconformity, as also shown in Beauchamp et al. (2022). It is worth noting that the excavation of the Carlin Canyon meander of the Humboldt River (Fig. 6) was strongly controlled by the trend of these folds, which are orthogonal to the Carboniferous ones.

References

- Beauchamp, B., Henderson, C.M., Dehari, E., Waldbott von Bassenheim, D., Elliot, S. and Calvo Gonzalez, D., 2022. Carbonate Sedimentology and Conodont Biostratigraphy of Late Pennsylvanian-Early Permian stratigraphic sequences, Carlin Canyon, Nevada: new insights into the tectonic and oceanographic significance of an iconic succession of the Basin and Range. In Henderson, C.M., Ritter, S. and Snyder, W.S. (eds). Late Paleozoic and Early Mesozoic Tectonostratigraphy and Biostratigraphy of western Pangea, Special Publication 113: SEPM (Society for Sedimentary Geology), Broken Arrow, Oklahoma, p. 34–71.
- Chernykh, V.V., Chuvashov, B.I., Davydov, V.I., and Schmitz, M.D., 2012. Mechetlino Section: A candidate for the Global Stratotype and Point (GSSP) of the Kungurian Stage

- (Cisuralian, Lower Permian). *Permophiles*, n. 56, p. 21–34.
- Chernykh, V.V., 2020. A brief account of the Mechetlino Section (Southern Urals, Russia) - potential candidate for a GSSP to define the base of the Kungurian stage in the global chronostratigraphic scale. *Permophiles*, n. 69, p. 14–22.
- Head, M.J., Aubry, M.P., Piller, W.E., and Walker, M., 2022. The Standard Auxiliary Boundary Stratotype: a proposed replacement for the Auxiliary Stratotype Point in supporting a Global boundary Stratotype Section and Point (GSSP). *Episodes*, online doi:10.18814/epiugs/2022/022012.
- Henderson, C.M., Wardlaw, B.R., Davydov, V.I., Schmitz, M.D., Schiappa, T.A., Tierney, K.E., and Shen, S.Z., 2012. Proposal for the base-Kungurian GSSP. *Permophiles*, n. 56, p. 8–21.
- McPhee J., 1981. *Basin and Range: Farrar, Straus and Giroux*, New York. 215 pp.
- Trexler, J.H., Cashman, P.H., Snyder, W.S., and Davydov, V.I. 2004. Late Paleozoic tectonism in Nevada: timing, kinematics, and tectonic significance: *Geological Society of America Bulletin*: 116, p. 525–538.
- Zhang, Y.C., Yuan, D.X., Qiao, F., Xu, H.P., Ju, Q., and Shen, S.Z., 2022. Late Early Permian timescale correlations between International scale and Tethyan scale: new evidence from the Lugu Formation in the South Qiangtang Block, Tibet. *Permophiles*, n. 73, p. 28–31.

Correlation chart for the Lower Permian of the western USA

Charles M. Henderson

Department of Geoscience, University of Calgary, Calgary, Alberta, Canada T2N 1N4

Michael T. Read

Department of Earth Sciences & Geologic Resources, Stephen F. Austin State University, Nacogdoches, Texas, USA

The accompanying chart (Fig. 1) is our work in progress highlighting some of the correlation changes resulting from conodont and fusulinacean biostratigraphic revisions. The most significant changes are reflected in the recognition that the cyclothems of the Chase Group do not extend into the Artinskian, but instead are no younger than lower Sakmarian. This revision was necessitated by the recognition of parallel evolution and consequent homeomorphy within the conodont genus *Sweetognathus* that demonstrates that *Sw. whitei* is late Asselian and *Sw. asymmetricus* is early to mid-Artinskian (Henderson, 2018; Petryshen et al., 2020; Chernykh et al., 2021). This taxonomic reevaluation has affected correlation in the western USA, but also in many other global localities. The following provides some important references for each of the columns illustrated in this correlation chart.

I. The north-central Nevada column includes correlations from Beauchamp et al. (2022). This location may become the site for the Standard Auxiliary Boundary Stratotype for the Sakmarian and Artinskian. The diagonal line within the Sakmarian indicates that in distal locations the Buckskin Mountain Formation is

Sakmarian to mid-Artinskian, but because there are several progradational carbonate platforms the Buckskin facies could be interpreted to correlate with the lower to mid-Artinskian (see figures 4&8 in Beauchamp et al., 2022) in proximal locations.

II. The eastern Nevada column is discussed in Read and Nestell (2018, 2019) and for the Kungurian (Henderson et al., 2012). The Rockland section in eastern Nevada is proposed to become the Global Stratotype Section and Point for the base-Kungurian.

III. The Wyoming column is based on the locus typicus for *Sweetognathus whitei* (Rhodes, 1963) with new correlations discussed in Henderson (2018).

IV. The southern New Mexico column is based on data presented in Kozur and Lemone (1995), Lucas et al. (2015, 2022), and Calvo Gonzalez et al. (2023).

V. The Hueco and Franklin mountains, West Texas column is based on data from Williams (1963, 1966), Ritter (1986), and Wahlman (2019) with some discussion in Calvo Gonzalez et al. (2023). Note the apparent time-transgressive nature of the Abo Formation in columns IV and V.

VI. The Glass Mountains, West Texas column is based on Ross (1963), Behnken (1975), Ross and Ross (2003a, b), Wahlman (2019), and Wardlaw and Nestell (2019) with some recent reinterpretation noted in Lucas et al. (2022).

VII. The Midland Basin, West Texas column is based on Kohn et al. (2019) and Tian et al. (2022).

VIII. The Eastern Shelf, central Texas column is based on various sources including Wardlaw (2005), Holterhoff et al. (2013), and Wardlaw and Nestell (2014) with some reinterpretations in Henderson (2018). Note in figure 2 of Tabor and Montanez (2004) that the upper part of the Admiral Formation and lower part of the Elm Creek Formation appear to represent a maximum flooding interval (restricting areal extent of fluvial channel succession) that is close to the base-Sakmarian. The lower part of the Bead Mountain Formation also represents a maximum flooding interval close to the base-Artinskian.

IX. The Midcontinent (Kansas) column is based on Boardman et al. (2009) with reinterpretations in Henderson (2018). Boardman et al. indicated the occurrence of *Sweetognathus whitei* (the real, Asselian taxon and not the Artinskian form) in association with *Streptognathodus florensis*. However, Chernykh (2005) indicated the latter taxon occurs in bed 26/2 at the Usolka section, which is the very top of the Asselian within the *S. postfusus* zone. In our view, *S. florensis* is synonymous with *S. fusus* or *S. postfusus*. Schmitz and Davydov (2012) used cyclostratigraphy to correlate the Council Grove and Chase groups; they interpreted cryptic 404Kyr cyclothem within lowstand shale units to represent the time needed to support a base-Artinskian age for the Barneston Limestone, but they did indicate this depended on accurate correlation of *Sweetognathus* lineages. These lineages have been reinterpreted (see Henderson's Harangue #11 in this issue) and the cyclostratigraphy correlates well if the limestone with *Sw. whitei* is uppermost Asselian. The age of the red beds and evaporite units of the Sumner and Nippewalla groups are generally regarded as Leonardian, as we indicate in Figure 1. However, this age is in part constrained by the previous Artinskian age interpretation for the underlying

Chase Group. It is possible that some of these units (Sumner?) are older (i.e., upper Wolfcampian). For example, figure 2 in Schneider et al. (2019) shows the lower part of the Sumner Group to be both correlative with the Yeso Group (Kungurian/Leonardian) and the Waggoner Ranch Formation (lower to mid-Artinskian/upper Wolfcampian). Insects and conchostrachans in the lower part of the Sumner Group (Wellington Formation) may resolve this question.

Finally, we regard Figure 1 as a work in progress. We welcome any comments on the correlations as suggested in Figure 1; please send to both of us at cmhender@ucalgary.ca and michael.read@sfasu.edu.

References

- Behnken, F.H., 1975. Leonardian and Guadalupian (Permian) conodont biostratigraphy in western and southwestern United States. *Journal of Paleontology*, v. 49, p. 284–315.
- Beauchamp, B., Henderson, C.M., Dehari, E., Waldbott von Bassenheim, D., Elliot, S. and Calvo Gonzalez, D., 2022. Carbonate Sedimentology and Conodont Biostratigraphy of Late Pennsylvanian-Early Permian stratigraphic sequences, Carlin Canyon, Nevada: new insights into the tectonic and oceanographic significance of an iconic succession of the Basin and Range. In Henderson, C.M., Ritter, S. and Snyder, W.S. (eds.), *Late Paleozoic and Early Mesozoic Tectonostratigraphy and Biostratigraphy of western Pangea*, Special Publication 113: SEPM (Society for Sedimentary Geology), Broken Arrow, Oklahoma, p. 34–71.
- Boardman, D.R., Wardlaw, B.R. and Nestell, M.K., 2009. Stratigraphy and conodont biostratigraphy of uppermost Carboniferous and Lower Permian from North American Midcontinent. *Kansas Geological Survey Bulletin*, v. 255, 253 pp.
- Calvo Gonzalez, D., Beauchamp, B. and Henderson, C.M., 2023. High-frequency sequence stratigraphy of Pennsylvanian-Lower Permian carbonate successions of the Robledo Mountains, New Mexico and the Carnic Alps, Austria: a record of the acme and demise of the late Paleozoic ice age. *Facies*, v. 69, no. 2, doi.org/10.1007/s10347-022-00658-z.
- Chernykh V.V., 2005. Zonal method in biostratigraphy, zonal conodont scale of the Lower Permian in the Urals. *Institute of Geology and Geochemistry of RAN, Ekaterinburg*, 217 pp. (in Russian)
- Chernykh, V.V., Henderson, C.M., Kutygin, R.V., Filimonova, T.V., Sungatullina, G.M., Afanasieva, M.S., Isakova, T.N., Sungatullin, R.K., Stephenson, M.H., Angiolini, L. and Chuvashov, B.I., 2021. Proposal for the Global Stratotype Section and Point (GSSP) for the base-Artinskian Stage (Lower Permian). *Permophiles*, n. 71, p. 45–72.
- Henderson, C.M., 2018. Permian conodont biostratigraphy. In Lucas, S.G. and Shen S.Z. (eds.), *The Permian Timescale*. Geological Society, London, Special Publication 450, p. 119–142.
- Henderson, C.M., Wardlaw, B.R., Davydov, V.I., Schmitz, M.D., Schiappa, T.A., Tierney, K.E. and Shen, S.Z., 2012. Proposal for the base-Kungurian GSSP. *Permophiles*, n. 56, p. 8-21.
- Henderson, C.M. and Shen, S.Z., 2020. Chapter 24-The Permian

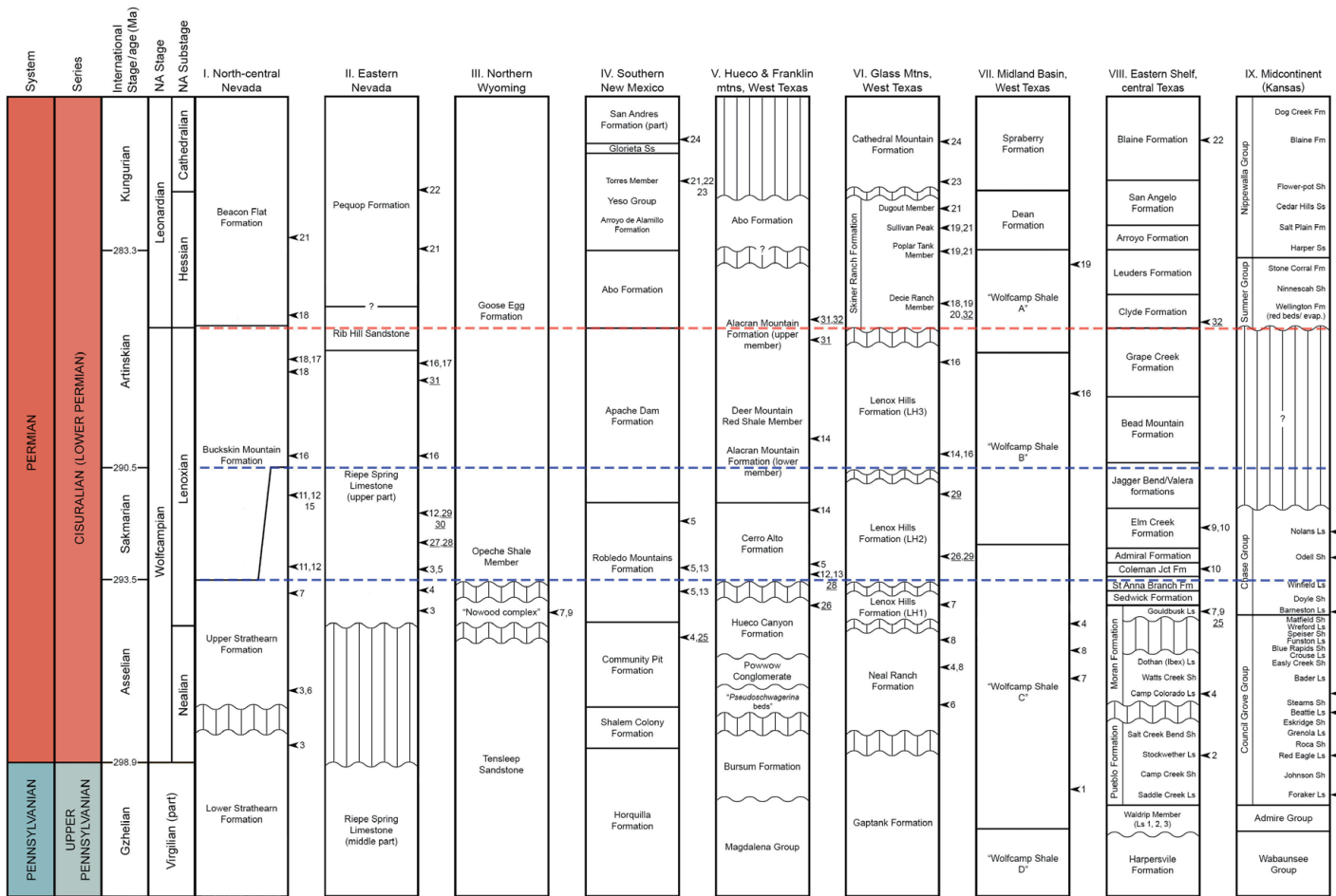


Fig. 1. Correlation chart of Lower Permian units in selected regions of the western USA. The position of the first occurrence as well as other significant levels of 32 different key conodont and fusulinacean taxa are indicated by numbers. Fusulinacean numbers are underlined. 1. *Streptognathodus wabaunsensis*; 2. *Streptognathodus isolatus*; 3. “*Sweetognathus complex*” (e.g., *Sw. duplex*, *Sw. trexleri*, *Sw. wardlawi*); 4. *Sweetognathus merrilli*; 5. *Sweetognathus sulcatus*; 6. *Streptognathodus constrictus*; 7. *Streptognathodus fusus/postfusis*; 8. *Streptognathodus barskovi*; 9. *Sweetognathus whitei*; 10. *Sweetognathus buccaramangus*; 11. *Mesogondolella monstra*; 12. *Sweetognathus binodosus*; 13. *Sweetognathus posterus*; 14. *Sweetognathus huecoensis*; 15. *Sweetognathus obliquidentatus*; 16. *Sweetognathus asymmetricus*; 17. *Sweetognathus behnkeni*; 18. *Neostreptognathodus pequopensis*; 19. *Sweetognathus exsculptus*; 20. *Mesogondolella gujoensis*; 21. *Neostreptognathodus pnevi*; 22. *Neostreptognathodus clinei*; 23. *Neostreptognathodus prayi*; 24. *Neostreptognathodus sulcopicatus*; 25. *Pseudoschwagerina texana*; 26. *Schwagerina diversiformis*; 27. *Schwagerina wellsensis*; 28. *Schwagerina neolata*; 29. *Eoparafusulina linearis*; 30. *Schwagerina glassensis*; 31. *Schwagerina franklinensis*; 32. *Schwagerina crassitectoria*. The two dashed blue lines represent two maximum flooding surfaces that approximate the base-Sakmarian and base-Artinskian. The dashed red line represents a sequence boundary that correlates with the Wolfcampian-Leonardian boundary. Chronostratigraphy of the Permian time scale is after Henderson and Shen (2020).

Period. In Gradstein F.M., Ogg J.G., Schmitz M.D., and Ogg G.M. (eds.), The Geologic Time Scale 2020. v. 2. Elsevier, p. 875–902.

Holterhoff, P.F., Walsh, T.R. and Barrick, J.E., 2013. Artinskian (Early Permian) conodonts from the Elm Creek Limestone, A heterozoan carbonate sequence on the eastern shelf of the Midland Basin, West Texas, USA. In Lucas, S.G. et al., (eds.), The Carboniferous-Permian transition. New Mexico Museum of Natural History and Science, Bulletin 60, p. 109–119.

Kohn, J., Barrick, J.E., Wahlman, G.P. and Baumgardner, R. 2019. Late Pennsylvanian (Virgilian) to Early Permian (Leonardian) conodont biostratigraphy of the “Wolfcamp Shale,” northern Midland basin, Texas. SEPM Special Publication, v. 111, p. 245–261.

Kozur, H.W. and Lemone, D.V., 1995. The Shalem Colony section of the Abo and upper Hueco members of the Hueco

Formation of the Robledo Mountains, Dona Ana County, New Mexico: Stratigraphy and new conodont-based age determinations. In Lucas, S.G. and Heckert, A.B. (eds.), Early Permian footprints and facies. New Mexico Museum of Natural History and Science, Bulletin 6, p. 39–55.

Lucas, S.G., Henderson, C.M., Barrick, J.E. and Krainer, K., 2022. Conodonts and the correlation of the Lower Permian Yeso Group, New Mexico, USA. Stratigraphy, v. 19, n.2, p. 77-94.

Lucas, S.G., Krainer, K. and Vachard, D., 2015. The Lower Permian Hueco Group, Robledo Mountains, New Mexico (USA). In Lucas S.G. and DiMichelle, W.A., (eds.), Carboniferous–Permian Transition in the Robledo Mountains, Southern New Mexico. New Mexico Museum of Natural History and Science, Bulletin 65, p. 43–95.

Petryshen, W., Henderson, C.M., de Baets, K. and Jarochowska,

- E., 2020. Evidence of parallel evolution in the dental elements of *Sweetognathus* conodonts. *Proceedings of the Royal Society B*, 287, 20201922.
- Read, M.T. and Nestell, M.K., 2018. Cisuralian (Early Permian) sweetognathid conodonts from the upper part of the Riepe Spring Limestone, north Spruce Mountain ridge, Elko County, Nevada. In Over, D.J and Henderson, C.M. (eds.), *Conodont studies dedicated to the careers and contributions of Anita Harris, Glenn Merrill, Carl Rexroad, Walter Sweet, and Bruce Wardlaw*. *Bulletins of American Paleontology*, v. 395–396, p. 89–113.
- Read, M.T. and Nestell, M.K., 2019. Lithostratigraphy and fusulinid biostratigraphy of the Upper Pennsylvanian-Lower Permian Riepe Spring Limestone at Spruce Mountain Ridge, Elko County, Nevada, USA. *Stratigraphy* v. 16, no. 4, p. 195–247. <https://doi.org/10.29041/strat.16.4.195-247>
- Rhodes, F.H.T., 1963. Conodonts from the topmost Tensleep sandstone of the Eastern Big Horn Mountains, Wyoming. *Journal of Paleontology*, v. 37, no. 2, p. 401–408.
- Ritter, S. M., 1986. Taxonomic revision and phylogeny of post-early crisis bisselli-whitei Zone conodonts with comments on Late Paleozoic diversity. *Geologica et Palaeontologica*, v. 20, p. 139–165.
- Ross, C.A., 1963. Standard Wolfcampian Series (Permian), Glass Mountains, Texas. *GSA Memoir*, v. 88, 205 pp.
- Ross, C.A. and Ross, J.R.P., 2003a. Sequence evolution and sequence extinction: Fusulinid biostratigraphy and species-level recognition of depositional sequences, Lower Permian, Glass Mountains, West Texas, U.S.A. *Micropaleontologic Proxies for Sea-level Change and Stratigraphic Discontinuities*, *SEPM Special Publication*, v. 75, p. 317–359.
- Ross, C.A. and Ross, J.R.P., 2003b. Fusulinid sequence evolution and sequence extinction in Wolfcampian and Leonardian Series (Lower Permian), Glass Mountains, West Texas. *Rivista Italiana di Paleontologia e Stratigrafia*, v. 109, n. 2, p. 281–306.
- Schmitz, M.D. and Davydov, V.I., 2012. Quantitative radiometric and biostratigraphic calibration of the Pennsylvanian–Early Permian (Cisuralian) time scale and pan-Euramerican chronostratigraphic correlation. *GSA Bulletin*, v. 124, n. 3–4, p. 549–577.
- Schneider, J.W., Lucas, S.G. Scholze, F., Voigt, S., Marchetti, L., Klein, H., Oplustil, S., Werneberg, R., Golubev, V.K., Barrick, J.E., Nemyrovksa, T., Ronchi, A., Day, M.O., Silantiev, V.V., Robler, R., Saber, H., Linnemann, U., Zharinova, V. and Shen, S.Z., 2019. Late Paleozoic-early Mesozoic continental biostratigraphy – Links to the Standard Global Chronostratigraphic Scale. *Palaeoworld*, v. 29, n. 2, p. 186–238. doi.org/10.1016/j.palwor.2019.09.001.
- Tabor, N.J. and Montanez, I.P., 2004. Morphology and distribution of fossil soils in the Permo-Pennsylvanian Wichita and Bowie Groups, north-central Texas, USA: Implications for western equatorial Pangean paleoclimate during icehouse-greenhouse transition. *Sedimentology*, v. 51, p. 851–884.
- Tian, H., Fan, M., Valencia, V.A., Chamberlain, K., Waite, L., Stern, R.J. and Loocke, M., 2022. Rapid Early Permian tectonic reorganization of Laurentia’s plate margins: Evidence from volcanic tuffs in the Permian Basin, USA. *Gondwana Research*, v. 111, p. 76–94.
- Wahlman, G. P., 2019. Pennsylvanian and Lower Permian fusulinid biostratigraphy of the Permian Basin region, southwestern USA. *AAPG Memoir*, v. 118, p. 167–227.
- Wardlaw, B.R., 2005. Age assignment of the Pennsylvanian–Early Permian succession of North Central Texas. *Permophiles*, n. 46, p. 21–22.
- Wardlaw, B.R. and Nestell, M.K., 2014. The first appearance of *Streptognathodus isolatus* in the Permian of Texas. *Permophiles*, n. 59, p. 17–20.
- Wardlaw, B.R. and Nestell, M.K., 2019. Conodont biostratigraphy of Lower Permian (Wolfcampian–Leonardian) stratotype sections of the Glass and Del Norte Mountains, West Texas, USA. *AAPG Memoir*, v. 118, p. 229–249.
- Williams, T.E., 1963. Fusulinidae of the Hueco Group (Lower Permian), Hueco Mountains, Texas. *Yale University Peabody Museum of Natural History Bulletin*, v. 18, 122pp.
- Williams, T.E., 1966. Permian Fusulinidae of the Franklin Mountains, New Mexico-Texas. *Journal of Paleontology*, v. 40, p. 1142–1156.

Additional conodonts from the Cisuralian-Guadalupian boundary interval in South China

Dong-xun Yuan

School of Resources and Geosciences, China University of Mining and Technology, Xuzhou 221116, China
Email: dxyuan@cumt.edu.cn

Shu-zhong Shen

State Key Laboratory for Mineral Deposits Research, School of Earth Sciences and Engineering, Frontiers Science Center for Critical Earth Material Cycling, Nanjing University, Nanjing, 210023, China

Hua Zhang

State Key Laboratory of Palaeobiology and Stratigraphy, Nanjing Institute of Geology and Palaeontology and Center for Excellence in Life and Palaeoenvironment, Chinese Academy of Sciences, Nanjing 210008, China

Hai-peng Xu

State Key Laboratory for Mineral Deposits Research, School of Earth Sciences and Engineering, Frontiers Science Center for Critical Earth Material Cycling, Nanjing University, Nanjing, 210023, China

Zhang-shuai Hou

State Key Laboratory for Mineral Deposits Research, School of Earth Sciences and Engineering, Frontiers Science Center for Critical Earth Material Cycling, Nanjing University, Nanjing, 210023, China

Quan-feng Zheng

State Key Laboratory of Palaeobiology and Stratigraphy, Nanjing Institute of Geology and Palaeontology and Center for Excellence in Life and Palaeoenvironment, Chinese Academy of Sciences, Nanjing 210008, China

Wen-qian Wang

State Key Laboratory for Mineral Deposits Research, School of Earth Sciences and Engineering, Frontiers Science Center for Critical Earth Material Cycling, Nanjing University, Nanjing, 210023, China

The Global Stratotype Section and Point (GSSP) of the Cisuralian-Guadalupian boundary (CGB) was ratified at the Stratotype Canyon section in the Guadalupe Mountains National Park in Texas, USA two decades ago. It is recognized and correlated by the first appearance datum (FAD) of the conodont *Jinogondolella nankingensis*. Although the official paper to define this GSSP has not been published, this section has been widely used to correlate the CGB globally.

A recent comprehensive review including biostratigraphy, geochronology and chemostratigraphy at the GSSP section (Shen et al., 2020) indicated the lack of multiple reliable markers at the GSSP section in addition to conodonts. This makes precise correlation difficult. Actually, both the holotype of *J. nankingensis* and the geochronologic age of the CGB in the official International Chronostratigraphic Chart were obtained from the base of the Kuhfeng Formation in South China. Therefore, South China plays a practical role in the international standard sections for the correlation of the CGB.

Jin (1960) established *Jinogondolella nankingensis* (= *Gondolella nankingensis*) based on the specimens from the lowest part (~0.25 m above the base) of the Kuhfeng Formation at the Zhengpanshan section in Nanjing, Jiangsu Province (Fig. 1). Since its original holotype was missing, Wang (1995) proposed a neotype which was from the base part of the Kuhfeng Formation at the same section. The conodont fauna of Wang (1995) also contains *Sweetognathus subsymmetricus*, *Hindeodus minutus* and *Pseudohindeodus ramovsi*. Wu et al. (2017) reported two high-precision CA-ID-TIMS dates, 272.95 ± 0.11 Ma and 271.038 ± 0.097 Ma, from the base part of the Kuhfeng Formation at the



Fig. 1. The locations of the studied sections in South China.

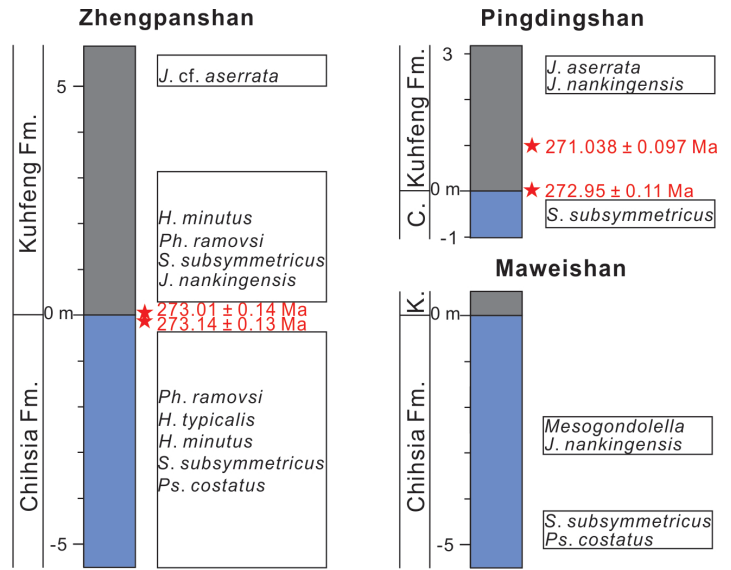


Fig. 2. Conodonts and U-Pb dates from the Chihhsia-Kuhfeng boundary interval at the studied sections in South China.

Pingdingshan section in Chaohu, Anhui Province (Figs. 1, 2). The Pingdingshan section is about 130 km from the Zhengpanshan section, and also yielded *Sweetognathus subsymmetricus* and a *Jinogondolella nankingensis*-*J. aserrata* mixed fauna from the topmost part of the Chihhsia Formation and the lower part of the Kuhfeng Formation respectively. Shen et al. (2020) reported two other high-precision CA-ID-TIMS dates, 273.14 ± 0.13 Ma and 273.01 ± 0.14 Ma, from the Chihhsia-Kuhfeng boundary interval at the Zhengpanshan section. In view of the first occurrence (FO) of *J. nankingensis* at this section, 273.01 ± 0.14 Ma was adopted as the current absolute age of the Cisuralian-Guadalupian boundary in the International Chronostratigraphic Chart (2022/10). Yuan and Shen (2022) reviewed previous reported data and illustrated newly recovered conodonts from the topmost part of the Chihhsia Formation to the middle part of the Kuhfeng Formation at the Zhengpanshan section. The updated conodont fauna includes *Pseudosweetognathus costatus*, *Sweetognathus subsymmetricus*, *Hindeodus minutus*, *H. typicalis* and *Pseudohindeodus ramovsi* in the topmost part of the Chihhsia Formation, *Jinogondolella nankingensis*, *Sweetognathus subsymmetricus*, *Hindeodus minutus* and *Pseudohindeodus ramovsi* in the base part of the Kuhfeng Formation, and *Jinogondolella* cf. *aserrata* in the middle part of the Kuhfeng Formation (Fig. 3). Three conodont zones, *Sweetognathus subsymmetricus*-*Pseudosweetognathus costatus*, *Jinogondolella nankingensis* and *J. cf. aserrata* zones, were recognized across the Chihhsia-Kuhfeng lithologic boundary interval at the Zhengpanshan section.

Here, new abundant *Jinogondolella nankingensis* in association with some smooth *Mesogondolella* from one sample are found from the uppermost part of the Chihhsia Formation at the Maweishan section in Chaohu, Anhui Province, which is about 10 km from the Pingdingshan section. Some *Sweetognathus subsymmetricus* and *Pseudosweetognathus costatus* are also yielded from another sample two meters below. The discovery of abundant *Jinogondolella nankingensis* from the uppermost part of the Chihhsia Formation suggests that this species occurred slightly below the international Cisuralian-Guadalupian boundary. This

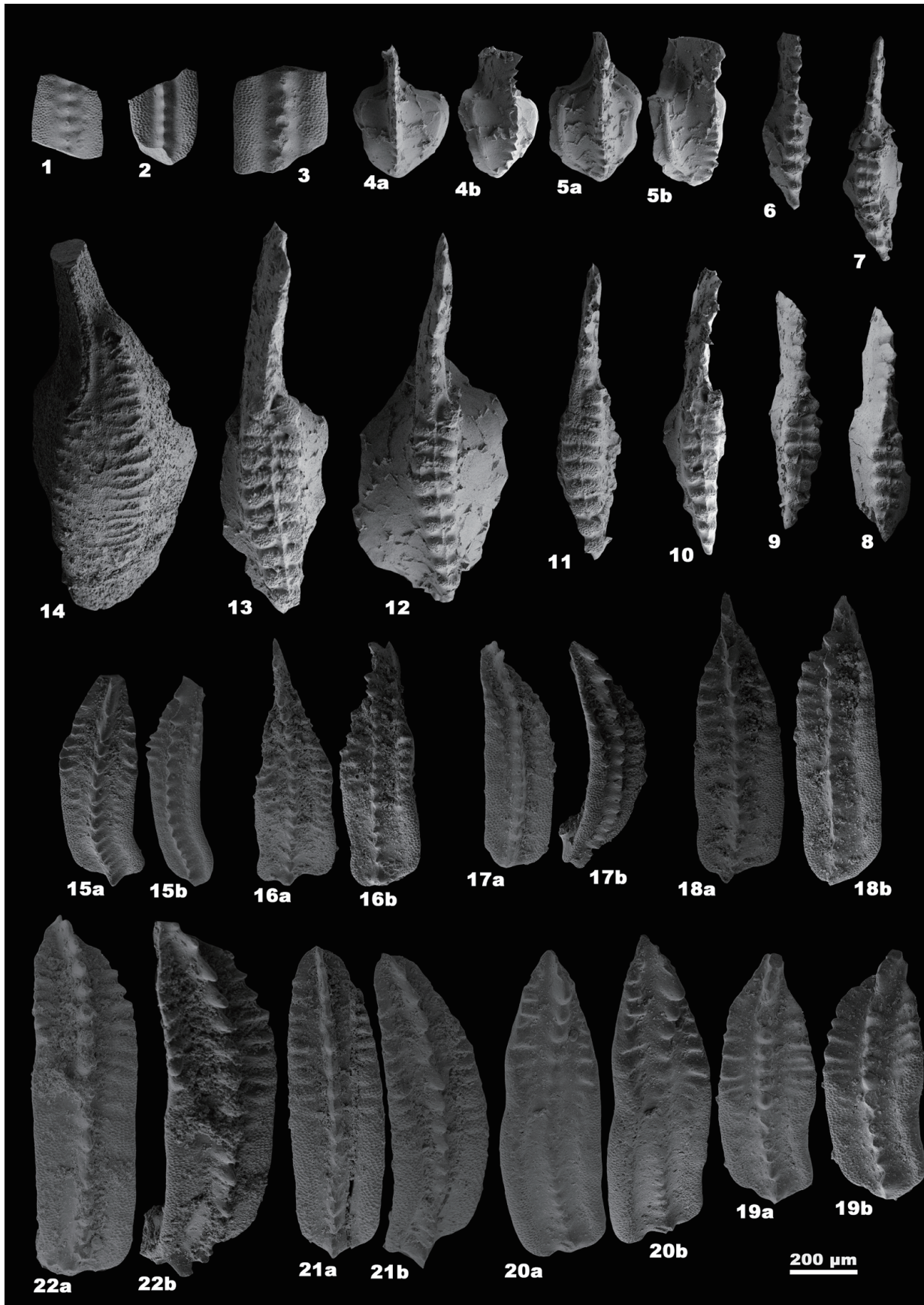


Fig. 3. Conodont specimens from the Chihhsia-Kuhfeng boundary interval at the studied sections in South China. 1-14. from the Zhengpanshan section. 1-3. *Jinogondolella* cf. *aserrata* (Clark and Behnken); 4, 5. *Pseudohindeodus ramovsi* Gullo and Kozur; 6-13. *Sweetognathus subsymmetricus* Wang, Ritter and Clark; 14. *Pseudosweetognathus costatus* Wang, Ritter and Clark. 15-22. from the Maweishan section, *Jinogondolella nankingensis* (Jin).

conodont fauna will provide pivotal materials for restricting the FO of *Jinogondolella nankingensis* in South China and understanding the evolutionary lineage from *Mesogondolella* to *Jinogondolella* (Fig. 3).

Acknowledgements

The fieldwork at Maweishan was guided by Huang Di-ying and Cai Chen-yang. The work is supported by the National Natural Science Foundation of China (NSFC 42072013, 41830323, 41702007) and Strategic Priority Research Program (B) of the Chinese Academy of Sciences (XDB26000000).

References

- Jin, Y.G. (Ching Y.K.), 1960. Conodonts from the Kufeng Suite (Formation) of Lungtan, Nanking. *Acta Palaeontologica Sinica*, v. 8, p. 230–248 (in Chinese with English abstract).
- Shen, S.Z., Yuan D.X., Henderson, C.M., Wu, Q., Zhang, Y.C., Zhang H., Mu, L., Ramezani J, Wang X.D., Lambert, L.L., Erwin, D.H., Hearst, J.M., Xiang L., Chen, B., Fan, J.X., Wang, Y., Wang, W.Q., Qi, Y.P., Chen, J., Qie, W.K. and Wang, T.T., 2020. Progresses, problems and prospects: An overview of the Guadalupian Series of South China and North America. *Earth-Science Reviews*, v. 211, 103412.
- Wang C.Y., 1995. A conodont fauna from the lowermost Kufeng Formation (Permian). *Acta Micropalaeontologia Sinica*, v. 12, n.3, p. 293–297 (in English with Chinese abstract).
- Wu, Q., Ramezani, J, Zhang, H., Wang, T.T., Yuan, D.X., Mu, L., Zhang, Y.C., Li, X.H. and Shen, S.Z., 2017. Calibrating the Guadalupian Series (Middle Permian) of South China. *Palaeogeography, Palaeoclimatology, Palaeoecology*, v. 466, p. 361–372.
- Yuan, D.X. and Shen, S.Z., 2022. A reinvestigation of the conodonts from the boundary interval between the Permian Kuhfeng and Chihhsia formations at the Zhengpanshan section in Longtan, Nanjing City. *Acta Palaeontologica Sinica*, v. 61, n.3, p. 358–370 (in English with Chinese abstract).

Do Permian-Triassic boundary microbialites contain keratose sponges?

Stephen Kershaw

Department of Life Sciences, Brunel University, Uxbridge, UB8 3PH, UK; and Earth Sciences Department, The Natural History Museum, Cromwell Road, London SW7 5BD, UK (E-mail: stephen.kershaw@brunel.ac.uk)

Introduction

Starting about 25 years ago with Szulc's (1997) study of Triassic stromatolites containing structures that he interpreted as sponges, there is increasing interest in the possibility of keratose sponge preservation in carbonates. The idea was made popular in landmark papers by Luo and Reitner (2014, 2016) using meticulous methods to construct the 3D shape of network structures in Devonian and Triassic limestones; thus keratose sponges were proposed. Since then there are numerous publications of various network structures in carbonates,

explaining these fabrics as keratose sponges. The idea is that the tough organic net made of the protein spongin (think here of the common bath sponges) was replaced by calcite; in contrast, the space between the spongin net branches, where the other soft tissue of the sponge existed when it was alive, is now occupied by micrite, and in almost all cases the micrite is structureless, seemingly particulate, with minor recrystallisation. Here it is worth noting that keratose sponges are a group of Demosponges; Demosponges are normally typified by silica spicules that build the sponge shape, enwrapped by spongin, with other soft tissue filling the remaining space, forming various chambers and canals to support sponge function. However, keratose sponges lack the spicules, so they are made of only soft tissues.

Keratose sponge preservation is an innovative concept in carbonate rocks; we normally consider fossils in limestones laid down in oxygenated shelf environments to be composed of mineral structure without soft tissues, so the notion that a soft-bodied material can be preserved in these environments is an advance on usual concepts of preservation. Normally we think of oxygen-poor environments, such as the Burgess Shale, as the places where soft tissues are represented.

The keratose sponge idea seems an ideal way to account for common occurrence of networks of curved and branching sparitic structure embedded in micrite, recorded from at least Neoproterozoic to possibly as recent as Eocene strata; such structures are commonly referred to as vermiform (alternative is vermicular), although structures with some variation have been interpreted as sponges (see Neuweiler et al. 2022 for discussion, where 5 different types of structure are recognized, all have been interpreted as keratose sponges by various authors). Sponges are very common in modern seas, so their preservation might be expected; but the problem is that modern sponges almost always break down and disappear on death, leaving no remains. There is also a problem of how to explain a pathway for mineralization of spongin. So, there is an interesting contradiction, between poor sponge preservation potential on one hand, and the desire to explain the nature of vermiform structures on the other hand.

Permian-Triassic Boundary Microbialite (PTBM) vermiform structures

Against the background of the scenario outlined above, vermiform structures occur in some cases of PTBMs (Fig. 1) in the immediate aftermath of the end-Permian event, in Tethyan sites. Some reports of these in the literature have interpreted the vermiform fabrics as keratose sponges, prominent examples being Baud et al. (2021), Friesenbichler et al. (2018), Heindel et al. (2018), Luo et al. (2022) and Wu et al. (2021). Those in Fig. 1 are typical of their preservation: narrow curved and branching structures composed of sparitic calcite, embedded in micrite, sitting in between the largely recrystallized calcimicrobial branches that constructed the PTBM biostromal deposits found across large areas of the South China Block. The idea of keratose sponges in the PTBM carbonates opens up a new avenue of research into these enigmatic structures, but there seems to be incongruity for the presence of sponges in these facies. Consider the following.

Positives

PTBMs follow the end-Permian extinction, and the PTBM fabrics are likely unique in Earth history. In South China, the principal fabric is a branching structure composed of lobate elements (Fig. 1) recognized by Kershaw et al. (2021a) as a new taxon of calcimicrobe (*Calcilobes wangshenghaii*), one that is similar to the Cambrian calcimicrobe called *Tarthinia*, and indeed may be a variant of *Tarthinia*.

Marine biodiversity took a significant hit at the extinction (e.g. Chen and Benton 2012), yet recovery was rapid, with numerous fossil groups being present, even within the microbialites, including ostracods, molluscs and others. So the logic that sponges could be represented is a reasonable interpretation, corresponding with possible sponge development during low-oxygen conditions associated with the extinction. In modern environments sponges are increasing in modern coral reef systems that may be response to decline of corals under worsening conditions in the oceans. So there is some reasonable basis for sponge expansion after the mass extinction.

Negatives

However, despite what we would like to believe in ecosystem development, we do need proof. The biggest barrier to acceptance of keratose sponges as an explanation of vermiform structure is the lack of a demonstrated process to explain how the soft-bodied spongin network gets replaced by calcite. Note that the infill

between network branches is made of essentially structureless, likely deposited, micrite, that is commonly expressed as microspar-to-pseudospar, which is most easily interpreted as minor recrystallisation of an original micritic carbonate mud (pictures in Fig. 1). One possible pathway is that the sponge soft tissue decayed leaving the spongin network alone, and the inter-network space was infiltrated by micrite that lithified early; then the spongin network decayed leaving an open cavity system subsequently infilled by sparite cement, preserving the form of the network as a cast.

The sequence above seems quite feasible, until we consider what happens with mineralized sponges in the rock record, most notably represented by the lithistid sponges (Fig. 2), another group of Demosponges. Lithistids are constructed of a tight network of particular spicules called desmas, that essentially lock together to form a solid mass (hence their common name of rock sponge); desmas are wrapped in spongin. Lithistids are very common as fossils, but there are no cases reported of the desma mineral structure wrapped by a replaced spongin calcite; thus a two-component preservation. Perhaps this is just a matter of interpretation, but if keratose spongin replacement by calcite was common, then it is very odd that there nowhere has anybody found evidence of replaced spongin in lithistids. Another problem is that no cases of compressed vermiform fabrics are known; these might be expected in the case of a spongin network buried in sediment becoming compressed by overburden before

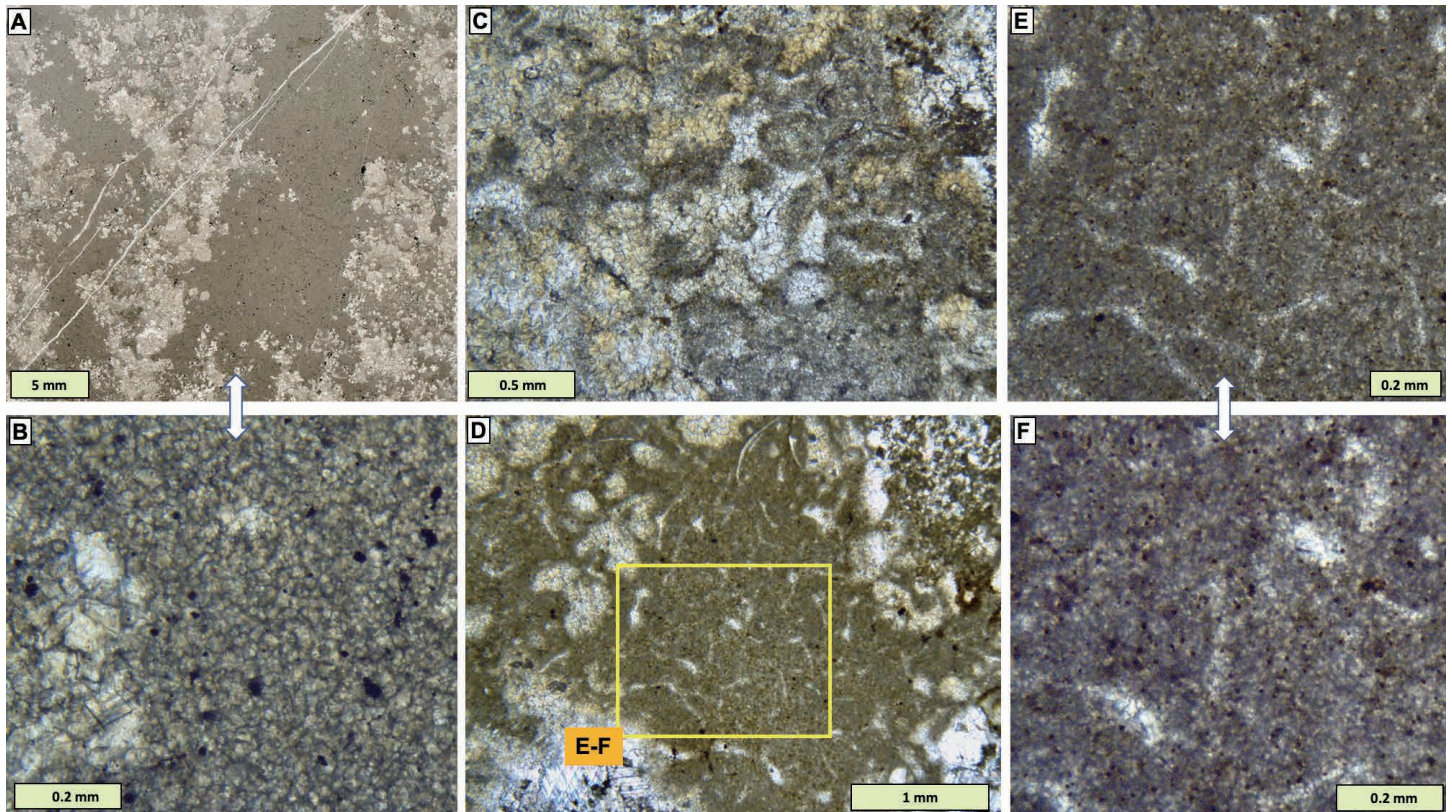


Fig. 1. Permian-Triassic boundary microbialites (PTBMs) showing vermiform and non-vermiform fabrics within the branching calcimicrobe frame. All photographs are in plane-polarised light and are vertical sections. A & B are from one sample, C-F are from another in the same location. A. enlargement in B. Microbial frame and interstitial micritic sediment. In B the light sparitic patch (left) is recrystallised calcimicrobes, and the remaining material is microspar interpreted to represent slightly recrystallised deposited micrite. C. Calcimicrobe frame of partially to strongly recrystallised lobate structure enclosing small primary porosity. D-F. vermiform micrite in the space between recrystallised calcimicrobe branches; enlargements in E and F show the structure comprises thin sparite areas with interstitial micrite that is interpreted as slightly recrystallised sediment. Baizhuyuan locality, Huaying Mountains, eastern Sichuan, China.

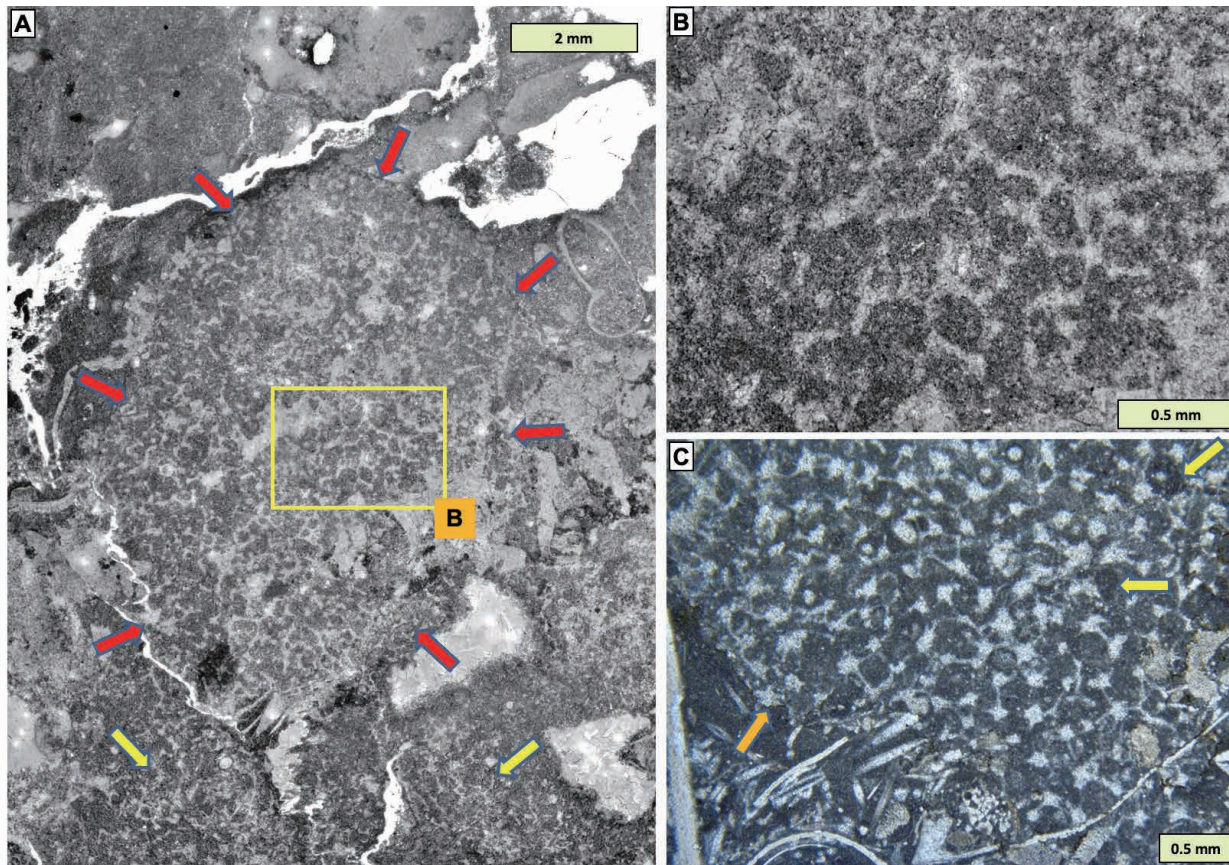


Fig. 2. Mineral sponges (in this case lithistids) showing the discrete masses of spicules of the type called desmas. A, B. A single sponge body (defined by red arrows at its margin), plus poorly-defined areas indicated by two yellow arrows). The sponge is surrounded by sediment matrix with shell remains. B shows the altered nature of the mineral desmas, with micrite sediment between them. Reef limestone, Högklint Fm, lower Wenlock; Korpklint Locality, northwest Gotland. C. Lithistid sponge with prominent network of spicules and interstitial micrite. Yellow arrows indicate round dark patches, interpreted as borings that cut both the spicule skeleton and the interstitial sediment fill. Orange arrow highlights the sharp margin of the sponge body, noting that the adjacent sediment is rich in bioclasts and is a similar dark colour to the round patches within the sponge. Filimore Fm, Lower Ordovician; Churches Reef, Utah.

lithification occurred. Of course the lack of these two is not proof that these structures are not keratose sponges, but adds to the doubt about their sponge status. Indeed, it seems that proponents of the keratose sponge hypothesis consider the spongin network to be equivalent in preservation potential to the mineral structure of spicule-bearing sponges, and this mismatch of our normal understanding of preservation potentials is a major stumbling block to the acceptance of the keratose sponge hypothesis.

Sponge mummies, or how to preserve a sponge body

A controversial aspect is that vermiform structures lack evidence of a process called mummification found in some mineralized sponges (see Neuweiler et al. 2022 for discussion); mummification is the replacement of sponge soft tissue by micrite, preserved as automicrite due to the complexity of geochemistry to permineralise the soft tissue components, and the result is a normally complex fabric inconsistent with the homogenous micritic fabrics found in vermiform structures. The outcome is preservation of a discrete sponge object that has internal sediment but with a sharp contact against surrounding sedimentary matrix. But there is a problem here because some cases of discrete sponge bodies have rather homogenous internal micrite, examples in Fig. 2. It seems difficult to accept that homogenous micrite can be considered as automicrite, because

the permineralization of soft tissues into micritic preservation would not be expected to result in homogenous micritic material. In the cases in Fig. 2, it is easier to interpret them as having solid desma frameworks that became infilled with micrite, then were lithified, with possible reworking on the sea bed to leave sharp margins. For vermiform structures, in contrast, cases where the vermiform structure has a defined form, and sharp contact against its enclosing matrix, are thus problematic to interpret; they don't have to be sponges (see below). Vermiform structures in PTBMs are not described as having sharp boundaries against the enclosing micrite, but Fig. 1 shows that some samples from a locality have vermiform structure, whereas other samples from the same place lack this structure. Again, this is not proof either for, or against, keratose sponges in the PTBMs, but it sharpens the need for searching for criteria to prove whether these structures are sponges or not.

Alternatives

Neuweiler et al. (2022) discussed in detail alternative interpretations of network fabrics, a key one being that they may represent burrow networks associated with the under-researched area of meiofauna, that is, very small faunal elements abundant in sediment in modern environments, but poorly known in the fossil record. The possibility also is open that vermiform fabrics are not

fossils at all, but fall into the concepts of structures created by unexplained early burial processes. These alternatives have not been much investigated in the rocks where vermiform structures occur. A nice example of such issues is given by Kershaw et al. (2021b) and Kershaw & Li (2022), from reefs of the lower Silurian of South China, where vermiform structures of different forms are abundant; some of these can be readily interpreted as burrows, but others are enigmatic.

Other

Although the network sparite in vermiform structure consists of very narrow elongate patches of sparite, we might eventually find geopetals in the network, if it was an empty space in shallow burial. Geopetals would be proof that the network was an open cavity system in shallow burial. It also might be expected that geopetals would occur in the inter-network space, in cases where the spongin network was not completely infiltrated by micrite; but none have yet been found. We need to search for geopetals in vermiform fabric.

A key area of new work that is needed is to develop more understanding of the vermiform fabrics in 3D; so far the only attempts have been by Luo & Reitner (2014) and Luo et al. (2021). These intricate micro-reconstructions are highly valuable and much more needs to be done, also at a meso-scale to map out the overall shape of the vermiform body, and see if the published claims (from thin section studies) that canals exist can be confirmed in 3D.

Finally, Lee and Riding (2021, fig. 9) found that Phanerozoic vermiform fabrics match the stratigraphic distribution of reefal microbialite carbonates, but a lot depends on the interpretation of the vermiform fabrics as being keratose sponges. I am not doubting that the distributions are matched, but confirmation is needed as to whether the keratose sponges are accurately identified. If the vermiform fabrics in Lee & Riding's (2021) plot mix together different kinds of formation processes, then more work will be needed to disentangle the stratigraphic match with reef microbialites, which of course makes it all the more interesting to try to understand.

Conclusion

The possibility of keratose sponges in carbonate rocks is tantalizing; it seems to challenge our normal thinking that preservation of soft-bodied tissues in open-marine shelf settings doesn't happen. But the jury is very much still out in relation to the validity of keratose sponges in the aftermath of the end-Permian extinction, and more effort is needed to validate the claims for their presence within PTBMs. I therefore very much hope that caution will be applied in such interpretations in future publications, and ask that the research community does not "build a house on sand" in this topic, pending absolute knowledge of what formed vermiform structures in these rocks.

Acknowledgments

I thank: Fritz Neuweiler (Laval University, Québec City, Canada) for inspirational discussion of processes regarding sponge preservation; Robert Riding (University of Tennessee, Knoxville, USA) for a great field trip in Utah in 2014 that opened

my eyes on sponges in those lower Ordovician limestones; and Nigel Watts (Calgary, Canada) for providing samples of limestones from the Silurian of Gotland, containing lithistid sponges.

References

- Baud, A., Richoz, S., Brandner, R., Krystyn, L., Heindel, K., Mohtat, T., Mohtat-Aghai, P. and Horacek, M., 2021. Sponge Takeover from End-Permian Mass Extinction to Early Induan Time: Records in Central Iran Microbial Buildups. *Frontiers in Earth Science*, n. 9, 586210.
- Chen, Z.Q. and Benton, M., 2012. The timing and pattern of biotic recovery following the end-Permian mass extinction. *Nature Geoscience*, v. 5, p. 373–383.
- Friesenbichler, E., Richoz, S., Baud, A., Krystyn, L., Sahakyan, L., Vardanyan, S., Peckmann, J., Reitner, J. and Heindel, K., 2018. Sponge-microbial buildups from the lowermost Triassic Chanakhchi section in southern Armenia: microfacies and stable carbon isotopes. *Palaeogeography Palaeoclimatology Palaeoecology*, v. 490, p. 653–672.
- Heindel, K., Foster, W. J., Richoz, S., Birgel, V. J., Roden, D., Baud, A., Brandner, R., Krystyn, L., Mohtat, T., Kosun, E., Twitchett, R., Reitner, J. and Peckmann, J., 2018. The formation of microbial-metazoan bioherms and biostromes following the latest Permian mass extinction. *Gondwana Research*, v. 61, p. 187–202.
- Kershaw, S., Zhang, T. and Li, Y., 2021a. *Calcilobes wangshenghaii* n. gen., n. sp., microbial constructor of Permian-Triassic boundary microbialites of South China, and its place in microbialite classification. *Facies*, v. 67, p. 28.
- Kershaw, S., Li, Q.J. and Li, Y., 2021b. Addressing a Phanerozoic carbonate facies conundrum-sponges or clotted micrite? Evidence from Early Silurian reefs, South China Block. *The Sedimentary Record*, v. 19, n. 1, p. 3–10, doi: 10.2110/sedred.2021.1.03.
- Kershaw, S. and Li, Y., 2022. Ningqiang Formation reefs, lower Silurian, South China: and atlas of images. https://figshare.com/articles/online_resource/Ningqiang_Formation_reefs_lower_Silurian_South_China_an_atlas_of_images/21786314.
- Lee, J.H. and Riding, R., 2021. Keratolite–stromatolite consortia mimic domical and branched columnar stromatolites, *Palaeogeography, Palaeoclimatology, Palaeoecology*, v. 571, 10288.
- Luo, C. and Reitner, J., 2014. First report of fossil “keratose” demosponges in Phanerozoic carbonates: Preservation and 3-D reconstruction. *Naturwissenschaften*, v. 101, p. 467–477.
- Luo, C. and Reitner, J., 2016. ‘Stromatolites’ built by sponges and microbes—a new type of Phanerozoic bioconstruction. *Lethaia*, v. 49, p. 555–570.
- Luo, C., Pei, Y., Richoz, S., Li, Q. and Reitner, J., 2022. Identification and current palaeobiological understanding of “Keratosa”-type nonspicular demosponge fossils in carbonates: with a new example from the lowermost Triassic, Armenia. *Life*, v. 12, p. 1348. doi: 10.3390/life12091348.
- Neuweiler, F., Kershaw, S., Boulvain, F., Matysik, M., Sendino, C., McMenamin, M. and Munnecke, A., 2022. Keratose sponges in ancient carbonates – a problem of interpretation.

Sedimentology. <https://doi.org/10.1111/sed.13059>.
 Szulc, J., 1997. Middle Triassic (Muschelkalk) sponge-microbial stromatolites, diplopores and Girvanella-oncoids from the Silesian Cracow Upland. In: 3rd IFAA Regional Symposium and IGCP 380 International Meeting, Guidebook. Cracow, p. 10–15.
 Wu, S., Chen, Z.Q., Su, C., Fang, Y. and Yang, H., 2021. Keratose sponge fabrics from the lowermost Triassic microbialites in South China: geobiologic features and Phanerozoic evolution. *Global and Planetary Change*. doi.org/10.1016/j.gloplacha.2022.103787.

understand taxa, but not their full variability, their ‘taxonomic distance’ from their nearest neighbours or the way that they ‘grade’ into their taxonomic neighbours. We should use the internet more to create galleries of images of key taxa and not be constrained by journal page and plate limits.

Gallery of images

Categorization of any collection of objects involves seeing the similarities and differences between things where there might be an amount of continuous variation. In palynology, palaeontology, botany and zoology we call this taxonomy - a hierarchical system which can be used to organise and index knowledge.

For a palynologist dealing with objects that may or may not have a biological expression in morphology, taxonomy can be difficult. A palynologist is faced with a slide with possibly thousands of palynomorphs. If there are no taxon names for some of the palynomorphs, he/she is faced with the task of looking at the palynomorphs and grouping them into individuals that have similar characteristics using her judgement and knowledge. He/she may want to then give the group a name and ally it with other groups or place it inside other groups higher in the hierarchy – again using her judgement and knowledge.

If he/she decides that the entity he/she has ‘defined’ is ‘new’ to science, he/she may want to give the entity a taxon name. He/she will choose a type specimen of some kind which is an embodiment of the category or taxon that he/she has envisaged.

All this is good. It’s a way of organising and indexing knowledge. If he/she has chosen a good characteristic type and written a good enough diagnosis and description, other palynologists can come along and make a judgement as to whether a specimen that they have found is also a member of the group. The taxon name and the type has to be published and peer reviewed so that the taxon has some validity and so that the concept of the taxon is accessible to others. Palynologists

Tackling species variation in palynology

Michael H Stephenson

Stephenson Geoscience Consulting, Keyworth, Nottingham;
 British Geological Survey, Keyworth, Nottingham
 Email: mikepalyno@me.com

Introduction

In palynology, one of the ways to correlate distant sections in different palaeophytogeographic provinces is to use ‘bridge’ taxa – the few taxa which appear to be common to the provinces, despite their other differences. Bridge taxa become very important when there are no other ways to correlate, for example in non-marine sequences with no other fossils, or in sequences that have no dateable ash horizons. The problem is that bridge taxa may not be well described, or that conceptions of them in different palaeophytogeographic provinces may be different where different ‘schools’ of palynology have grown up. Traditional and formal (‘legal’) documentation in scientific journals - with a description, diagnosis and types can help us



Fig. 1. Variation in *Reduviasporonites catenulatus* illustrated in the BGS Taxonomy online Reduviasporonites gallery

use journals to publish this information. Journals are tight on space, so publication may take place in the journal but only a few photographs may be published - and text is required to be succinct.

As a practising taxonomist I've always been frustrated by the fact that the brevity of descriptions and paucity of photography have meant that it is sometimes difficult to understand the variation within a taxon, where its limits are, and how far it is from the nearest similar taxon - in other words the 'taxonomic space' between one taxon and the next. In the case of what appears to be continuous variation between one taxon and another, how (and where) do you 'draw the line' that separates the taxa? You might have thought that the internet would have come along to provide extra photos dealing with variation within a taxon and continuous variation between taxa, but in the majority of cases this has not happened. Taxonomy continues as it always has: based on and limited by the strictures of journal publishing.

Only a few publications and websites stand out, as least in Permian palynology, to deal with variation within a taxon and continuous variation between taxa. One is the lavishly illustrated monograph by J. M. Anderson on the Permian and Triassic palynology of South Africa (Anderson 1977). The paper uses some unorthodox taxonomic names but in a way that does not matter because most taxa are so well illustrated. Each taxon is illustrated as a population. It is possible at a stroke to understand a bit more about the natural variation of a taxon and its neighbours in taxonomic space just by flicking through the pages. Anderson's paper was used heavily by Backhouse (1991) to make correlations using 'bridge' taxa between quite distant parts of the Gondwana continent in the Permian. Using the many plates of Anderson's paper, Backhouse was able to reassure himself that specimens that he thought belonged to bridge taxa that existed in both the Australian and South African parts of Gondwana were indeed one and the same. A case in point is the spore *Verrucosiporites pseudoreticulatus*, an important biozonal index in Australia. The taxon was well known in Australia and the series of photographs published by Anderson allowed some assurance that it was indeed present in South Africa. Using a series of such bridge taxa, Backhouse (1991) was able to make a close correlation between the Collie Basin and the northern Karoo Basin.

The internet is of course the best place to illustrate variation within a taxon and continuous variation between taxa. A great source of data on two enigmatic taxa which is rich in imagery is the BGS' Taxonomy online [Reduviasporonites database or gallery](#). This gallery features almost 200 light microscope and SEM pictures of the variation within, and variation between, two species of the genus *Reduviasporonites* (Figs.1, 2). This genus was of great interest and importance a number of years ago because of its disputed connection with the Permian-Triassic mass extinction.

In particular two of the species - *R. chalastus* and *R. catenulatus* - were hard to separate and there is a lot of variation within each species. Also, the affinities of *Reduviasporonites* were ambiguous and disputed - algae or fungus? The huge gallery of specimens helps other palynologists decide on the taxonomy of their specimens, and helped mycologists and

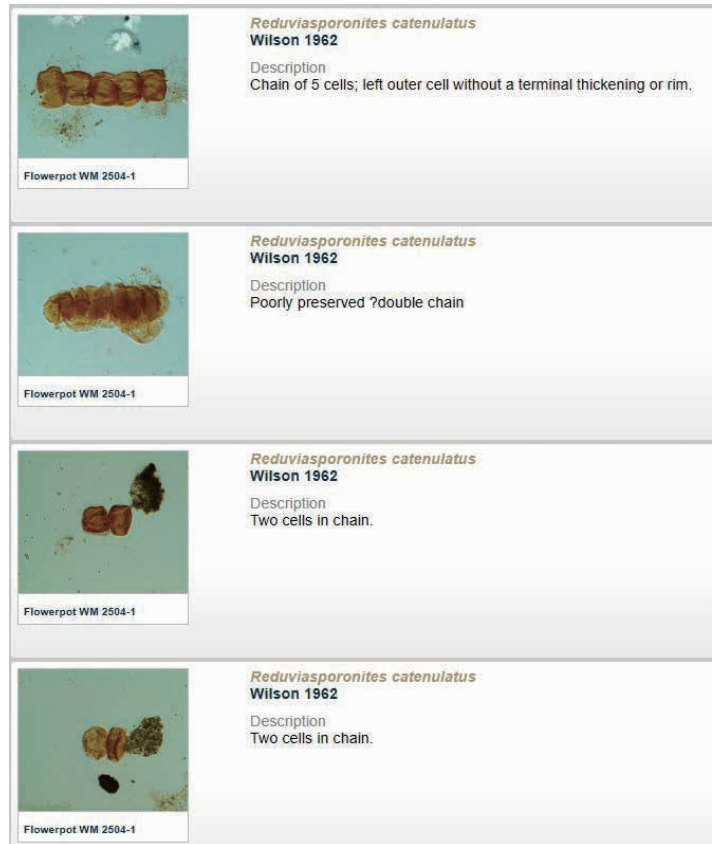


Fig. 2. Details of some *Reduviasporonites catenulatus* specimens in the BGS Taxonomy online *Reduviasporonites* gallery

phycologists think about the affinity of these important species without having to look at small pictures in journals that allow only a few illustrations and small amounts of description.

Useful resource for groups of palynological taxonomists making decisions about important taxa

At the moment, as a practising palynologist I am interested in a few problems that are taxonomic at heart. One is the use of the bisaccate, bitaeniate pollen *Lueckisporites virkkiae* as a marker for the Middle and Upper Permian; the other is the continuous variation between the genera *Falcisporites* and *Alisporites*.

The first problem is important, I think, because *Lueckisporites virkkiae* is one of the few taxa that could be regarded as a bridge between different parts of the highly phytogeographically differentiated Permian world. *Lueckisporites virkkiae* has long been considered useful for correlation in the Permian phytogeographical province of Euramerica because it is widespread in the province (Stephenson 2016), and because the taxon is very distinctive with a diploxylonoid outline, a thin corpus intexine and a prominent cappa formed chiefly by two reniform exoexinal taeniae (see Klaus 1963; fig. 27). The biostratigraphic value of *Lueckisporites virkkiae* also stems from its well-established first occurrence in the lower part of the Kazanian (Roadian) in its type area in the Russian Platform (Stephenson 2016), and therefore was useful for correlating to the then international scale of the Upper Permian before the Guadalupian Epoch was established in the United States. Early confirmation of a Guadalupian first occurrence for *Lueckisporites*

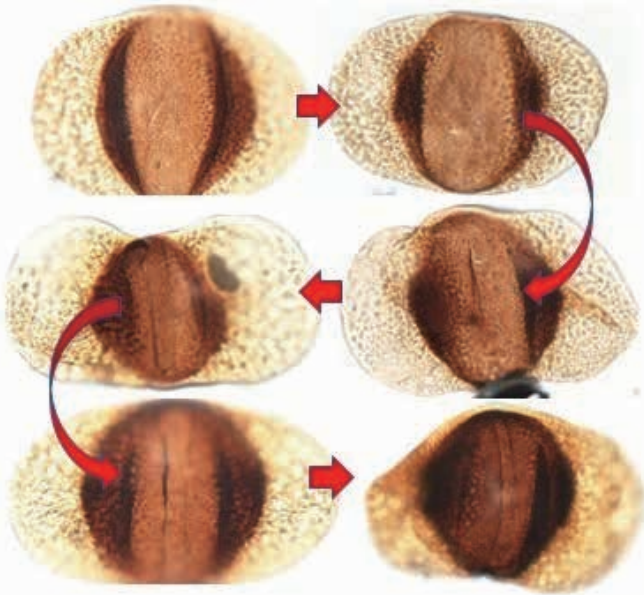


Fig.3. Where is the 'boundary' between *Falcisporites* and *Alisporites* in a continuously variable space?

virkkiae in the Gondwana phytogeographic province came from radioisotopic dating of the Argentinian Striatites Biozone (Archangelsky and Vergel, 1996), at the base of which that taxon makes its first appearance, though other identifications of *Lueckisporites virkkiae* in the Gondwana province may use a wider conception of the species (for example that used by Clark 1965) than was perhaps intended by Klaus (1963). *Lueckisporites virkkiae* therefore seems to me to a prime candidate as a bridge taxon which needs investigation and a clearer (or tighter) circumscription – if Gondwana/Euramerica correlation is to be achieved in palynology.

The difference between *Falcisporites* and *Alisporites* is important because these taxa, which both occur in the Upper Permian Umm Irna Formation in Jordan, were produced by plants which in the last few years have been under intense study by a team from Münster University in Germany. The Münster team believe that the Umm Irna Formation was an evolutionary cradle for a number of plant types that appeared early there (e.g. Blomenkemper et al. 2018), for example the seed fern *Dicroidium* that was once thought to be a Triassic-only species. *Dicroidium* produced the pollen *Falcisporites stabilis* which is extremely common pollen in the Umm Irna Formation. However *Falcisporites stabilis* is known to grade continuously into *Alisporites nuthallensis*. What is the relationship between the two and where is the 'boundary' between *Falcisporites stabilis* and *Alisporites nuthallensis* in a continuously variable space (Fig. 3)? Again to foster discussion and good taxonomic decision making it seems useful to be able to display these variations via photographs and maybe short videos that indicate the character of change between species. This and a gallery of *Lueckisporites virkkiae* specimens from many locations could form a useful resource for groups of palynological taxonomists making

decisions about important taxa.

Correlating GSSPs with palynology

Recently the Gondwana-Euramerica Working Group of the Sub-Commission on Permian Stratigraphy has been considering some of these problems and intends to set up galleries for key sections and taxa that relate to correlation between Gondwana and Euramerica in the Permian. One section that could be important is Usolka, which was ratified as the GSSP for the Sakmarian in 2020 (Chernykh et al. 2020). Palynological samples were taken from the section, and reported on in Chernykh et al. (2020), though due to space constraints a palynological plate was not included. Although palynomorphs in the section are rather poorly preserved there were a considerable number of unidentified specimens particularly of a suspected algal origin that may have correlation potential and there may be value in displaying specimens that could be recognised by palynologists working in other palaeophytogeographic provinces. The Sakmarian is problematic for correlation between Gondwana and Euramerica because its GSSP is based on conodonts which are extremely rare in Gondwana in the Cisuralian. Thus an SPS Usolka palynology gallery is planned, so watch this space!

References

- Anderson, J. M., 1977. The biostratigraphy of the Permian and Triassic. Part 3. A review of Gondwana Permian palynology with particular reference to the northern Karroo Basin of South Africa. *Memoirs of the Botanical Survey of South Africa.*, v. 41, p. 1–133
- Archangelsky, S. and Vergel, M., 1996. Paleontología, biostratigrafía y paleoecología. In *El sistema Permico en la Republica Argentina y en la Republica Oriental del Uruguay*, Academia Nacional de Ciencias, Cordoba, Rep. Argentina, 1996, p. 40–44.
- Backhouse, J., 1991. Permian Palynostratigraphy of the Collie Basin, Western Australia. *Rev. Palaeobot. Palynol.*, v. 67, p. 237–314.
- Blomenkemper, P., Kerp, H., Hamad, A. A., DiMichele W. A. and Bomfleur B., 2018. A hidden cradle of plant evolution in Permian tropical lowlands. *Science*, v. 362, n. 6421, p. 1414–1416. doi: 10.1126/science.aau4061
- Clarke, R. F. A., 1965. British Permian saccate and monosulcate miospores. *Palaeontology*, v. 8, p. 322–354.
- Chernykh, V V, Chuvashov, B I, Shen, S.Z., Henderson, C.M., Yuan, D.X., and Stephenson, M H., 2020. The Global Stratotype Section and Point (GSSP) for the base-Sakmarian Stage (Cisuralian, Lower Permian). *Episodes* v. 43, n. 4, p. 961–979
- Klaus, W., 1963. Sporen aus dem südalpinen Perm. *Jb. Geol. Bundesanst., Wien*, v. 106, p. 229–363.
- Stephenson, M.H., 2016. Permian palynostratigraphy: a global overview. In Lucas, S. G. and Shen, S. Z. (eds.) *The Permian Timescale*. Geological Society, London, Special Publications, v. 450; p. 321–347.

Rebuilding terrestrial Gondwana: challenges and opportunities of a palynological approach

Annette E. Götz

State Authority for Mining, Energy and Geology, Hannover, Germany

Email: annette.goetz@lbeg.niedersachsen.de

Alexander Wheeler

Leibniz University Hannover, Hannover, Germany

Email: wheeler@geowi.uni-hannover.de

Introduction

The terrestrial successions of Permian Gondwana capture a period of significant climatic change across the southern hemisphere as well as a significant shift in the dominant assemblage of land plants leading to the dominance of the *Glossopteris* flora across most of the continent. Correlating the terrestrial basins of Gondwana with one another and to the standard Permian stages (Henderson and Shen, 2020) using palynology has proved challenging and imprecise largely because these stages are often defined by the first appearance of marine organisms such as fusulinids, conodonts or ammonites. In terrestrial basins, palynology is ideal for biostratigraphy as other microfossil groups are not present or abundant enough, and macrofossils only offer biostratigraphic utility limited to individual basins, such as the therapsids in the Main Karoo Basin (Lucas, 2006), or have relatively poor time resolution such as macrofloral zonation schemes (Cleal, 2018).

Quaternary palynologists can reconstruct detailed vegetation histories examining climate amelioration at the end of the last glacial period at an extremely high temporal resolution (Huntley and Webb, 2012; Feurdean et al., 2014; Stojakowits and Mayr, 2022). In the Permian, several factors render this difficult (poor sampling resolution, preservation, poorly understood botanical affinities). However, by examining floral shifts over a longer timescale, identifying variation in different localities, and broadening our knowledge through multidisciplinary analyses, we can deepen our understanding of the dynamic earth systems of the Permian. Permian Gondwana offers a significant opportunity to study long-term processes associated with deglaciation and global climate amelioration and also offers a deep-time comparison to the more recent Late Cenozoic Ice Age and modern climate warming. Gondwana's many sedimentary basins capture the acme and ending of the Late Palaeozoic Ice Age and the subsequent climatic and vegetation changes from low to high latitudes (Birgenheier et al., 2010; Isbell et al., 2012). This offers a chance to understand climatic and vegetational changes on a local as well as inter-basinal and intra-continental scale (Ruckwied et al., 2014; Götz and Wheeler, 2018). However, the tectonic and depositional setting of different basins can vary dramatically. Correlation of the coal seams developed in a foreland setting of the Main Karoo Basin and the rift basins of Mozambique has proven difficult due to the very different nature of the basin infill (Götz et al., 2018; Lopes et al., 2021). Glacial-derived diamictites and tillites of the Dwyka Group form the basal unit of the Main

Karoo Basin in South Africa, directly underlying the coal seams, whereas in the Moatize Basin in Mozambique, conglomerate units underlie and interfinger the coal units and are more likely related to the rifting as opposed to glaciation. These processes also affect on the palynological content of the sediments as depositional setting and base-level changes place environmental controls on the in-situ floras, and subsequent sedimentary processes affect the transport and preservation of the pollen and spores (Gregory and Hart, 1992; Holz and Dias, 1998). Using palynology in concert with other stratigraphic and geochemical tools is also essential for more accurate correlation.

Calibration with radiometric ages

Recent work successfully calibrating biostratigraphic schemes to the Permian stages has provided the greatest opportunity for future interregional correlations. The most well-calibrated biostratigraphic scheme is found in Australia, particularly in the east represented mainly by the foreland Bowen-Gunnedah-Sydney Basin System, and the intracratonic Galilee and Cooper basins. Zircon-yielding tuffs were sampled from several different basins and have been used to calibrate the ages of most of the major palynozones, with a high level of precision using CA-ID-TIMS (Metcalfe et al., 2015; Laurie et al., 2016; Ayaz et al., 2016; Phillips et al., 2018; Fielding et al., 2019). This has also allowed for much higher resolution examinations of the Permian-Triassic Boundary (Fielding et al., 2019; Mays et al., 2020; Wheeler et al., 2020; McLoughlin et al., 2021). New age dates defining the bases of the Permian stages (Cohen et al., 2022) necessitate an update to this calibration (Fig. 1).

Progress has also been made in South America, both in refining the biostratigraphy in several basins (Limarino and López-Gamundí, 2021) and in collecting radiometric ages and using them to calibrate both the litho- and palynostratigraphy (Césari, 2007; Césari et al., 2022; Guerra-Sommer et al., 2008; Mori et al., 2012; Simas et al., 2012) (Fig. 1). The *Vittatina costabilis* Zone in the Paraná Basin has now been well constrained using up to thirty-two radiometric ages (summarised in Souza et al., 2021). In South Africa, radiometric ages have been provided for the Abrahamskraal Formation to calibrate the *Tapinocephalus vertebrate* assemblage zone (Day et al., 2022). These ages are consistent with the assignment of the K8/K9 palynozones to the Capitanian in the southern Main Karoo Basin (Barbolini et al., 2018). Whilst other age dates have been collected in the Main Karoo Basin, these have yet to be assessed alongside palynological data, which could help to further refine the biostratigraphic scheme in the future (Prevec et al., 2022).

Future challenges

The challenges associated with palynology-based regional correlation are numerous. Regarding the terrestrial basins of Permian Gondwana, several factors require addressing before progress can be made.

Subprovinciality and diachroneity

While the *Glossopteris* flora is relatively ubiquitous across Gondwana, subprovinciality can be identified in the palynological record, hindering attempts at correlation (Jha, 2006; Lindström

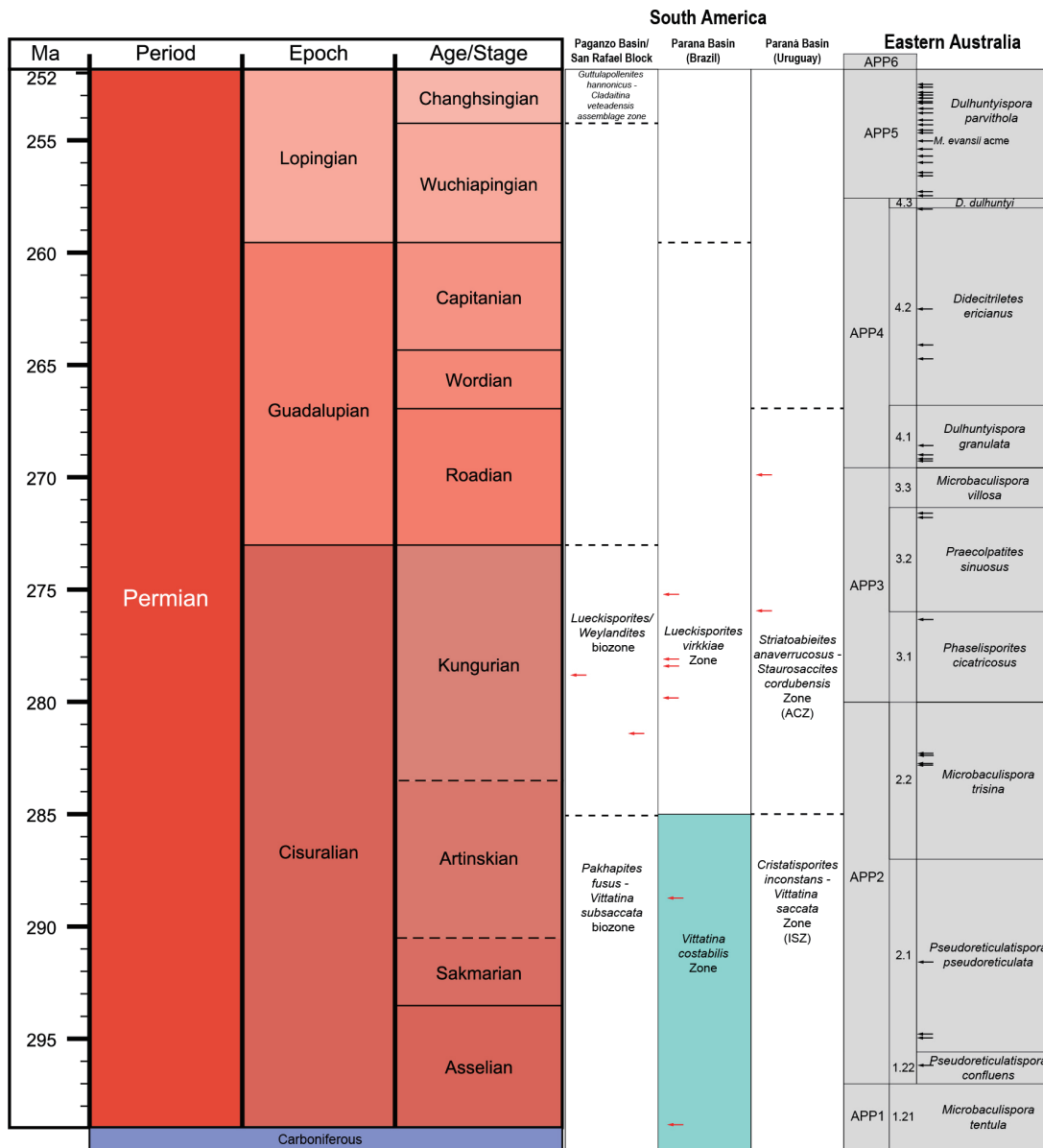


Fig. 1. Palynological zonation schemes of South America and eastern Australia calibrated to the global Permian stages (Henderson and Shen, 2020; Cohen et al., 2022) using radiometric age dates. Note the recent corrections to the time scale. Red arrows refer to ages referred to in Césari et al. (2022). Black arrows refer to ages referred to in Laurie et al. (2016). The highlighted *Vittatina costabilis* Zone is further calibrated by thirty-two age dates (Souza et al., 2021).

and McLoughlin, 2007; Stephenson, 2018; Jha et al., 2018). *Dulhuntyispora* has particular biostratigraphic utility in the Late Permian of Australia but is rare or absent in central and western Gondwana, where subregions are defined by the common occurrence of *Guttulapollenites* and *Lueckisporites*, respectively (Jha et al., 2018).

Many index taxa which are biostratigraphically significant in one region/basin, do not appear contemporaneously across all Gondwana, hindering interregional correlation. This can be seen when correlating Australia to both South Africa (Barbolini et al., 2016), and to the Middle East (Lindström and McLoughlin, 2007). Taxa that appear in the Middle Permian in Oman (Stephenson et al., 2003; Stephenson, 2006, 2008) appear only in the Late Permian or are even markers for the earliest Triassic in Australia (e.g., *Playfordiaspora crenulata*, *Triplexisporites playfordii*). This reflects the spread of floras evolving in low

latitude evolutionary centres to the high latitude zones as the climate became more amenable, something that similarly occurred with *Dicroidium* (Kerp et al., 2006; Abu Hamad et al., 2008). On a much smaller scale, diachroneity is observed on an intra- and inter-basinal scale in Southern Africa, between the northern and southern parts of the Main Karoo Basin and to the basins of Namibia (Barbolini et al., 2016; 2018).

Biostratigraphic suitability and temporal resolution

For a palynomorph taxon to fit the criteria as an index taxon for a biostratigraphic interval, it ideally fulfils the criteria of being relatively widespread geographically, temporally restricted and common. Many taxa used as index markers do not fulfil all these criteria. The subprovinciality of stratigraphically useful taxa in Gondwana limits their utility for regional correlation, but taxa that are more common and widespread (e.g., *Protohaploxylinus*)

have low temporal resolution. In Australia, Price (1997) defined further subzones for the eastern Australian biostratigraphic scheme for better temporal resolution. However, these subzones are poorly defined (i.e. using informal taxa or using the appearance of “large” forms of certain taxa or taxa that are restricted to specific areas within a basin). A better understanding of the utility of these higher resolution subzones is crucial for further development of Australia’s biostratigraphy. In South America, biostratigraphy relies mainly on assemblage zones with many zones covering intervals of tens of millions of years (Césari, 2007). Biostratigraphic schemes with higher temporal resolution are necessary to facilitate useful correlations between basins. To achieve this, future studies must thoroughly examine candidate taxa in terms of the geographical and temporal distribution. In this endeavour, analyses of large compilations of data, potentially using machine learning techniques may prove useful.

Conclusions and outlook

In order to effectively correlate using palynology, we as palynologists must always consider the processes that produce and affect the pollen and spores we examine. We must understand the floras that produce them, the environments and climates that influence the distribution of those floras, and the sedimentological processes that affect a palynomorph as it is deposited and preserved. It is worth remembering that earth systems, biotic and abiotic, are dynamic and their processes will always elude our attempts at neat categorisation. It is our job to build our classifications and correlations to fit the observations as opposed to cutting corners to make things fit neatly. In this regard, we must always be aware that our data records a vegetation history that is influenced by climatic change and tectonic processes and in this way, the Permian becomes a natural laboratory for better understanding the effects of deglaciation in deep time for comparison to the present.

References

Abu Hamad, A., Kerp, H., Vörding, B. and Bandel, K., 2008. A Late Permian flora with *Dicroidium* from the Dead Sea region, Jordan. *Review of Palaeobotany and Palynology*, v. 149, n. 3–4, p. 85–130.

Ayaz, S.A., Martin, M., Esterle, J., Amelin, Y. and Nicol, R.S., 2016. Age of the Yarrabee and accessory tuffs: implications for the upper Permian sediment-accumulation rates across the Bowen Basin. *Australian Journal of Earth Sciences*, v. 63, n.7, p. 843–856.

Barbolini, N., Bamford, M.K. and Rubidge, B., 2016. Radiometric dating demonstrates that Permian spore-pollen zones of Australia and South Africa are diachronous. *Gondwana Research*, v. 37, p. 241–251.

Barbolini, N., Rubidge, B. and Bamford, M.K., 2018. A new approach to biostratigraphy in the Karoo retroarc foreland system: Utilising restricted-range palynomorphs and their first appearance datums for correlation. *Journal of African Earth Sciences*, v. 140, p. 114–133.

Birgenheier, L.P., Frank, T.D., Fielding, C.R. and Rygel, M.C., 2010. Coupled carbon isotopic and sedimentological records from the Permian system of eastern Australia reveal the

response of atmospheric carbon dioxide to glacial growth and decay during the Late Palaeozoic age. *Palaeogeography, Palaeoclimatology, Palaeoecology*, v. 286, n. 3–4, p. 178–193.

Césari, S.N., 2007. Palynological biozones and radiometric data at the Carboniferous–Permian boundary in western Gondwana. *Gondwana Research*, v. 11, n. 4, p. 529–536.

Césari, S.N., Limarino, C.O., Marensi, S., Ciccioli, P.L., Bello, F.C., Ferreira, L.C., Scarlatta, L.R. and Friedman, R., 2022. High-precision U-Pb CA-ID-TIMS calibration of the Permian Lueckisporites-dominated assemblages in westernmost Gondwana: inferences for correlations. *Palynology*, v. 46, n. 2, p. 1–20.

Cleal, C.J., 2018. A global review of Permian macrofloral biostratigraphical schemes. In Lucas, S.G. and Shen, S.Z., eds. *The Permian Timescale*. Geological Society, London, Special Publications, v. 450, p. 349–364.

Cohen, K.M., Harper, D.A.T. and Gibbard, P.L., 2022. ICS International Chronostratigraphic Chart 2022/10. International Commission on Stratigraphy, IUGS. www.stratigraphy.org (visited: 2022/11/07)

Day, M.O., Ramezani, J., Frazer, R.E. and Rubidge, B.S., 2022. U-Pb zircon age constraints on the vertebrate assemblages and palaeomagnetic record of the Guadalupian Abrahamskraal Formation, Karoo Basin, South Africa. *Journal of African Earth Sciences*, v. 186, 104435.

Feurdean, A., Perşoiu, A., Tanţău, I., Stevens, T., Magyari, E.K., Onac, B.P., Marković, S., Andrič, M., Connor, S., Fărcaş, S., Gałka, M., Gaudeny, T., Hoek, W., Kolaczek, P., Kuneš, P., Lamentowicz, M., Marinova, E., Michczyńska, D.J., Perşoiu, I., Plóciennik, M., Słowiński, M., Stancikaite, M., Sumegi, P., Svensson, A., Tămaş, T., Timar, A., Tonkov, S., Toth, M., Veski, S., Willis, K.J. and Zernitskaya, V., 2014. Climate variability and associated vegetation response throughout Central and Eastern Europe (CEE) between 60 and 8 ka. *Quaternary Science Reviews*, v. 106, p. 206–224.

Fielding, C.R., Frank, T.D., McLoughlin, S., Vajda, V., Mays, C., Tevyaw, A.P., Winguth, A., Winguth, C., Nicoll, R.S. and Bocking, M., 2019. Age and pattern of the southern high-latitude continental end-Permian extinction constrained by multiproxy analysis. *Nature Communications*, v. 10, n. 1, p. 1–12.

Götz, A.E. and Wheeler, A., 2018. Challenges of Gondwanan Marine-Nonmarine Correlations – A Palynological Perspective. *Paleontological Journal*, v. 52, n. 7, p. 748–754.

Götz, A.E., Ruckwied, K. and Wheeler, A., 2018. Marine flooding surfaces recorded in Permian black shales and coal deposits of the Main Karoo Basin (South Africa): implications for basin dynamics and cross-basin correlation. *International Journal of Coal Geology*, v. 190, p. 178–190.

Henderson, C.M. and Shen, S.Z., 2020. The Permian Period. In Gradstein, F.M., Ogg, J.G., Schmitz, M.D. and Ogg, G.M., eds. *Geological Time Scale 2020, Volume 2*, Amsterdam, Elsevier, p. 875–902.

Gregory, W.A. and Hart, G.F., 1992. Towards a predictive model for the palynologic response to sea-level changes. *Palaios*, v. 7, p. 3–33.

Guerra-Sommer, M., Cazzulo-Klepzig, M., Formoso, M.L.L.,

- Menegat, R. and Fo, J.G.M., 2008. U–Pb dating of tonstein layers from a coal succession of the southern Paraná Basin (Brazil): a new geochronological approach. *Gondwana Research*, v. 14, n. 3, p. 474–482.
- Holz, M. and Dias, M.E., 1998. Taphonomy of palynological records in a sequence stratigraphic framework: an example from the Early Permian Paraná Basin of southern Brazil. *Review of Palaeobotany and Palynology*, v. 99, n. 3-4, p. 217–233.
- Huntley, B. and Webb III, T., 2012. *Vegetation history*, Volume 7, Springer Science & Business Media.
- Isbell, J.L., Henry, L.C., Gulbranson, E.L., Limarino, C.O., Fraiser, M.L., Koch, Z.J., Ciccioli, P.L. and Dineen, A.A., 2012. Glacial paradoxes during the late Paleozoic ice age: Evaluating the equilibrium line altitude as a control on glaciation. *Gondwana Research*, v. 22, n. 1, p. 1–19.
- Jha, N., 2006. Permian palynology from India and Africa – a phytogeographical paradigm. *Journal of the Palaeontological Society of India*, v. 51, n. 1, p. 43–55.
- Jha, N., Aggarwal, N. and Mishra, S., 2018. A review of the palynostratigraphy of Gondwana sediments from the Godavari Graben, India: Global comparison and correlation of the Permian-Triassic palynoflora. *Journal of Asian Earth Sciences*, v. 163, p. 1–21.
- Kerp, H., Abu Hamad, A., Vörding, B. and Bandel, K., 2006. Typical Triassic Gondwanan floral elements in the Upper Permian of the paleotropics. *Geology*, v. 34, n. 4, p. 265–268.
- Laurie, J.R., Bodorkos, S., Nicoll, R.S., Crowley, J.L., Mantle, D.J., Mory, A.J., Wood, G.R., Backhouse, J., Holmes, E.K., Smith, T.E. and Champion, D.C., 2016. Calibrating the middle and late Permian palynostratigraphy of Australia to the geologic time-scale via U-Pb zircon CA-IDTIMS dating. *Australian Journal of Earth Sciences*, v. 63, n. 6, p. 701–730.
- Limarino, C.O. and López-Gamundí, O.R., 2021. Late Paleozoic basins of South America: Insights and progress in the last decade. *Journal of South American Earth Sciences*, v. 107, 103150.
- Lindström, S. and McLoughlin, S., 2007. Synchronous palynofloristic extinction and recovery after the end-Permian event in the Prince Charles Mountains, Antarctica: implications for palynofloristic turnover across Gondwana. *Review of Palaeobotany and Palynology*, v. 145, n. 1–2, p. 89–122.
- Lopes, G., Pereira, Z., Fernandes, P., Marques, J., Mendes, M. and Götz, A.E., 2021. Permian stratigraphy and palynology of the Karoo Group in Mozambique – a 2020 perspective. *Newsletters on Stratigraphy*, v. 54, n. 3, p. 335–362.
- Lucas, S.G., 2006. *Global Permian tetrapod biostratigraphy and biochronology*. Geological Society, London, Special Publications, v. 265, n. 1, p. 65–93.
- Mays, C., Vajda, V., Frank, T.D., Fielding, C.R., Nicoll, R.S., Tevyaw, A.P. and McLoughlin, S., 2020. Refined Permian-Triassic floristic timeline reveals early collapse and delayed recovery of south polar terrestrial ecosystems. *GSA Bulletin*, v. 132, n. 7–8, p. 1489–1513.
- McLoughlin, S., Nicoll, R.S., Crowley, J.L., Vajda, V., Mays, C., Fielding, C.R., Frank, T.D., Wheeler, A. and Bocking, M., 2021. Age and paleoenvironmental significance of the Frazer Beach Member – A new lithostratigraphic unit overlying the End-Permian Extinction Horizon in the Sydney Basin, Australia. *Frontiers in Earth Science*, v. 8, 600976.
- Metcalfe, I., Crowley, J.L., Nicoll, R.S. and Schmitz, M., 2015. High-precision U-PbCA-TIMS calibration of middle Permian to lower Triassic sequences, mass extinction and extreme climate-change in eastern Australian Gondwana. *Gondwana Research*, v. 28, no. 1, p. 61–81.
- Mori, A.L.O., Souza, P.A., Marques, J.C. and Lopes, R.C., 2012. A new U–Pb zircon age dating and palynological data from a Lower Permian section of the southernmost Paraná Basin, Brazil: biostratigraphical and geochronological implications for Gondwanan correlations. *Gondwana Research*, v. 21, no. 2-3, p. 654–669.
- Phillips, L.J., Crowley, J.L., Mantle, D.J., Esterle, J.S., Nicoll, R.S., McKellar, J.L. and Wheeler, A., 2018. U-Pb geochronology and palynology from Lopingian (upper Permian) coal measure strata of the Galilee Basin, Queensland, Australia. *Australian Journal of Earth Sciences*, v. 65, n. 2, p. 153–173.
- Prevec, R., Nel, A., Day, M.O., Muir, R.A., Matiwane, A., Kirkaldy, A.P., Moyo, S., Staniczek, A., Cariglino, B., Maseko, Z., Kom, N., Rubidge, B.S., Garrouste, R., Holland, A. and Barber-James, H.M., 2022. South African Lagerstätte reveals middle Permian Gondwanan lakeshore ecosystem in exquisite detail. *Communications Biology*, v. 5, n. 1, p. 1–14.
- Price, P.L., 1997. Permian to Jurassic palynostratigraphic nomenclature of the Bowen and Surat Basins. In Green, P.M., ed. *The Surat and Bowen Basins, Southeast Queensland*. Queensland Department of Mines and Energy, Brisbane, p. 137–178.
- Ruckwied, K., Götz, A.E. and Jones, P., 2014. Palynological records of the Permian Ecca Group (South Africa): Utilizing climatic icehouse–greenhouse signals for cross basin correlations. *Palaeogeography, Palaeoclimatology, Palaeoecology*, v. 413, p. 167–172.
- Simas, M.W., Guerra-Sommer, M., Cazzulo-Klepzig, M., Menegat, R., Santos, J.O.S., Ferreira, J.A.F. and Degani-Schmidt, I., 2012. Geochronological correlation of the main coal interval in Brazilian Lower Permian: Radiometric dating of tonstein and calibration of biostratigraphic framework. *Journal of South American Earth Sciences*, v. 39, p. 1–15.
- Souza, P.A., Boardman, D.R., Premaor, E., Félix, C.M., Bender, R.R. and Oliveira, E.J., 2021. The *Vittatina costabilis* Zone revisited: New characterization and implications on the Pennsylvanian-Permian icehouse-to-greenhouse turnover in the Paraná Basin, Western Gondwana. *Journal of South American Earth Sciences*, v. 106, 102968.
- Stephenson, M.H., 2006. Stratigraphic Note: update of the standard Arabian Permian palynological biozonation; definition and description of OSPZ5 and 6. *GeoArabia*, v. 11, n. 3, p. 173–178.
- Stephenson, M.H., 2008. Spores and pollen from the middle and upper Gharif members (Permian) of Oman. *Palynology*, v. 32, n. 1, p. 157–182.
- Stephenson, M.H., 2018. Permian palynostratigraphy: a global

- overview. In Lucas, S.G. and Shen, S.Z., eds. The Permian Timescale. Geological Society, London, Special Publications, v. 450, p. 321–347.
- Stephenson, M.H., Osterloff, P.L. and Filatoff, J., 2003. Palynological biozonation of the Permian of Oman and Saudi Arabia: progress and challenges. *GeoArabia*, v. 8, n. 3, p. 467–496.
- Stojakowits, P. and Mayr, C., 2022. Quaternary Palynostratigraphy of Germany with special emphasis on the Late Pleistocene. In Montenari, M. (ed.), *Integrated Quaternary Stratigraphy. Stratigraphy and Timescales, Volume 7*, Amsterdam, Elsevier. <https://doi.org/10.1016/bs.sats.2022.09.001>
- Wheeler, A., Van de Wetering, N., Esterle, J. and Götz, A.E., 2020. Palaeoenvironmental changes recorded in the palynology and palynofacies of a Late Permian Marker Mudstone (Galilee Basin, Australia). *Palaeoworld*, v. 29, n. 2, p. 439–452.

Wuchiapingian brachiopods from Iran: potential and perspectives as archives of the past

Marco Viaretti

Dipartimento di Scienze della Terra “A. Desio”, Via Mangiagalli 34, 20133 Milano.

Email: marco.viaretti@unimi.it

Gaia Crippa

Dipartimento di Scienze della Terra “A. Desio”, Via Mangiagalli 34, 20133 Milano.

Email: gaia.crippa@unimi.it

Lucia Angiolini

Dipartimento di Scienze della Terra “A. Desio”, Via Mangiagalli 34, 20133 Milano

Email: lucia.angiolini@unimi.it

The Wuchiapingian (Lopingian) time interval is well-represented in sedimentary successions across Iran, often bearing rich brachiopod faunas (Angiolini and Carabelli, 2010; Garbelli et al., 2014; Ghaderi et al., 2014; Viaretti et al., 2021). Given the complex tectonic setting of the region (see Viaretti et al., 2021 and references therein for an overview), consisting of a mosaic of microplates compressed between the Arabian and Eurasian plates, correlation is challenging, also because of different depositional settings recorded by the Lopingian successions (Angiolini and Carabelli, 2010; Ghaderi et al., 2014). Using brachiopod faunas, Viaretti et al. (2021) correlated the Abadeh (Taraz et al., 1981) and Ali Bashi Mountains Main Valley (Julfa; Ghaderi et al., 2014) sections, both considered very important records of the Permian-Triassic transition in the Neotethys ocean (Fig. 1). The correlation has been made using the Unitary Association method (Guex, 1991), demonstrating the value of brachiopods as correlation tools at the regional scale.

Geochemical analyses of the brachiopod shells from the

Hambast Formation in the Abadeh section (Viaretti et al., 2022) have been performed on selected taxa, based on their shell microstructure. The Strophomenata *Araxilevis intermedius* (Abich, 1878), *Leptodus nobilis* (Waagen, 1883), *Leptodus* cf. *richthofeni* Kayser, 1883, *Spinomarginifera helica* (Abich, 1878), *Spinomarginifera iranica* Fantini Sestini, 1965, and *Spinomarginifera* sp. were selected among those taxa bearing a laminar secondary layer; whereas the Rhynchonellata *Araxathyris bruntoni* Angiolini and Carabelli, 2010, *?Rectambitus* sp., *Transcaucasathyris araxensis* (Grunt in Ruzhentsev and Sarytcheva, 1965), *T. kandevani* (Fantini Sestini and Glaus, 1966) and *T. lata* (Grunt in Ruzhentsev and Sarytcheva, 1965) were selected among the taxa with a fibrous secondary layer. The main aim of the study was to detect the best taxa from the Abadeh succession to use for isotopic analyses, considering the importance of the selection of a certain shell microstructure in geochemical analyses (i.e. Garbelli et al., 2012, 2014) and given the poor preservation and the very small size of most of the taxa, particularly the species of the genera *Araxathyris*, *Transcaucasathyris* and *?Rectambitus*.

Prior to the isotopic analysis, a study of the microstructure of all the specimens has been performed using the SEM; however, the shell of many specimens showed signs of local to complete alteration, without any evident pattern linked to taxon-specificity or stratigraphic position. The microstructure of the Strophomenata specimens is characterized by a laminar secondary layer, made of cross-bladed laminae, which show signs of amalgamation and disruption across the entire length of each microstructural element (laminae). Except for the specimens of *Araxilevis intermedius*, where this layer has a thickness of 300–1000 μm , the occurrence of the laminar layer is generally limited due to the small size of the specimens and the decortication of the shell. The shell of *Araxilevis intermedius* also shows the presence of pseudopunctae. The Rhynchonellata microstructure instead consists of a fibrous secondary layer. In this case, the alteration is manifested by the microstructural elements (fibers) mainly through amalgamation, sometimes with the deformation of their shape in transverse section. This layer is consistently limited, with a thickness of 50–200 μm . Some specimens, belonging to both Strophomenata and Rhynchonellata, possess a columnar tertiary layer, variably preserved. The isotopic analysis was performed using a Finnigan GasBench connected to a Delta V (Thermo Fisher Scientific Inc., Waltham, Massachusetts, USA) mass spectrometer at Dipartimento di Scienze della Terra “A. Desio”, Università degli Studi di Milano on 200–250 μg of powders collected from pristine shells. The powders were collected using a hand-held drill equipped with a tungsten carbide drill bit in case of specimens embedded in resin (too small to be worked without any physical support), in which only the longitudinal section of the shell was available as a sampling surface. The powder from all the other specimens (larger than 15 mm in length or width) was collected through a manual abrasion of the shell with a file and an awl, a simple and fast method to collect enough powder. Isotope values ($\delta^{18}\text{O}$, $\delta^{13}\text{C}$) are reported as per mil (‰) deviations of the isotopic ratios ($^{18}\text{O}/^{16}\text{O}$, $^{13}\text{C}/^{12}\text{C}$) calculated to the V-PDB scale using two within-run internal laboratory standards (MAQ and MOKA) calibrated against the International standards IAEA-

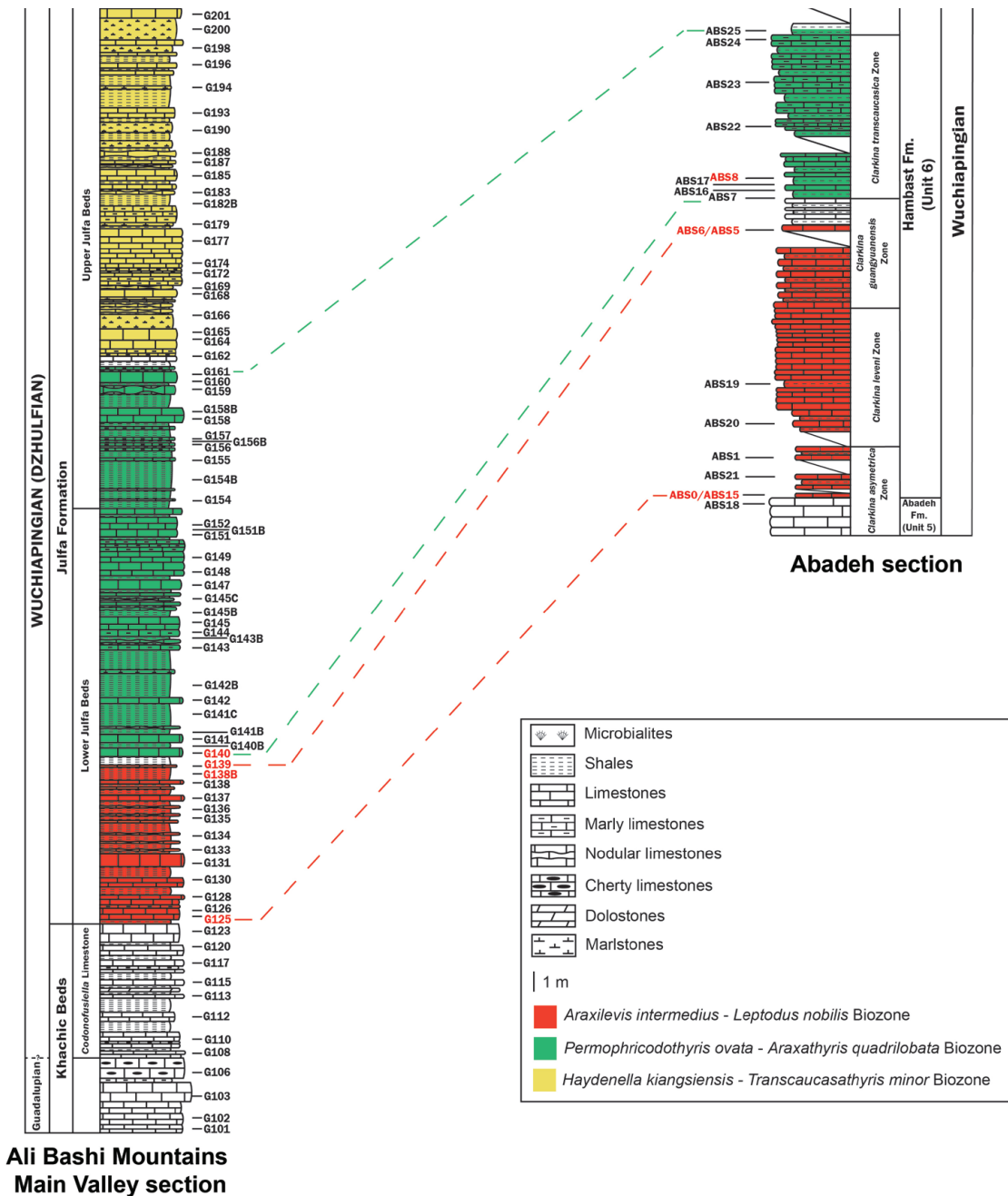


Fig. 1. Correlation between the Abadeh (Viaretti et al., 2021) and Julfa (Ghaderi et al., 2014) sections. Red labels indicate the beds with the specimens selected for the isotopic analyses. Modified from Viaretti et al. (2021).

603 and NBS-18.

Here, we focus on the results of the analysis of the oxygen isotope composition which returned $\delta^{18}\text{O}$ values comprised between -2.0‰ and -5.9‰ . In a previous study, Garbelli et al. (2014) recorded values ranging from -3.2‰ to -4.8‰ for Rhynchonellata shells and from -3.3‰ to -5.5‰ for Strophomenata shells from the Wuchiapingian Nesen Formation of N Iran, all deemed to be pristine. However, the temperatures obtained from these low values, applying the newest brachiopod-based oxygen-isotope thermometer (Brand et al., 2019), would far exceed 30°C . These temperatures are unlikely for a depositional environment at water depth around 50-60 m at low paleolatitudes, as the one reconstructed for the Wuchiapingian

Hambast Formation (Viaretti et al., 2021). Temperatures reported at similar water depths in modern low latitudes basins, such as the Persian Gulf, are around $20^\circ\text{-}25^\circ\text{C}$ (Guinehut et al., 2012). We thus considered likely that only the specimens of the two classes recording $\delta^{18}\text{O}$ values higher than -3.5‰ could be considered pristine (Fig. 2).

Among all the analyzed specimens from the Hambast Formation in the Abadeh section, only the *Araxilevis intermedius* ones show $\delta^{18}\text{O}$ values consistently above the -3.5‰ threshold, a result most probably linked to their large size and very thick shell, which, even if partially altered during diagenetic processes, could have maintained some shell portions pristine, thus representing a good taxon to be used for isotopic analyses.

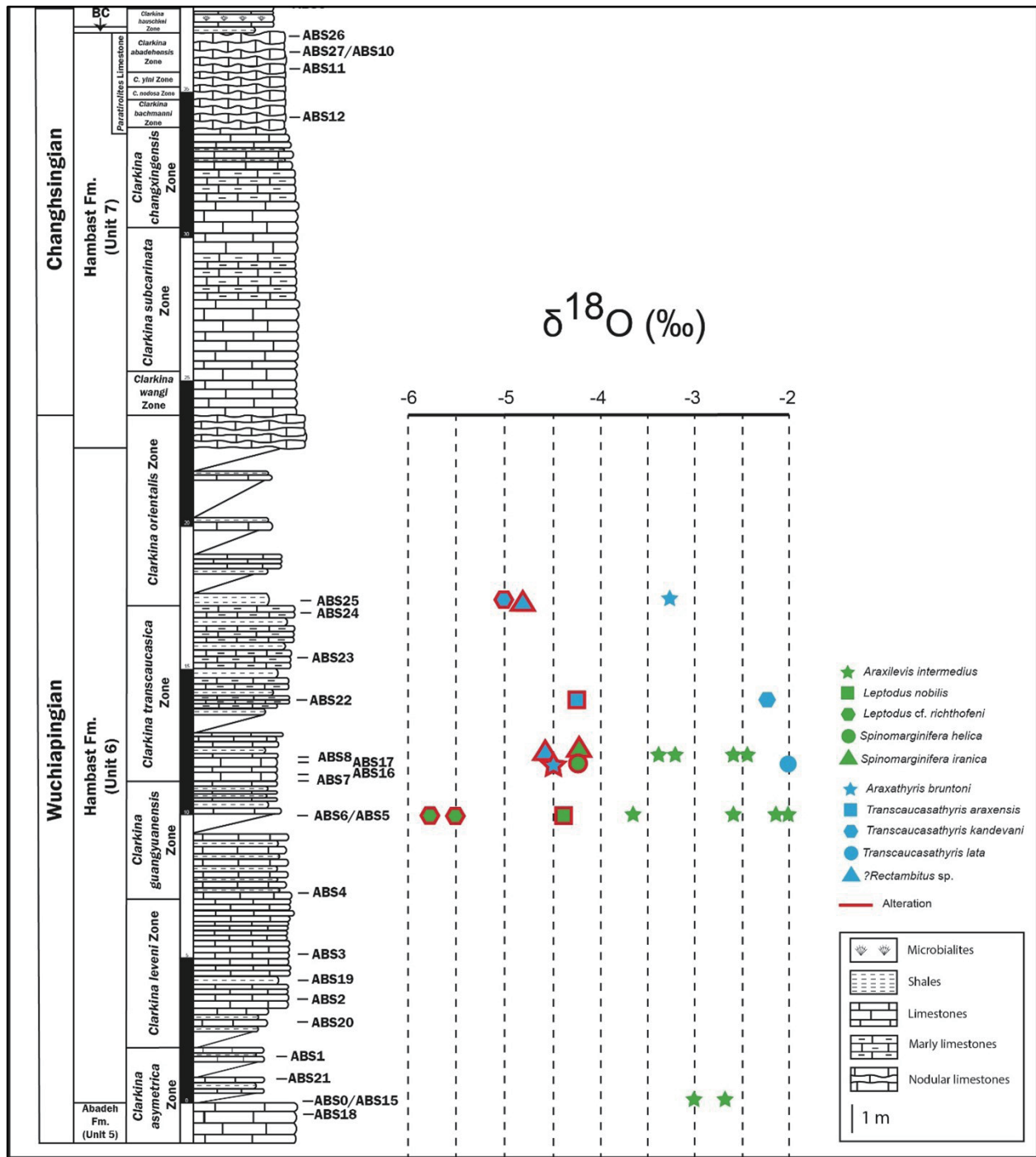


Fig. 2. Shell $\delta^{18}\text{O}$ values and stratigraphic position of the analyzed brachiopods from the Hambast Formation in the Abadeh section.

For this reason, we selected further specimens of *Araxilevis intermedius* from the Julfa Formation in the Ali Bashi Mountains Main Valley section, comparing possibly coeval beds in the two sections following the correlation made by Viaretti et al. (2021) (Fig. 1). All the examined *A. intermedius* specimens from the Julfa Formation show a well preserved shell microstructure (Fig. 3a), differing from the locally-to-mostly altered specimens from Abadeh (Fig. 3b). To complete the evaluation of the preservation of the specimens from the two sections, we analyzed by cathodoluminescence shells from both Abadeh and Julfa

sections. This screening test showed that, except for one slightly luminescent specimen, all the shells of *A. intermedius* are non-luminescent, regardless of the section they come from and the morphological preservation of the secondary layer fabric (Fig. 4).

The data collected so far show that *Araxilevis intermedius* is the species best suited for isotopic analyses in the Wuchiapingian formations of Iran. Therefore, further detailed isotopic analyses will be performed on these specimens using a sclerochronological approach, following the method recently published by Garbelli et al. (2022). The analyses will be performed in collaboration with

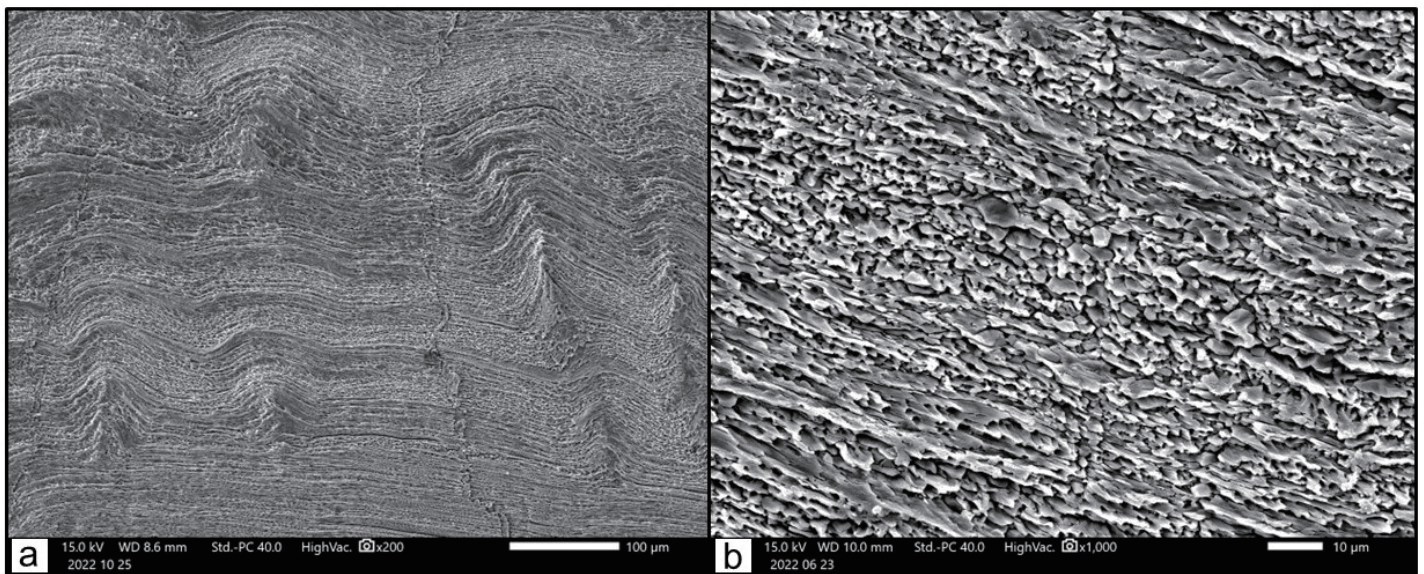


Fig. 3. a. SEM photomicrograph of the shell microstructure of *Araxilevis intermedius* (G140-12) from the Julfa Formation showing a well preserved laminar (cross-bladed) secondary layer with pseudopunctae; b. SEM photomicrograph of the shell microstructure of *Araxilevis intermedius* (ABS5-13) from the Hambast Formation showing local alteration of the laminae.

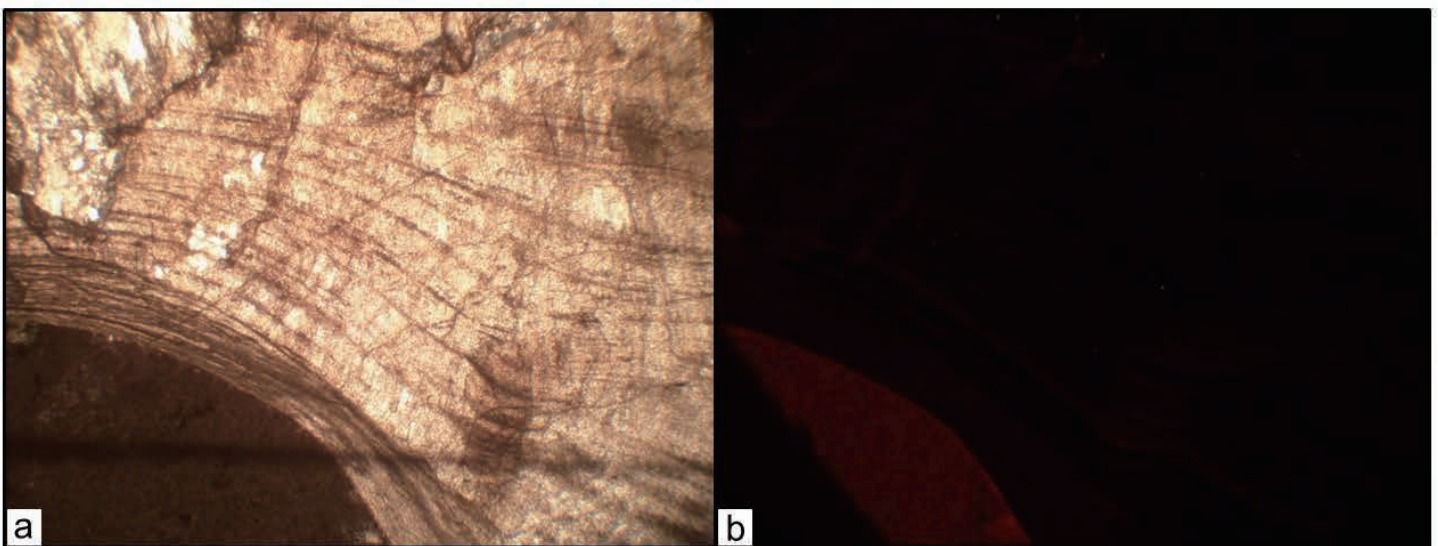


Fig. 4. *Araxilevis intermedius* (ABS8-6) from the Abadeh section. a. photomicrographs under parallel polarizers and b. cathodoluminescence.

Renato Posenato of the University of Ferrara.

Garbelli et al. (2022) analyzed, among others, shells of species of *Permophricodothyris* and *Araxathyris* (both genera of Rhynchonellata with a fibrous secondary layer and a tertiary layer) from the Julfa Formation, showing that they retain a good, even if narrow due to the low latitudes location, seasonal variation record; it will be interesting to compare the isotopic composition recorded by *Araxilevis intermedius* (Strophomenata) with that of *Permophricodothyris* and *Araxathyris*, and compare the seasonal signal in the two sections. In fact the analyses of specimens of species of *Permophricodothyris* and *Araxathyris* from the Abadeh section is not feasible, as the first taxon is questionably represented by one specimen only, and the second one only by small-sized and altered specimens.

The selection of the best archive to investigate past conditions

is not trivial, and it is crucial to correctly interpret paleoclimate and paleoenvironments, particularly during times of climatic, environmental and biotic turnover such as the Wuchiapingian, an interval not much considered so far, but which seems to record some important changes and a cooling phase before the end-Permian hothouse (Gong et al., 2022; Wang et al., 2022).

References

- Angiolini, L. and Carabelli, L., 2010. Upper Permian brachiopods from the Nesen Formation, North Iran. *Special Papers in Palaeontology*, v. 84, p. 41–90.
- Brand, U., Bitner, M.A., Logan, A., Azmy, K., Crippa, G., Angiolini, L., Colin, P., Griesshaber, E., Harper, E.M., Ruggiero, E.T. and Haussermann, V., 2019. Brachiopod-based oxygen-isotope thermometer: update and review. *Rivista*

- Italiana Di Paleontologia e Stratigrafia, v. 125, n. 3, p. 775–787.
- Garbelli, C., Angiolini, L., Jadoul, F. and Brand, U., 2012. Micromorphology and differential preservation of upper Permian brachiopod low-Mg calcite. *Chemical Geology*, v. 298–299, p. 1–10.
- Garbelli, C., Angiolini, L., Brand, U. and Jadoul, F., 2014. Brachiopod fabric, classes and biogeochemistry: implications for the reconstruction and interpretation of seawater carbon-isotope curves and records. *Chemical Geology*, v. 371, p. 60–67.
- Garbelli, C., Angiolini, L., Shen, S.Z., Crippa, G., Yuan, D., Bahramanesh, M., Abbasi, S. and Birjandi, M., 2014. Additional brachiopod findings from the Lopingian succession of the Ali Bashi Mountains, NW Iran. *Rivista Italiana Di Paleontologia e Stratigrafia*, v. 120, n. 1, p. 119–126.
- Ghaderi, A., Garbelli, C., Angiolini, L., Ashouri, A.R., Korn, D., Rettori, R. and Mahmudy Gharaie, M.H., 2014. Faunal changes near the End Permian Extinction: the brachiopods of the Ali Bashi Mountains, NW Iran. *Rivista Italiana di Paleontologia e Stratigrafia*, v. 120, n. 1, p. 27–59.
- Gong, Z., Zhang, M., Li, J. and Huang, C., 2022. Late Permian ~6 My cooling induced by basaltic weathering of the Emeishan large igneous province: Evidence from interbasaltic paleosols. *Palaeogeography, Palaeoclimatology, Palaeoecology*, v. 609, 111305.
- Guex, J., 1991. *Biochronological correlations*: Springer, Berlin. 252 pp.
- Guinehut, S., Dhomps, A.L., Larnicol, G. and Le Traon, P.Y., 2012. High resolution 3-D temperature and salinity fields derived from in situ and satellite observations. *Ocean Science*, v. 8, n. 5, p. 845–857.
- Taraz, H., Golshani, F., Nakazawa, K., Shimura, D., Bando, Y., Ishii, K.I., Maurata, M., Okimura, Y., Sakamura, S., Nakamura, K. and Tokuoka, T., 1981. The Permian and the Lower Triassic Systems in Abadeh Region, Central Iran. *Memoirs of the Faculty of Science, Kyoto University, Series of Geology and Mineralogy*, v. 47, p. 62–133.
- Viaretti, M., Crippa, G., Posenato, R., Shen, S.Z. and Angiolini, L., 2021. Lopingian brachiopods from the Abadeh section (Central Iran) and their biostratigraphic implications. *Bollettino della Società paleontologica Italiana*, v. 60, n. 3, p. 213–254.
- Viaretti, M., Crippa, G. and Angiolini, L., 2022. Brachiopods from the Upper Permian of Central Iran: shell microstructure and isotopic signature as archives of global changes in the geological past. In Carmina, B., Innamorati, G., Fascio, L., Pasero, M. and Petti, F.M. (eds), *Congresso SGI-SIMP 2022 - Geosciences for a sustainable future*. Abstract book, p. 708.
- Wang, W.Q., Garbelli, C., Zhang, F.F., Zheng, Q.F., Zhang, Y.C., Yuan, D.X., Shi, Y.K., Chen, B. and Shen, S.Z., 2020. A high-resolution Middle to Late Permian paleotemperature curve reconstructed using oxygen isotopes of well-preserved brachiopod shells. *Earth and Planetary Science Letters*, v. 540, 116245.
- News from the Permian of Northern Albania at the base of the Albanian Alps**
- Micha Horacek**
Department of Lithospheric Research, Vienna University, Austria
- Leopold Krystyn**
Department of Palaeontology, Vienna University, Austria
- Rainer Brandner**
Institut für Geologie und Paläontologie, Innsbruck Universität, Austria
- Cerciz Durmishi**
Faculty of Geology and Mining, Tirana Polytechnic University (UPT), Tirana, Albania
- Kujtim Onuzi**
Geosciences Institute, Tirana Polytechnic University (UPT), Tirana, Albania

Introduction

Albania is geologically a very interesting and fascinating spot for many reasons, starting with obducted ophiolites and the resulting ore deposits, and complex tectonic settings due to a multiphase Alpine orogeny (and older ones, already pre-Cimmerian tectonic activities). It is also interesting and relevant area with respect to tectonic correlation and palinspastic reconstruction of the wider Dinarid-Albanid-Hellenid realm. Well-developed Permian fossiliferous rocks of the Albanian Alps and/or neighbouring areas are of special interest, and can shed light on the still-ambiguous and controversial paleogeographic reconstructions of this time interval within the Mediterranean region (e.g. Schmid et al., 2020).

The Albanian Alps (Fig. 1) are confined tectonically by the Cukali Zone, which lies below, and the Gashi Zone and Vermoshi Zone which lies above (Xhomo et al., 2008). The Albanian Alps are composed of several tectonic blocks (Fig. 1C), as they have been termed in the literature. However, we prefer the term “thrust sheet”, as “block” might be understood in an autochthonous context. Thus, our “sheets” are identical with the “Blocks” mentioned in the respective literature (Gaetani et al., 2015; Muttoni et al., 1998; Xhomo et al., 2008). The lowermost one is the Bishkaz-Shale Sheet, which is overlain by the Teth Sheet and the Valbona Sheet (Xhomo et al., 2008), and towards the north and east there are further sheets, which are of no direct interest for the present work. First studies have been published by Muttoni et al. (1999) and Gaetani et al. (2015), basing on earlier Albanian works (Vetters, 1906; Xhomo et al., 1969, 1975, 2002; Toska and Bushati 1970; Gjata and Skela, 1972; Peza et al., 1973; Pirdeni, 1973, 1982; Biçoku et al., 1974; Theodori et al., 1978, 1988, 1993; Shima et al., 1980; Peza, 1981, 1983, 1985; Shehu et al., 1983; Toska and Selenica, 1988; Biçoku and Arkaxhiu, 1998; Lula et al., 1999; Meco, 1999; Meco et al., 2000, 2011). Muttoni et al. (1999) place the base of the Albanian Alps (see

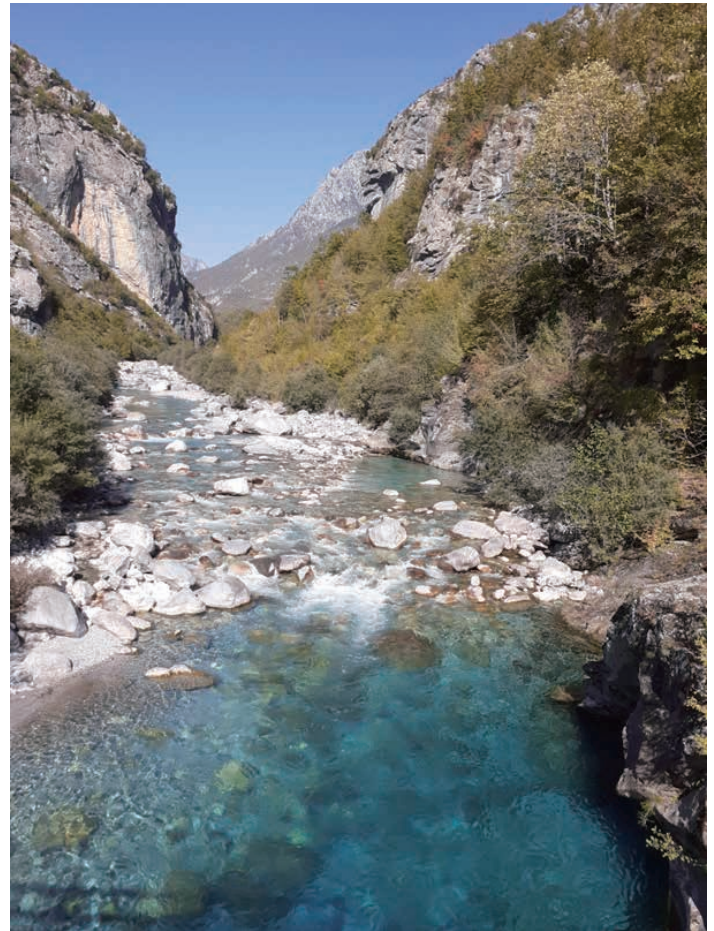
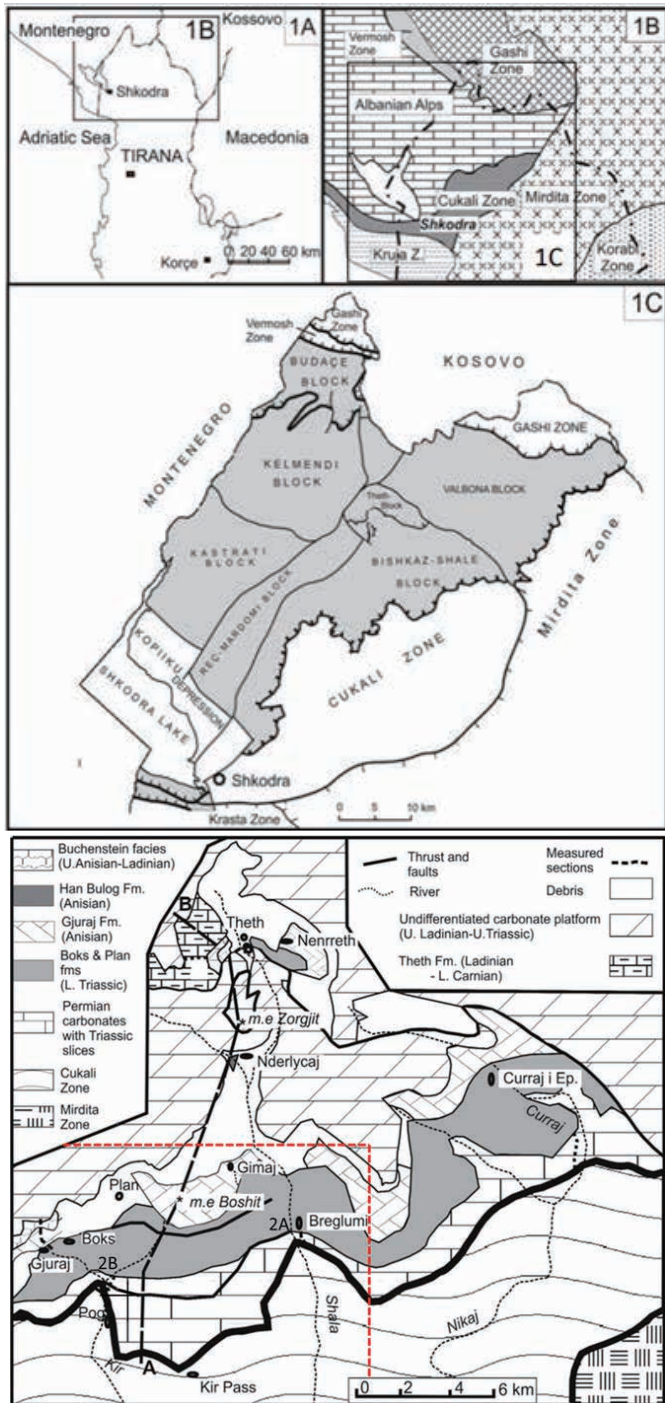


Fig. 2A. The “Shala Gate”, a short gorge of the Shala Valley passing through the Pog Formation consisting of debris flows of Permian carbonate. Position can be seen in Fig. 1 and in Fig. 7 nearby position 19/73.

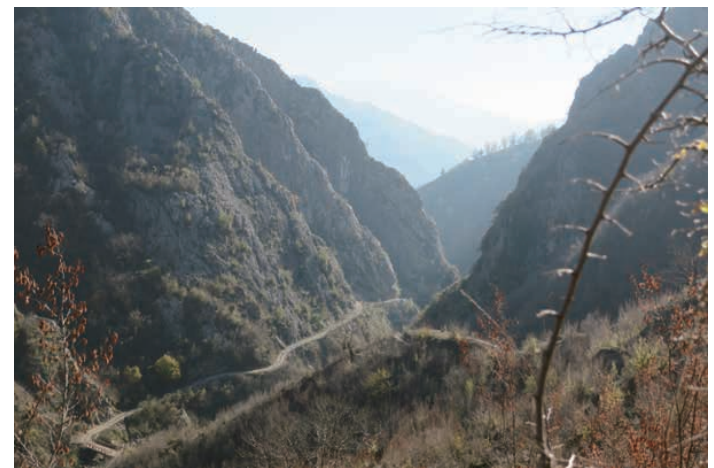


Fig. 2B. Kir Valley gorge through the Pog Formation, photo taken from the North towards south showing the road on the eastern side. Position can be seen in Fig. 1, and approximately 17/11 in Fig. 7.

Fig. 1. 1A and 1B. Index map of the study area, 1C. structural map of the Albanian Alps [modified after Xhomo et al. (2008) and Gaetani et al. (2015)]. Despite that the different units are termed “Block” we regard them as “sheet”, see text. 1D. Coarse sketch of the Albanian Alps (after Gaetani et al., 2015) showing the approximate area (dashed line) of investigation and of the aerial photo (Google photo) in Fig. 7. The thick black line indicating the thrust between the “Permian carbonates with Triassic slices” and the “Cukali Zone” is debated and questioned. “2A” and “2B” indicate the position of the photos shown in Figs. 2A and 2B.

their fig. 1B) below the Permian massive limestones (which have been investigated and named the “Pog Formation” of Middle Permian age by Gaetani et al.(2015)). The Pog Formation consists of a quite massive carbonate interval forming a kind of cliff and massive-looking carbonate unit, which builds the “Shala-Gate” (Fig. 2A) in the Shala River Valley and in which

the Kir River has excavated the “Kir-River-Gorge” (Fig. 2B) in the Kir Valley. Below the Pog Formation, Muttoni et al.(1999) report Cretaceous to Palaeogene flysch with Permian blocks belonging to the Cukali Zone, which is the adjacent tectonic unit below the Albanian Alps. Between the Kir and Shala valley, Muttoni et al. (1999) report a lower unit of the Permian massive

carbonates, which they also count to the Permian Pog Formation (perhaps as a kind of duplex structure, as briefly mentioned in Gaetani et al. (2015), and which is separated by the upper one (the Pog Formation sensu Gaetani et al., 2015) by the mentioned Cretaceous flysch containing Permian blocks. Slightly differently, Gaetani et al. (2015; see the inset in their fig. 4) report below the Pog Formation (the above-mentioned Permian massive limestones) “conglomerates and shales, possibly Triassic” which they seem to correlate with the Lower Triassic Boks Formation (resting on top of the Pog Formation) that also consists of shales and conglomerates, thereby separating the Pog Formation from the Permian carbonate unit below (the latter they also regard as duplex structure, as described above). Furthermore they write: “ ... the tectonic setting of the lower part of the Bishkaz-Shale Block is more complicated than reported in these [Albanian geological] maps. Important duplex structures intersect the Permian rocks, which are subdivided by Triassic slices [...]. We therefore decided to describe only part of the Permian succession, as exposed along the Kir Valley, north of Pog, leaving the basal



Fig. 4. Conglomerate (and debris-flow) at the top of the Pog Formation, resembling from its content/consistence the conglomerate below the Pog Formation (dominantly siliciclastic components, black components (lydite?), less large-sized components).

stack of the Albanian Alps, as exposed along the Shala and Curraj valleys, for a future study...” Our report continues here and is in line with earlier studies of Permian to Middle Triassic sediments in the Budva Zone (Krystyn et al., 2019; Horacek et al., 2020), regarded by many authors (e.g. Schmid et al., 2020) as the northward continuation of the Cukali Zone as well as in the external Dinarides (e.g. Aljinovic et al., 2018), known as the equivalent to the Hochkarst zone and the Albanian Alps.

**New observations:
Pog Formation**

Our field studies revealed, contrary to Gaetani et al.(2015), who report a continuous sedimentary succession, that the entire Pog Formation (in the Kir and Shala Valleys) can be regarded as succession of mass-flows/olistoliths (Fig. 3A), which disintegrate laterally and on the top into megabreccias of different clast sizes. We assume an almost syn-sedimentary and quick re-deposition of these large blocks and components, as we could not find evidence of younger sediments coexisting within the Pog Formation and there is (almost) no difference in age from the base to the top of this unit (Gaetani et al., 2015). Furthermore, the finding of Lower Permian conodonts in a carbonate block on top of the formation indicates redeposition of also older marine sediments (sample 18/90, Fig. 3B; Horacek et al., in prep.). Gaetani et al. (2015, text-fig. 4) did exclude this interval from the Pog Formation for which we see no good reason. Evidence for quick and more or less continuous deposition of these megabreccias is the obvious absence of a shale matrix between the blocks, as for example in the underlying Xhani Formation or the overlying Boks Formation. The “Boks-Shale”-like tectonic interlayers mentioned by Gaetani et al. (2015) have turned out as lenses of dark, thin-bedded coarse to fine-grained, biotrititic limestones containing also Middle Permian conodonts (Horacek et al., in prep.).

A local, wedge-shaped conglomerate body (Fig. 4) north of the Kir river gorge - directly east of the bridge- marks the boundary to the disconformally, on a regional scale already unconformably overlying Boks Shales/ Formation, interpreted by Gaetani et al. (2015) to represent most of the Lower Triassic. Still, this



Fig. 3A. Photograph from the west-side of the Kir Valley gorge through the Pog Formation. Thicker and thinner layers of debris flows, one on another, (almost) without any interruption by background sedimentation. In the upper right quarter of the photo can be seen a large carbonate block within a debris flow. Position approximately 17/11 on Fig. 7.

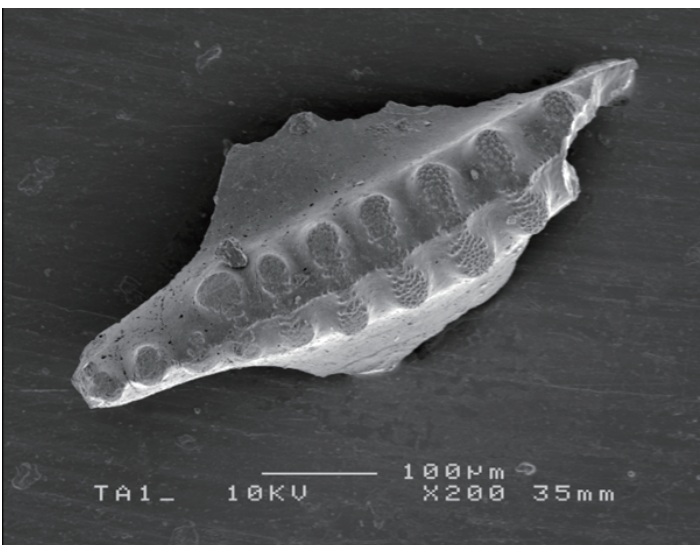


Fig. 3B. Lower Permian conodont *Sweetognathodus* cf. *whitei*, sample 18/90.



Fig. 5. Typical Boks-conglomerate/breccia with a large amount of Permian carbonate detritus. Position is from of the “2.Kgl” points in Fig. 7.

conglomerate contains siliciclastic and also some black (lydite?) components, differing from the strongly carbonate dominated Boks conglomerates (Fig. 5).

“Sub-Pog Beds”

Below the Pog Formation are two thick mass-flows (PDF: Permian Debris Flow, Fig. 7), containing mid-Permian carbonate components, underlain by a massive and thick conglomerate unit (Fig. 6, sample 21/21 in Fig. 7) which we tentatively name as the Sub-Pog Beds (SPK: Sub-Pog conglomerate in Fig. 7). These Sub-Pog Beds are separated by a thin shale layer (Fig. 7). Our first and preliminary investigations revealed that the conglomerates below the Pog Formation contain, besides Permian? shallow-water carbonate clasts, a considerable amount of siliciclastic and quartz pebbles. This is a significant difference to the Boks conglomerates (Fig. 5) dominated by carbonate components (except for the topmost Boks conglomerate). Some of the smaller conglomerate layers (under 10 m thickness) interfinger with black shales containing thin black, partly bituminous, pyrite rich mudstones which despite several attempts



Fig. 6. Uppermost massive conglomerate with well-rounded pebbles of siliciclastics and metamorphic rocks at the top of the Sub-Pog-Formation. Position is 21/21 in Fig. 7. Length of hammer is ca. 35cm.

unfortunately were barren. The conglomerate unit has a thickness of ca. 200m.

“Sub-Pog Shale”

The conglomerate unit rests on a massive and very thick shale (and sandstone?) unit (which might have a thickness greater than 2000 m, that contains discontinuous layers of a) carbonate mass-flows and b) conglomerates of varying thicknesses with blocks of carbonates, carbonate-shale (Fig. 8) or sandstones (Fig. 9A). One of the largest sandstone blocks exposed along the Kir valley road has an exposed length of minimal 200 m and thickness of up to 50 m. It contains a thin syndepositional limestone debris flow (20/69). In this, and in a component of the Sub-Pog conglomerate (Sub-Pog Beds) conodonts of Carboniferous age have been found (Fig. 9B, sample 20/69, Horacek et al., in prep.).

The identical ages of the limy clasts in the sandstone and conglomerates point to a genetic relationship between them, which is further corroborated by the presence of episodic and up to 1m thick conglomerate layers/wedges within the sandstones. Though presently no longer in direct sedimentary sequence, we conclude that sandstones and conglomerates and potentially also the shale-limestone matrix might have built together the Sub-Pog Beds and Shale and were formed in a relatively shallow and marginal basin with conglomerate and sandstone dominated sedimentation.

Due to the absence of any younger (post-Permian) markers, the assignment of this unit to the Cukali Shale (or Xhani Shale), which is the topmost unit of the underlying Cukali Zone and has a Cretaceous-Paleogene age (Fig. 10), is unlikely. We thus tentatively regard this unit as tectonically belonging to the Pog

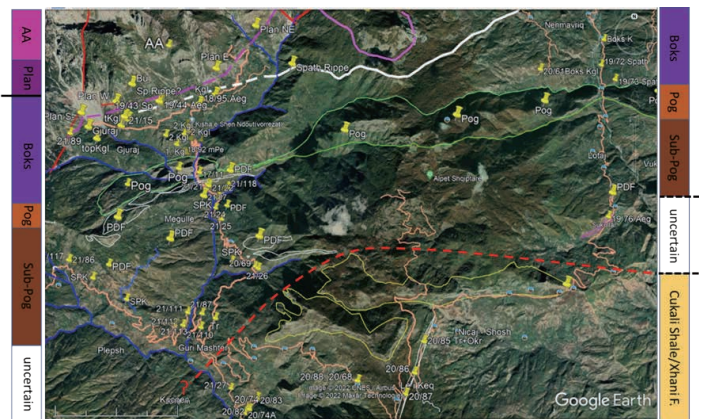


Fig. 7. Satellite image of the investigated area of the Kir River Valley. Kir River is shown as blue line, roads in light orange, green lines denote the Pog Formation. Note the lateral pinching out of the olistolithes and megabreccias. Thin white lines denote massive debris flows with olistolithes (PDF=Permian Debris Flow), SPK identifies conglomerates within the Sub-Pog unit (Sub-Pog-K/conglomerate). Yellow nails show points of interest (Pog=Pog Formation, PDF, SPK), sample locations, sections, etc... AA= Albanian Alps. The columns on the left and right side of the photo show the geological units, as they approximately end at the sides of the photo. Between the Plan and Boks Formations a tectonical boundary is assumed (shown by the pink line on photo/black line in column). Also between the Sub-Pog and Xhani formations a tectonical thrust is assumed. As the exact position is unknown it is shown dashed (dashed red line giving the approximate top of the Cukali Shale/Xhani Formation) with an “uncertain” interval in between. However, it is also possible that the megablocks (shown by yellow lines) regarded as top of the Xhani shale, indeed might be the base of the Sub-Pog Shale unit, in which case the boundary moves below these blocks. On the left-side column the “uncertain” interval was not investigated by us. Scale is 2310 m.



Fig. 8. Carbonate-shale intercalation within the Sub-Pog Formation on the lower right side and on the lower side of the photo below the road. Person for scale is ca. 1.8 m. In the centre, upper left and upper right of the photo are isolated blocks of debris flow breccias. Position 21/87 in Fig. 7.



Fig. 9A. Shale-sandstone-carbonate debris-flow. Position 20/69 in Fig. 7. The carbonate-sandstone is "boudinized" with shale matrix in-between. Hammer is ca. 35cm.

(and Boks) complex of the Bishkaz Shale sheet and thus to the Albanian Alps, differing in this view from Gaetani et al. (2015) and Muttoni et al. (1999).

The age of the Pog Formation and the conglomerate and shale-sandstone units below, which we tentatively name "Sub-Pog-Beds and Shale" is debated and still unclear, since besides redeposited Carboniferous and Early Permian marine fossils also one large carbonate block of Mid-Triassic age has been found (Horacek et al., in prep.). We assume that the Carboniferous and Lower Permian sediments have been redeposited by mass-flows, which might have happened episodically and over a longer (but presently unspecified) interval, with the shales (at least partially) representing background deeper-water sedimentation. However, also a quick (re-)deposition of dislocated blocks and mass-flows from a shallower level into the shale matrix in a deeper water setting might be a valid assumption.

Conclusions

Revisiting the Permian of the Albanian Alps, resulted in a different interpretation of the Permian deposits than previously reported, since no normal respectively continuous sedimentary sequence could be recognized. The Pog Formation, as the top Permian formation present, is now regarded as a succession of mass-flows/olistoliths laterally and on the top disintegrating into megabreccias of different size of almost syn-sedimentary and quick re-deposition. The deposits below are tentatively named „Sub-Pog Beds and Shale“, consisting of the upper Sub-Pog beds conglomerates of ca. 200 m thickness, and the lower „Sub-Pog Shale“. Those consist of thick shale (and sandstone?) that contains discontinuous layers of a) carbonate mass-flows and b) conglomerates of varying thicknesses, and also blocks of carbonates, carbonate-shale (Fig. 8) or sandstones, with a thickness of maybe (even exceeding) 1km. Both Sub-Pog units are regarded as belonging to the Bishkaz-Shale sheet and thus form the base of the Albanian Alps. We report the first findings of Carboniferous and Lower Permian sediments in Albania from the Pog and Sub-Pog units. These findings will have a significant impact on the reconstruction of the paleogeography and the evolution of the western Tethys.

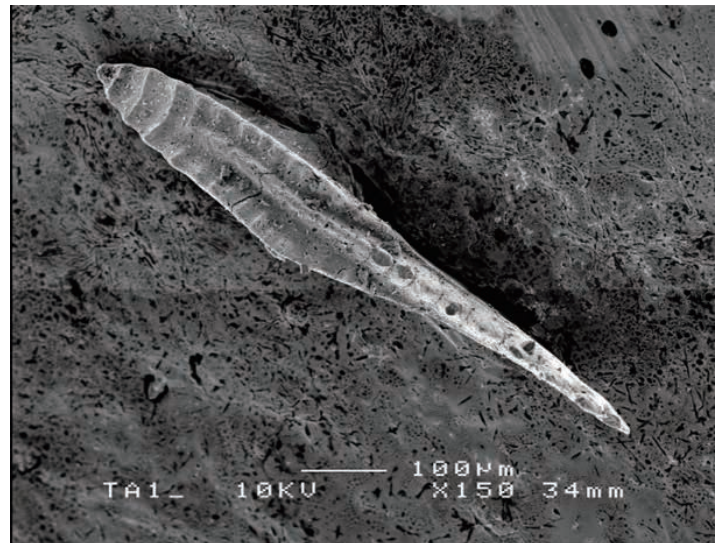


Fig. 9B. *Idiognathus* sp., sample 20/69 in fig. 7.

Acknowledgments

M. Horacek thankfully acknowledges partial financial support by the grant WTZ AL 05/2019. For conodont identifications respectively control we are indebted to Y. Sun (Erlangen).

References

- Aljinović, D., Horacek, M., Richoz, S., Kolar-Jurkovšek, T., Jurkovšek, B., Smirčić, D. and Krystyn, L., 2018, Western Tethyan epeiric ramp setting in the Early Triassic – an example from the central Dinarides (Croatia). *Journal of Earth Science*, v. 29, n. 4, p. 806–823.
- Biçoku, T., Papa, A., Xhomo, A. Pirdeni, A. and Jahja B., 1974. Nyja e Tepes, cak kalimtar nga zona e Alpeve Shqiptare për në zonën e Krastë-Cukalit. *Përmbledhje Studimesh*, v. 4, p. 15–40.
- Biçoku, T. and Arkaxhiu, F., 1998. Studjueshmëria e rievimeve dhe hartografimeve gjeologjike në Shqipëri. *Fondi Qendror i Gjeologjisë*.
- Gaetani, M., Meço, S., Rettori, R., Henderson, C.M. and Tulone, A., 2015, The Permian and Triassic in the Albanian Alps. *Acta Geologica Polonica*, v. 65, n. 3, p. 271–295.
- Gjata T.H. and Skela V., 1972. Përfytyrimi strukturor i zonave



Fig. 10. Scaglia/Couch rouge Tertiary carbonate sediment block in brown shale. Hammer is ca. 35cm.

të Kraste-Cukalit, Jonike dhe të Sazanit. Përmbledhje Studimesh, v. 1, p. 127–139.

Horacek, M., Dakovic, M. and Krystyn, L., 2020, The Permian of the Budva Zone, Montenegro, western Tethys. *Permophiles*, n. 69, p. 32–36.

Horacek, M., Krystyn, L., Onuzi, K., Sun, Y. and Durmishi, C., in prep., Evidence for Paleotethyan origin of Permo-Triassic sediments in Northern Albania: The carbonate blocks in the “Lotaj Shale” (part of the Xhani Shale) of the Cukali Zone, Northern Albania.

Krystyn, L., Brandner, R., Dakovic, M. and Horacek, M., 2019. The Lower Triassic of the Budva Zone. *Geoloski Glasnik/ Geological Bulletin Geological Survey of Montenegro*, v. 17, p. 9–20.

Lula, F., Sadushi, P., Meçaj, B. and Muska, K., 1999. Studim mbi modelin strukturor, shkallën e mbihipjes, karakteristikat sedimentologjike, gjeokimike e kolektorale të zonës Krasta-Cukali lidhur me perspektivën naftë-gazmbajtëse.

Meço, S., 1999. Studim i detajuar i depozitimeve të Permianit të sipërm dhe Triasikut të poshtëm e të mesëm në zonën e Alpeve Shqiptare dhe atë të Cukalit. *Fondi i F.G.J.M. Tiranë*.

Meço, S., 1999. Conodont biostratigraphy of Triassic pelagic strata Albania. *Rivista Italiana di Paleontologia e Stratigrafia*, v. 105, n. 2, p. 251–266.

Meço, S., Aliaj, Sh. and Turku, I., 2000. *Geology of Albania*. Gebrüder Borntraeger. Ser.28, 246f. Berlin-Shtutgart

Muttoni, M., Kent, D.V., Meço, S., Balini, M., Nicora, A., Rettori, R., Gaetani, M. and Krystyn, L. 1998. Towards a better definition of the Middle Triassic magnetostratigraphy and biostratigraphy in the Tethys Realm. *Earth and Planetary Sciences Letters*, v. 164, p. 285–302.

Muttoni, G., Gaetani, M., Kent, D.V., Sciunnach, D., Angiolini, L., Berra, F., Garzanti, E., Mattei M. and Zanchi, A., 2009. Opening of the Neo-Tethys Ocean and the Pangea B to Pangea A transformation during the Permian. *GeoArabia*, v. 14, n. 4, p. 17–48.

Onuzi, K, Vukaj, S. and Pajovic, M., 2011. Korrelimi hartave gjeologjike ne shkalle 1:50 000 te zones kufitare Shqiperi-Mali i Zi (Akademia e Shkencave e Shqipërisë&Akademia e Shkencave dhe e Arteve e Malit të Zi, Librat 105,Vellimi I, Podgorica-Shkoder (Podgorice2011)

Peza, L.H., Theodhori, P. and Xhomo, A., 1973. Depozitimet liasike në pjesën veriperëndimore të Alpeve Shqiptare. *Përmbledhje studimesh*, v.1.

Peza, L.H., 1981. Stratigrafia e depozitimeve kretake të zonës së Alpeve Shqiptare dhe studimi monografik i disa molusqeve. *Disertacion*, I.

Peza, L.H., 1983. Stratigrafia dhe disa gastropodë të depozitimeve të Baramianit në luginën e Valbonës. *Buletini i shkencave gjeologjike*, n. 2, p. 37–59.

Peza, L.H., 1985. Depozitimet e Baramian-Aptianit në nënzonën e M. Madhe (zona e Alpeve Shqiptare). *Buletini i shkencave gjeologjike*, n. 2, p. 33–43.

Pirdeni, A., 1973. Disa përfaqësues të gjinisë Globotruncana në zonën e Alpeve Shqiptare. *Përmbledhje Studimesh*, v. 2, p. 121–151.

Pirdeni, A., 1982. Biostratigrafia dhe mikrofauna e depozitimeve mesozoike të rajonit të Cukalit. *Disertacion*.

Schmid, S.M., Fügenschuh, B., Kounov, A., Matenco, L., Nievergelt, P., Oberhänsli, R., Pleuger, J., Schefer, S., Schuster, R., Tomljenovic, B., Ustaszewski, K. and van Hinsbergen, D.J.J., 2020. Tectonic units of the Alpine collision zone between Eastern Alps and western Turkey. *Gondwana Research*, v. 78, p. 308–374.

Shima, G., Naska, K. and Kalldani, G., 1980. Shfaqje të argjilave boksitike triasike në zonat tektonike të Alpeve Shqiptare. *Përmbledhje Studimesh*, v. 2.

Theodhori, P., Bushati, S.H. and Pirdeni, A., 1978. Stratigrafia e depozitimeve mesozoike të zonës së Cukalit dhe disa të dhëna mbi mineralmbajtjen. *I.S.P.G.J. Tiranë*.

Theodhori, P., 1988. Kushtet e sedimentimit dhe evolucioni paleogjeografik mesozoik në nënzonën e Cukalit. *Disertacion*.

Theodhori, P., Peza, L.H. and Pirdeni, A., 1993. Cretaceous pelagic and flysh facies of the Krasta- Cukali zone, Albania. *Cretaceous research*, nr.14.

Toska, Z. and Selenica Y., 1988. Horizonti i argjilave të bardha në zonën e Alpeve. *Buletini i shkencave gjeologjike*, n. 3, p. 45–54.

Toska, Z. and Bushati, Sh., 1970. Horizonti i argjilave boksit- mbajtëse jurasike në pjesën veriperëndimore të Alpeve Shqiptare. *Përmbledhje Studimesh*, v. 15, n. 2, p. 49–56.

Vetters, H., 1906. *Geologie des Nordlichen Albaniens-Beitrag zur Geologischen Kenntnis des Nordlichen Albaniens*. Wienn.

Xhomo, A., Peza, L.H. and Theodhori, P., 1969. Disa facie pelagjike të Juarsikut dhe Kretakut në zonën e Alpeve Shqiptare. *Përmbledhje Studimesh*, v. 11, p. 55–66.

Xhomo, A., Peza, L.H. and Pirdeni, A., 1975. Një kontribut për njohjen e stratigrafisë së zonës së Krastë- Cukalit (n/z. Cukalit). *Përmbledhje Studimesh*, v. 2, p. 5–36.

Xhomo, A., Kodra, A. and Gjata, K., 2002. Vendi i gjenezës së ofioliteve të Shqipërisë është baseni oqeanik Mirdita dhe jo baseni Krastë-Cukali (= Pindi). *Buletini i shkencave gjeologjike*, n. 1, p. 25–42.

Xhomo, A., Kodra, A. Xhafa, Z. and Shallo, M. 2008. Gjellogjia e Shqipërisë. *Stratigrafia, Magmatizmi, Metamorfismi, Tektonika, Neotektonika, Evolucioni Paleogjeografik dhe Gjeodinamik*. Sherbimi Gjellogjik Shqiptar, Tirana, 464 pp.

ANNOUNCEMENTS

1. The 4th International Congress on Stratigraphy Strati 2023, Lille, France, 11th-13th July 2023.
<https://stratigraphy.org/news/141>

2. A conference will be held at Lausanne University, Switzerland from 30th August to 2nd September 2023 to discuss Permian-Triassic field work crossing the great extinction to geological, sedimentological, paleontological, and geochemical results. For details, contact the organizing committee coordinator Aymon Baud (aymon.baud@unil.ch). Upcoming website will be at: <https://www.unil.ch/permiantriassic23/>

SUBCOMMISSION ON PERMIAN STRATIGRAPHY



Call for funded participation in STRATI 2023 Lille, France, 11th -13th July 2023

<https://stratigraphy.org/news/141>

SPS would like to fund two Conference Registration fees (Student fee), each to a maximum value of Euros 200.

The call is open to all PhD students and Postdocs studying the Permian.

To apply to the call please send a short CV and an abstract intended for Session “SC10: Correlation of glacial events and extinctions: The Permian and beyond” by email to Lucia Angiolini before 20 February 2023. The subject of the email should be: SPS call for STRATI.

SUBMISSION GUIDELINES FOR ISSUE 75

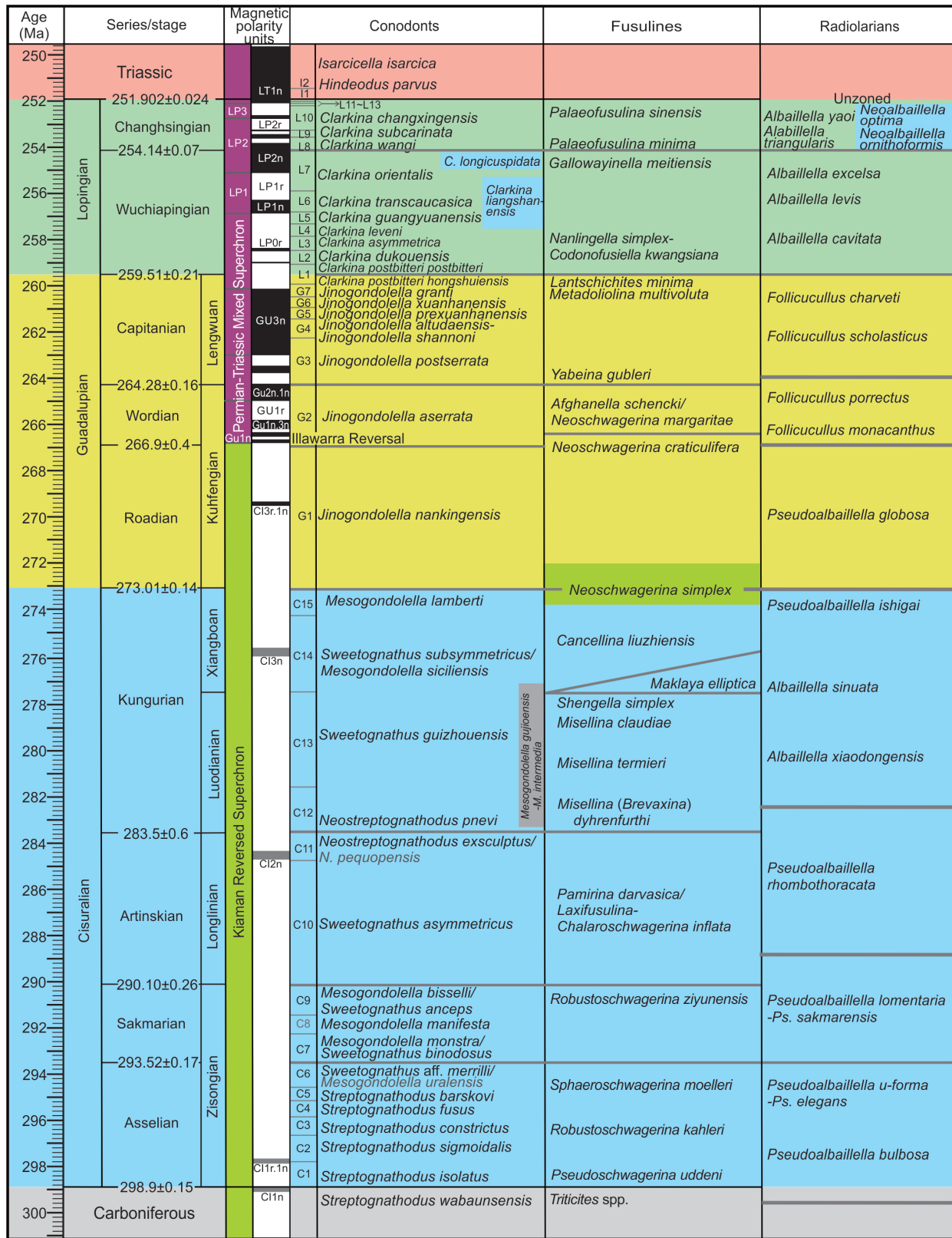
It is best to submit manuscripts as attachments to E-mail messages. Please send messages and manuscripts to Yichun Zhang's E-mail address. Hard copies by regular mail do not need to be sent unless requested. To format the manuscript, please follow the TEMPLATE that you can find on the SPS webpage at <http://permian.stratigraphy.org/>.

Please submit figures files at high resolution (600dpi) separately from text one. Please provide your E-mail addresses in your affiliation. All manuscripts will be edited for consistent use of English only.

Prof. Yichun Zhang (SPS secretary)

Nanjing Institute of Geology and Palaeontology, Chinese Academy of Sciences, Nanjing, Jiangsu, 210008, P.R.China, Email: yczhang@nigpas.ac.cn

The deadline for submission to Issue 75 is July, 31th, 2023



High-resolution integrative Permian stratigraphic framework (after Shen et al., 2019. Permian integrative stratigraphy and timescale of China. Science China Earth Sciences 62(1): 154-188. Guadalupian ages modified after (1) Shen et al., 2020. Progress, problems and prospects: An overview of the Guadalupian Series of South China and North America. Earth-Science Reviews, 211: 103412 and (2) Wu et al., 2020, High-precision U-Pb zircon age constraints on the Guadalupian in West Texas, USA. Palaeogeography, Palaeoclimatology, Palaeoecology, 548: 109668. Lopingian ages modified after Yang et al., 2018, Early Wuchiapingian cooling linked to Emeishan basaltic weathering? Earth and Planetary Science Letters, 492: 102-111.